ISSN 1949-8470 (online)

World Journal of *Radiology*

World J Radiol 2013 December 28; 5(12): 450-502

Baishideng Publishing Group
www.wjgnet.com

WJR World Journal of Radiology

A peer-reviewed, online, open-access journal of Radiology

Editorial Board

2009-2013

The *World Journal of Radiology* Editorial Board consists of 319 members, representing a team of worldwide experts in radiology. They are from 40 countries, including Australia (3), Austria (4), Belgium (5), Brazil (3), Canada (9), Chile (1), China (25), Czech (1), Denmark (1), Egypt (4), Estonia (1), Finland (1), France (6), Germany (17), Greece (8), Hungary (1), India (9), Iran (5), Ireland (1), Israel (4), Italy (28), Japan (14), Lebanon (1), Libya (1), Malaysia (2), Mexico (1), Netherlands (4), New Zealand (1), Norway (1), Saudi Arabia (3), Serbia (1), Singapore (2), Slovakia (1), South Korea (16), Spain (8), Switzerland (5), Thailand (1), Turkey (20), United Kingdom (16), and United States (82).

France

Alain Chapel, *Fontenay-Aux-Roses*
Nathalie Lassau, *Villejuif*
Youlia M Kirova, *Paris*
Géraldine Le Duc, *Grenoble Cedex*
Laurent Pierot, *Reims*
Frank Pilleul, *Lyon*
Pascal Pommier, *Lyon*

Germany

Ambros J Beer, *München*
Thomas Deserno, *Aachen*
Frederik L Giesel, *Heidelberg*
Ulf Jensen, *Kiel*
Markus Sebastian Juchems, *Ulm*
Kai U Juergens, *Bremen*
Melanie Kettering, *Jena*
Jennifer Linn, *Munich*
Christian Lohrmann, *Freiburg*
David Maintz, *Münster*
Henrik J Michaely, *Mannheim*
Oliver Micke, *Bielefeld*
Thoralf Niendorf, *Berlin-Buch*
Silvia Obenauer, *Duesseldorf*
Steffen Rickes, *Halberstadt*
Lars V Baron von Engelhardt, *Bochum*
Goetz H Welsch, *Erlangen*

Greece

Panagiotis Antoniou, *Alexandroupolis*
George C Kagadis, *Rion*
Dimitris Karacostas, *Thessaloniki*
George Panayiotakis, *Patras*
Alexander D Rapidis, *Athens*
C Triantopoulou, *Athens*
Ioannis Tsalafoutas, *Athens*
Virginia Tsapaki, *Anixi*
Ioannis Valais, *Athens*

Hungary

Peter Laszlo Lakatos, *Budapest*

India

Anil Kumar Anand, *New Delhi*
Surendra Babu, *Tamilnadu*
Sandip Basu, *Bombay*
Kundan Singh Chufal, *New Delhi*
Shivanand Gamanagatti, *New Delhi*
Vimoj J Nair, *Haryana*
R Prabhakar, *New Delhi*
Sanjeeb Kumar Sahoo, *Orissa*

Iran

Vahid Reza Dabbagh Kakhki, *Mashhad*
Mehran Karimi, *Shiraz*
Farideh Nejat, *Tehran*
Alireza Shirazi, *Tehran*
Hadi Rokni Yazdi, *Tehran*

Ireland

Joseph Simon Butler, *Dublin*

Israel

Amit Gefen, *Tel Aviv*
Eyal Sheiner, *Be'er-Sheva*
Jacob Sosna, *Jerusalem*
Simcha Yagel, *Jerusalem*

Italy

Mohssen Ansarin, *Milan*
Stefano Arcangeli, *Rome*
Tommaso Bartalena, *Imola*
Sergio Casciaro, *Lecce*
Laura Crocetti, *Pisa*
Alberto Cuocolo, *Napoli*
Mirko D'Onofrio, *Verona*
Massimo Filippi, *Milan*
Claudio Fiorino, *Milano*
Alessandro Franchello, *Turin*
Roberto Grassi, *Naples*
Stefano Guerriero, *Cagliari*
Francesco Lassandro, *Napoli*
Nicola Limbucci, *L'Aquila*
Raffaele Lodi, *Bologna*
Francesca Maccioni, *Rome*
Laura Martincich, *Candiolo*
Mario Mascalchi, *Florence*
Roberto Miraglia, *Palermo*
Eugenio Picano, *Pisa*
Antonio Pinto, *Naples*
Stefania Romano, *Naples*
Luca Saba, *Cagliari*
Sergio Sartori, *Ferrara*
Mariano Scaglione, *Castel Volturno*
Lidia Strigari, *Rome*
Vincenzo Valentini, *Rome*

Japan

Shigeru Ehara, *Morioka*
Nobuyuki Hamada, *Chiba*
Takao Hiraki, *Okayama*
Akio Hiwatashi, *Fukuoka*
Masahiro Jinzaki, *Tokyo*
Hiroshi Matsuda, *Saitama*
Yasunori Minami, *Osaka*
Jun-Ichi Nishizawa, *Tokyo*
Tetsu Niwa, *Yokohama*
Kazushi Numata, *Kanagawa*
Kazuhiko Ogawa, *Okinawa*
Hitoshi Shibuya, *Tokyo*
Akira Uchino, *Saitama*
Haiquan Yang, *Kanagawa*

Lebanon

Aghiad Al-Kutoubi, *Beirut*

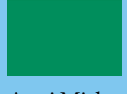

Libya

Anuj Mishra, *Tripoli*

Malaysia

R Logeswaran, *Cyberjaya*
Kwan-Hoong Ng, *Kuala Lumpur*

Mexico

Heriberto Medina-Franco, *Mexico City*

Netherlands

Jurgen J Fütterer, *Nijmegen*
Raffaella Rossin, *Eindhoven*
Paul E Sijens, *Groningen*

New Zealand

W Howell Round, *Hamilton*

Norway

Arne Sigmund Borthne, *Lørenskog*

Saudi Arabia

Mohammed Al-Omran, *Riyadh*
Ragab Hani Donkol, *Abha*
Volker Rudat, *Al Khobar*

Serbia

Djordjije Saranovic, *Belgrade*

Singapore

Uei Pua, *Singapore*
Lim CC Tchoyoson, *Singapore*

Slovakia

František Dubecký, *Bratislava*

South Korea

Bo-Young Choe, *Seoul*
Joon Koo Han, *Seoul*
Seung Jae Huh, *Seoul*
Chan Kyo Kim, *Seoul*
Myeong-Jin Kim, *Seoul*
Seung Hyup Kim, *Seoul*
Kyoung Ho Lee, *Gyeonggi-do*
Won-Jin Moon, *Seoul*
Wazir Muhammad, *Daegu*
Jai Soung Park, *Bucheon*
Noh Hyuck Park, *Kyunggi*
Sang-Hyun Park, *Daejeon*
Joon Beom Seo, *Seoul*
Ji-Hoon Shin, *Seoul*
Jin-Suck Suh, *Seoul*
Hong-Gyun Wu, *Seoul*

Spain

Eduardo J Aguilar, *Valencia*
Miguel Alcaraz, *Murcia*
Juan Luis Alcazar, *Pamplona*
Gorka Bastarrika, *Pamplona*
Rafael Martínez-Monge, *Pamplona*
Alberto Muñoz, *Madrid*
Joan C Vilanova, *Girona*

Switzerland

Nicolau Beckmann, *Basel*
Silke Grabherr, *Lausanne*
Karl-Olof Lövblad, *Geneva*
Tilo Niemann, *Basel*
Martin A Walter, *Basel*

Thailand

Sudsriluk Sampatchalit, *Bangkok*

Turkey

Olus Api, *Istanbul*
Kubilay Aydin, *İstanbul*
Işıl Bilgen, *Izmir*
Zulkif Bozgeyik, *Elazig*
Barbaros E Çil, *Ankara*
Gulgun Engin, *Istanbul*
M Fatih Evcimik, *Malatya*
Ahmet Kaan Gündüz, *Ankara*
Tayfun Hakan, *Istanbul*
Adnan Kabaalioglu, *Antalya*
Fehmi Kaçmaz, *Ankara*
Musturay Karcaaltincaba, *Ankara*
Osman Kizilkilic, *Istanbul*
Zafer Koc, *Adana*
Cem Onal, *Adana*
Yahya Paksoy, *Konya*
Bunyamin Sahin, *Samsun*
Ercument Unlu, *Edirne*
Ahmet Tuncay Turgut, *Ankara*
Ender Uysal, *Istanbul*

United Kingdom

K Faulkner, *Wallsend*
Peter Gaines, *Sheffield*
Balaji Ganeshan, *Brighton*
Nagy Habib, *London*
Alan Jackson, *Manchester*
Pradesh Kumar, *Portsmouth*
Tarik F Massoud, *Cambridge*
Igor Meglinski, *Bedfordshire*
Robert Morgan, *London*
Ian Negus, *Bristol*
Georgios A Plataniotis, *Aberdeen*
N J Raine-Fenning, *Nottingham*
Manuchehr Soleimani, *Bath*
MY Tseng, *Nottingham*
Edwin JR van Beek, *Edinburgh*
Feng Wu, *Oxford*

United States

Athanassios Argiris, *Pittsburgh*
Stephen R Baker, *Newark*
Lia Bartella, *New York*
Charles Bellows, *New Orleans*
Walter L Biffl, *Denver*
Homer S Black, *Houston*
Wessam Bou-Assaly, *Ann Arbor*
Owen Carmichael, *Davis*
Shelton D Caruthers, *St Louis*
Yuhchyau Chen, *Rochester*
Melvin E Clouse, *Boston*
Ezra Eddy Wyssam Cohen, *Chicago*
Aaron Cohen-Gadol, *Indianapolis*
Patrick M Colletti, *Los Angeles*
Kassa Darge, *Philadelphia*
Abhijit P Datir, *Miami*
Delia C DeBuc, *Miami*
Russell L Deter, *Houston*
Adam P Dicker, *Phil*
Khaled M Elsayes, *Ann Arbor*
Steven Feigenberg, *Baltimore*
Christopher G Filippi, *Burlington*
Victor Frenkel, *Bethesda*
Thomas J George Jr, *Gainesville*
Patrick K Ha, *Baltimore*
Robert I Haddad, *Boston*
Walter A Hall, *Syracuse*
Mary S Hammes, *Chicago*
John Hart Jr, *Dallas*
Randall T Higashida, *San Francisco*
Juebin Huang, *Jackson*
Andrei Iagaru, *Stanford*
Craig Johnson, *Milwaukee*
Ella F Jones, *San Francisco*
Csaba Juhasz, *Detroit*
Riyad Karmy-Jones, *Vancouver*
Daniel J Kelley, *Madison*
Amir Khan, *Longview*
Euishin Edmund Kim, *Houston*
Vikas Kundra, *Houston*
Kennith F Layton, *Dallas*
Rui Liao, *Princeton*
CM Charlie Ma, *Philadelphia*
Nina A Mayr, *Columbus*
Thomas J Meade, *Evanston*
Steven R Messé, *Philadelphia*
Nathan Olivier Mewton, *Baltimore*
Feroze B Mohamed, *Philadelphia*
Koenraad J Mortele, *Boston*
Mohan Natarajan, *San Antonio*
John L Nosher, *New Brunswick*
Chong-Xian Pan, *Sacramento*
Dipanjan Pan, *St Louis*
Martin R Prince, *New York*
Reza Rahbar, *Boston*
Carlos S Restrepo, *San Antonio*
Veronica Rooks, *Honolulu*
Maythem Saeed, *San Francisco*
Edgar A Samaniego, *Palo Alto*
Kohkan Shamsi, *Doylestown*
Jason P Sheehan, *Charlottesville*
William P Sheehan, *Willmar*
Charles Jeffrey Smith, *Columbia*
Monvadi B Srichai-Parsia, *New York*
Dan Stoianovici, *Baltimore*
Janio Szklaruk, *Houston*
Dian Wang, *Milwaukee*
Jian Z Wang, *Columbus*
Shougang Wang, *Santa Clara*
Wenbao Wang, *New York*
Aaron H Wolfson, *Miami*
Gayle E Woloschak, *Chicago*
Ying Xiao, *Philadelphia*
Juan Xu, *Pittsburgh*
Benjamin M Yeh, *San Francisco*
Terry T Yoshizumi, *Durham*
Jinxing Yu, *Richmond*
Jianhui Zhong, *Rochester*

WJR World Journal of Radiology

Contents

Monthly Volume 5 Number 12 December 28, 2013

AIM AND SCOPE

World Journal of Radiology (*World J Radiol*, *WJR*, online ISSN 1949-8470, DOI: 10.4329) is a peer-reviewed open access academic journal that aims to guide clinical practice and improve diagnostic and therapeutic skills of clinicians.

WJR covers topics concerning diagnostic radiology, radiation oncology, radiologic physics, neuroradiology, nuclear radiology, pediatric radiology, vascular/interventional radiology, medical imaging achieved by various modalities and related methods analysis. The current columns of *WJR* include editorial, frontier, diagnostic advances, therapeutics advances, field of vision, mini-reviews, review, topic highlight, medical ethics, original articles, case report, clinical case conference (clinicopathological conference), and autobiography.

We encourage authors to submit their manuscripts to *WJR*. We will give priority to manuscripts that are supported by major national and international foundations and those that are of great basic and clinical significance.

INDEXING/ABSTRACTING

World Journal of Radiology is now indexed in PubMed Central, PubMed, Digital Object Identifier, and Directory of Open Access Journals.

NAME OF JOURNAL
World Journal of Radiology

ISSN
ISSN 1949-8470 (online)

LAUNCH DATE
December 31, 2009

FREQUENCY
Monthly

EDITOR-IN-CHIEF
Filippo Cademartiri, MD, PhD, FESC, FSCCT, Professor, Cardio-Vascular Imaging Unit-Giovanni XXIII Hospital, Via Giovanni XXIII, 7-31050-Monastier di Treviso (TV), Italy

EDITORIAL OFFICE
Jin-Lei Wang, Director
Xiu-Xia Song, Vice Director

World Journal of Radiology
Room 903, Building D, Ocean International Center, No. 62 Dongsihuan Zhonglu, Chaoyang District, Beijing 100025, China
Telephone: +86-10-85381891
Fax: +86-10-85381893
E-mail: bpgoffice@wjgnet.com
http://www.wjgnet.com

PUBLISHER
Baishideng Publishing Group Co., Limited
Flat C, 23/F., Lucky Plaza, 315-321 Lockhart Road, Wanchai, Hong Kong, China
Fax: +852-65557188
Telephone: +852-31779906
E-mail: bpgoffice@wjgnet.com
http://www.wjgnet.com

PUBLICATION DATE
December 28, 2013

INSTRUCTIONS TO AUTHORS
Full instructions are available online at http://www.wjgnet.com/1949-8470/g_info_20100316162358.htm.

ONLINE SUBMISSION
http://www.wjgnet.com/esps/

World Journal of Radiology

Online Submissions: http://www.wjgnet.com/esps/
bpgoffice@wjgnet.com
doi:10.4329/wjr.v5.i12.450

World J Radiol 2013 December 28; 5(12): 450-454
ISSN 1949-8470 (online)

EDITORIAL

Interventional neuroradiology of stroke, still not dead

Vitor Mendes Pereira, Karl-Olof Lövblad

Vitor Mendes Pereira, Karl-Olof Lövblad, Department of Diagnostic and Interventional Neuroradiology, Geneva University Hospitals, 1224 Geneva, Switzerland
Author contributions: Pereira VM wrote the manuscript; Lövblad KO discussed and revised the manuscript.
Correspondence to: Karl-Olof Lövblad, MD, Department of Diagnostic and Interventional Neuroradiology, Geneva University Hospitals, 4 rue Gabrielle-Perret-Gentil, 1224 Geneva, Switzerland. karl-olof.lovblad@hcuge.ch
Telephone: +41-22-3727033 Fax: +41-22-3727072
Received: May 28, 2013 Revised: November 11, 2013
Accepted: November 15, 2013
Published online: December 28, 2013

Abstract

Since the National Institute of Neurological Disorders and Stroke trial, intravenous thrombolysis has been gaining wide acceptance as the modality of treatment for acute embolic stroke, with a current therapeutic window of up to 4.5 h. Both imaging [with either magnetic resonance imaging (MRI) or computed tomography (CT)] and interventional techniques (thrombolysis and/or thrombectomy) have since improved and provided us with additional imaging of the penumbra using CT or MRI and more advanced thrombolysis or thrombectomy strategies that have been embraced in many centers dealing with patients with acute cerebral ischemia. These techniques, however, have come under scrutiny due to their accrued healthcare costs and have been questioned following major recent studies. These studies basically showed that interventional techniques were not superior to the traditional intravenous thrombolysis techniques and that penumbra imaging could not determine what patients would benefit from more aggressive (*i.e.*, interventional) treatment. We discuss this in the light of the latest developments in both diagnostic and interventional neuroradiology and point out why further studies are needed in order to define the right choices for patients with acute stroke. Indeed, these studies were in part conducted with suboptimal patient recruitment strategies and did not always use the latest interventional techniques available today. So, while these studies may have raised some relevant questions, at the same time, definitive answers have not been given, in our opinion.

Key words: Stroke; Interventional neuroradiology thrombolysis; Magnetic resonance imaging; Computed tomography

Core tip: While intravenous thrombolysis has gained wide acceptance as a major breakthrough for the acute treatment of stroke, interventional and diagnostic neuroradiology tools have also evolved at a very high rate, providing us with very sophisticated techniques to demonstrate brain tissue damage and revascularization techniques. However, these methods have not been evaluated properly until recently and have been adopted quickly by part of the clinical neuroscience community. A number of recent studies question the impact of these techniques.

Pereira VM, Lövblad KO. Interventional neuroradiology of stroke, still not dead. *World J Radiol* 2013; 5(12): 450-454 Available from: URL: http://www.wjgnet.com/1949-8470/full/v5/i12/450.htm DOI: http://dx.doi.org/10.4329/wjr.v5.i12.450

INTERVENTIONAL NEURORADIOLOGY OF STROKE-STILL NOT DEAD

The position of diagnostic neuroradiology and interventional neuroradiology and their role in stroke have been questioned recently by some randomized controlled studies[1-4]. The role and position of imaging in the diagnosis and management of stroke has changed extensively since the 1990s. Overall, stroke and its management have changed drastically: while initially patients were

considered to be future candidates for reeducation if they survived, with new advances in the management this perspective has changed considerably. Indeed, the concept of stroke units where these patients were seen with an emphasis on their acute disease has already improved their outcome significantly. Then, thrombolysis was introduced with groundbreaking results following the National Institute of Neurological Disorders and Stroke trials[5-7]; initially this implied a rather strict therapeutic window, as well as the sole intravenous administration of drugs and with the presence of significant potential complications due to treatment, such as hemorrhage. Thus, strict guidelines for the management of patients with stroke have been developed in order to improve management and outcomes[8]. However, during that same decade, the radiological side, both diagnostic and interventional techniques, evolved in ways that were important: in a period of a few years, we additionally had diffusion magnetic resonance imaging (MRI)[9], perfusion computed tomography (CT)[10] and additional interventional procedures, such as local intra-arterial thrombolysis[11], followed by mechanical thrombectomy and stenting[12]. On the one hand, dramatic increases were observed in advances that led to an improved understanding of the acute disease and eventually its treatment. However, while the initial results were encouraging, their use was also more time and money consuming, all without real state of the art validation. For anyone who has been involved in the management, diagnosis and treatment of these patients, it is important to know that we saw advances in a very short period in patients where before nothing was expected. This also caused a shift from stroke being a globally managed disease to one that would be more reasonably treated within specialized stroke units and centers. Thus, in addition to a higher technicality and cost, there was a shift away from the primary gatekeepers, the general practitioners or internists, because if time was more and more brain, it meant that these patients had to have a change in clinical pathway for which not everyone was ready. Therapy was moving fast, while at the same time the scientific evidence was not and this was bound to make the whole system collapse. Fortunately, we are not at that point but the recently published papers in the New England Journal raise some valid points while being inherently flawed.

Interventional neuroradiology, different to medical pharmaceutical treatments, does inherently rely on not being fully standardizable; indeed, in order to obtain a certain level of quality, a certain number of interventions must be performed at the center to assure a good level as well as the whole chain from the arrival at the hospital to the post-operative management. Acute stroke treatment is, in fact, a process that involves different disciplines, divisions and teams at the health network and hospital. High volume centers mean that they are able to bring patients through the detection of stroke, diagnosis and therapeutic steps constantly that imply increased effectiveness over time. If we consider a stroke treatment study, where the acute treatment is evaluated but, in fact, the whole stroke pathway is involved, it is hard to imagine that low volume or inexperienced centers will be able to demonstrate any difference between any kinds of treatment. While a drug such as aspirin can be given by any physician or nurse in a standardized way, this is unfortunately not the case with interventional techniques which, like surgery, rely on expertise (relying on experience and talent) which is also at the same time difficult or impossible to quantify. Thus, to some degree, per se interventional techniques are not best suited to fully randomized studies and are almost always certain to fail. We did read with interest the two recent papers published in the New England Journal of Medicine[13,14] as well as the accompanying editorial[4]. What is worrisome is the potential message that these papers may send out: that interventional therapy as such is a failure in improving outcomes in stroke. The introduction of intravenous thrombolysis was a breakthrough for patients with cerebral ischemia, but clinicians, investigators and patients have been frustrated by the limitations due to the rather limited time window and even associated potential complications if exclusion criteria were not followed. Indeed, even with improved outcomes, a high number of hemorrhagic events have been observed with thrombolysis, forcing many clinicians to look for another alternative therapy that might induce less bleeding. There has also been a striking lack of translation of the knowledge about ischemic events into daily practice due to the failure of any kind of alternative neuroprotective therapy to function clinically. Besides simple intravenous thrombolysis based on the exclusion of other pathologies, many investigators have over the years explored the use of imaging for the detection of still viable tissue and the use of interventional techniques. Anybody who has been confronted with utilizing these methods has been able to see that they have indeed improved patient management to some degree, maybe not to the degree we would like, but at least substantially. A further paper also questioned the use of advanced imaging techniques to help identify patients using penumbra imaging in order to determine what candidates may be best suited for another type of therapy. This is an excellent idea but fails, probably because it did only look at penumbral patterns, whereas when one looks at imaging findings, it is very often important to take all parameters into account and additionally look at the parenchyma (on diffusion weighted imaging or unenhanced CT) and the angiographic appearance of the vessels; indeed, this last factor should not be underappreciated since thrombolysis or thrombectomy target the vessel. However, both CT and MRI have become powerful techniques, at least for the exclusion of hemorrhage and the detection of an early insult[15,16]. Despite the fact that both MR and CT techniques have been able to provide more information than merely the absence or presence of hemorrhage, the main role of imaging is still central to exclude another pathology before initiating treatment. Indeed, one area where the role of neuroimag-

ing has always been more problematic, has been with regard to what we call the penumbra[17,18]. From a theoretical point of view, the penumbra is a state of hypoperfusion associated with synaptic dysfunction but not yet membrane dysfunction[19-22]; thus, this is a state where the neurons are not able to function normally but may recover if flow is recovered. The penumbra that we see on imaging with either MRI[22-37] or CT[38-48] is, due to methodological factors, not a representation of the real penumbra as most people understand it: instead of having a pure metabolic model, we have a model based on hemodynamics and which has limitations whether one uses CT or MRI. The validation of these techniques have been rendered more difficult by the fact that most centers use homemade software that is constantly evolving[49,50] and, while these limitations exist, the technique has been shown to be useful. Indeed, very often, one can demonstrate a larger than expected area of hypoperfusion and sometimes demonstrate other causes that may mimic strokes[51]. Interventional techniques can be time-consuming and prone to potential complications but, if used early on in a setting where the angiography suite is placed ideally close to the emergency room or where the time to puncture can be reduced[52,53], definitely has great value. Indeed, the technique, since it includes angiography with direct luminography of the affected vessel, also allows direct visualization of the thrombus as well as vascular revascularization. Additionally, over the last decade, we have moved from pharmacological local intra-arterial fibrinolysis to more complex interventions requiring stenting and/or clot retrieval systems. The evolution of these techniques that have become more efficient, safer and easier to use has been striking over the last few years. This is unfortunately the period when most of the randomized studies were conducted in centers with low volume or with no significant experience of interventional treatment (we can see this by the recruitment numbers and the techniques and devices used in those studies). Thus, it does not represent the results obtained with current state of the art interventional techniques. These studies are a call to sobriety and show us that we should probably not be too enthusiastic when looking at single patient data compared to larger studies. We are, however, in an era where interventional neuroradiology is trying to become more evidence-based but in order to do so, it has to provide larger series than those presented to date, taking into account the very impressive technological advances we have seen recently, and maybe then more encouraging results can be produced. On the one hand, the studies are not encouraging but they represent the first attempts at investigating interventional stroke therapies with state of the art statistics. What the studies maybe lack in "patient selection criteria", they make up for in study design. Indeed, the recent years or months have seen a shift from aspiration to thrombectomy using stent retrievers with a rapidity that requires that they be taken into account before making a final assessment of the method[4]. The fact that most of the studies, including the recently published randomized ones, put techniques that are completely different into the same basket. Recent studies demonstrated that there are two generations of devices to date and their results are completely different (swift and trevo 2). How can we analyze data using those two generation devices together? Or how can we consider the results of a study using techniques that have not been used on high volume and experienced centers for at least 3-4 years? It is not the fault of those responsible for the studies as they declared they had many issues in order to include high volume centers, to keep a constant and unbiased recruitment, and with many competitive studies. The high volume centers that refused to randomize patients in the past are paying an expensive price now that intra-arterial therapy is being proven. This, in parallel with constant evolution in imaging and post-processing techniques, has made it difficult sometimes to evaluate the situation in the way it still merits before being relegated to history. Thus, efforts should focus on designing further studies involving centers of excellence with a high flow of patients and where time to treatment is reduced to a minimum; then it will be possible to obtain data as homogenous as possible in order to fully appreciate the efficacy of endovascular management of stroke. We feel that, in the worst case, these techniques may be used for a while for more extensive clots but this may be proven wrong if studies are conducted in a more fair way.

Only when new studies have been performed with more relevant study criteria (faster inclusion times, faster time to needle, done in centers with high volumes *etc*.) can we really appreciate the failures and successes of interventional neuroradiology coupled by modern imaging techniques used in a correct way[54]; these paradigms may require using many parameters in order to function correctly[55]. Only then can we avoid being too distracted by the main problem we may still encounter, that the technologies keep evolving in this field faster than the evaluation, thus making validation difficult.

REFERENCES

1 **Kidwell CS**, Jahan R, Gornbein J, Alger JR, Nenov V, Ajani Z, Feng L, Meyer BC, Olson S, Schwamm LH, Yoo AJ, Marshall RS, Meyers PM, Yavagal DR, Wintermark M, Guzy J, Starkman S, Saver JL. A trial of imaging selection and endovascular treatment for ischemic stroke. *N Engl J Med* 2013; **368**: 914-923 [PMID: 23394476 DOI: 10.1056/NEJMoa1212793]

2 **Broderick JP**, Palesch YY, Demchuk AM, Yeatts SD, Khatri P, Hill MD, Jauch EC, Jovin TG, Yan B, Silver FL, von Kummer R, Molina CA, Demaerschalk BM, Budzik R, Clark WM, Zaidat OO, Malisch TW, Goyal M, Schonewille WJ, Mazighi M, Engelter ST, Anderson C, Spilker J, Carrozzella J, Ryckborst KJ, Janis LS, Martin RH, Foster LD, Tomsick TA; Interventional Management of Stroke (IMS) III Investigators. Endovascular therapy after intravenous t-PA versus t-PA alone for stroke. *N Engl J Med* 2013; **368**: 893-903 [PMID: 23390923 DOI: 10.1056/NEJMoa1214300]

3 **Ciccone A**, Valvassori L, Nichelatti M, Sgoifo A, Ponzio M, Sterzi R, Boccardi E. Endovascular treatment for acute ischemic stroke. *N Engl J Med* 2013; **368**: 904-913 [PMID: 23387822 DOI: 10.1056/NEJMoa1213701]

4 **Chimowitz MI**. Endovascular treatment for acute ischemic

stroke--still unproven. *N Engl J Med* 2013; **368**: 952-955 [PMID: 23394477]
5 Tissue plasminogen activator for acute ischemic stroke. The National Institute of Neurological Disorders and Stroke rt-PA Stroke Study Group. *N Engl J Med* 1995; **333**: 1581-1587 [PMID: 7477192]
6 **Hacke W**, Kaste M, Fieschi C, Toni D, Lesaffre E, von Kummer R, Boysen G, Bluhmki E, Höxter G, Mahagne MH. Intravenous thrombolysis with recombinant tissue plasminogen activator for acute hemispheric stroke. The European Cooperative Acute Stroke Study (ECASS) *JAMA* 1995; **274**: 1017-1025 [PMID: 7563451]
7 **Hacke W**, Kaste M, Bluhmki E, Brozman M, Dávalos A, Guidetti D, Larrue V, Lees KR, Medeghri Z, Machnig T, Schneider D, von Kummer R, Wahlgren N, Toni D. Thrombolysis with alteplase 3 to 4.5 hours after acute ischemic stroke. *N Engl J Med* 2008; **359**: 1317-1329 [PMID: 18815396 DOI: 10.1056/NEJMoa0804656]
8 **Adams HP**, del Zoppo G, Alberts MJ, Bhatt DL, Brass L, Furlan A, Grubb RL, Higashida RT, Jauch EC, Kidwell C, Lyden PD, Morgenstern LB, Qureshi AI, Rosenwasser RH, Scott PA, Wijdicks EF. Guidelines for the early management of adults with ischemic stroke: a guideline from the American Heart Association/American Stroke Association Stroke Council, Clinical Cardiology Council, Cardiovascular Radiology and Intervention Council, and the Atherosclerotic Peripheral Vascular Disease and Quality of Care Outcomes in Research Interdisciplinary Working Groups: the American Academy of Neurology affirms the value of this guideline as an educational tool for neurologists. *Stroke* 2007; **38**: 1655-1711 [PMID: 17431204 DOI: 10.1161/STROKEAHA.107.181486]
9 **Lövblad KO**, Laubach HJ, Baird AE, Curtin F, Schlaug G, Edelman RR, Warach S. Clinical experience with diffusion-weighted MR in patients with acute stroke. *AJNR Am J Neuroradiol* 1998; **19**: 1061-1066 [PMID: 9672012]
10 **Wintermark M**, Sincic R, Sridhar D, Chien JD. Cerebral perfusion CT: technique and clinical applications. *J Neuroradiol* 2008; **35**: 253-260 [PMID: 18466974 DOI: 10.1016/j.neurad.2008.03.005]
11 **Gönner F**, Remonda L, Mattle H, Sturzenegger M, Ozdoba C, Lövblad KO, Baumgartner R, Bassetti C, Schroth G. Local intra-arterial thrombolysis in acute ischemic stroke. *Stroke* 1998; **29**: 1894-1900 [PMID: 9731615 DOI: 10.1161/01.STR.29.9.1894]
12 **Pereira VM**, Narata AP, Gonzalez AM, Sztajzel R, Lovblad KO. Use of stentrievers in acute stroke: tips, tricks, and current results. *Tech Vasc Interv Radiol* 2012; **15**: 68-77 [PMID: 22464305 DOI: 10.1053/j.tvir.2011.12.009]
13 **Warach S**, Pettigrew LC, Dashe JF, Pullicino P, Lefkowitz DM, Sabounjian L, Harnett K, Schwiderski U, Gammans R. Effect of citicoline on ischemic lesions as measured by diffusion-weighted magnetic resonance imaging. Citicoline 010 Investigators. *Ann Neurol* 2000; **48**: 713-722 [PMID: 11079534]
14 **Dávalos A**, Alvarez-Sabín J, Castillo J, Díez-Tejedor E, Ferro J, Martínez-Vila E, Serena J, Segura T, Cruz VT, Masjuan J, Cobo E, Secades JJ. Citicoline in the treatment of acute ischaemic stroke: an international, randomised, multicentre, placebo-controlled study (ICTUS trial). *Lancet* 2012; **380**: 349-357 [PMID: 22691567 DOI: 10.1016/S0140-6736(12)60813-7]
15 **Kidwell CS**, Chalela JA, Saver JL, Starkman S, Hill MD, Demchuk AM, Butman JA, Patronas N, Alger JR, Latour LL, Luby ML, Baird AE, Leary MC, Tremwel M, Ovbiagele B, Fredieu A, Suzuki S, Villablanca JP, Davis S, Dunn B, Todd JW, Ezzeddine MA, Haymore J, Lynch JK, Davis L, Warach S. Comparison of MRI and CT for detection of acute intracerebral hemorrhage. *JAMA* 2004; **292**: 1823-1830 [PMID: 15494579 DOI: 10.1001/jama.292.15.1823]
16 **Chalela JA**, Kidwell CS, Nentwich LM, Luby M, Butman JA, Demchuk AM, Hill MD, Patronas N, Latour L, Warach S. Magnetic resonance imaging and computed tomography in emergency assessment of patients with suspected acute stroke: a prospective comparison. *Lancet* 2007; **369**: 293-298 [PMID: 17258669 DOI: 10.1016/S0140-6736(07)60151-2]
17 **Astrup J**, Symon L, Branston NM, Lassen NA. Cortical evoked potential and extracellular K+ and H+ at critical levels of brain ischemia. *Stroke* 1977; **8**: 51-57 [PMID: 13521]
18 **Astrup J**, Siesjö BK, Symon L. Thresholds in cerebral ischemia - the ischemic penumbra. *Stroke* 1981; **12**: 723-725 [PMID: 6272455]
19 **Symon L**, Astrup J. Phenomena associated with focal ischaemia in the central nervous system. *Acta Neurochir Suppl (Wien)* 1979; **28**: 215-217 [PMID: 225935]
20 **Fisher M**, Takano K. The penumbra, therapeutic time window and acute ischaemic stroke. *Baillieres Clin Neurol* 1995; **4**: 279-295 [PMID: 7496621]
21 **Touzani O**, Roussel S, MacKenzie ET. The ischaemic penumbra. *Curr Opin Neurol* 2001; **14**: 83-88 [PMID: 11176222 DOI: 10.1097/00019052-200102000-00013]
22 **Heiss WD**, Forsting M, Diener HC. Imaging in cerebrovascular disease. *Curr Opin Neurol* 2001; **14**: 67-75 [PMID: 11176220]
23 **Kidwell CS**, Villablanca JP, Saver JL. Advances in neuroimaging of acute stroke. *Curr Atheroscler Rep* 2000; **2**: 126-135 [PMID: 11122736 DOI: 10.1007/s11883-000-0107-z]
24 **Schlaug G**, Benfield A, Baird AE, Siewert B, Lövblad KO, Parker RA, Edelman RR, Warach S. The ischemic penumbra: operationally defined by diffusion and perfusion MRI. *Neurology* 1999; **53**: 1528-1537 [PMID: 10534263 DOI: 10.1212/WNL.53.7.1528]
25 **Baird AE**, Benfield A, Schlaug G, Siewert B, Lövblad KO, Edelman RR, Warach S. Enlargement of human cerebral ischemic lesion volumes measured by diffusion-weighted magnetic resonance imaging. *Ann Neurol* 1997; **41**: 581-589 [PMID: 9153519 DOI: 10.1002/ana.410410506]
26 **Baird AE**, Lövblad KO, Dashe JF, Connor A, Burzynski C, Schlaug G, Straroselskaya I, Edelman RR, Warach S. Clinical correlations of diffusion and perfusion lesion volumes in acute ischemic stroke. *Cerebrovasc Dis* 2000; **10**: 441-448 [PMID: 11070374 DOI: 10.1159/000016105]
27 **Wu O**, Koroshetz WJ, Ostergaard L, Buonanno FS, Copen WA, Gonzalez RG, Rordorf G, Rosen BR, Schwamm LH, Weisskoff RM, Sorensen AG. Predicting tissue outcome in acute human cerebral ischemia using combined diffusion- and perfusion-weighted MR imaging. *Stroke* 2001; **32**: 933-942 [PMID: 11283394 DOI: 10.1161/01.STR.32.4.933]
28 **Ay H**, Buonanno FS, Rordorf G, Schaefer PW, Schwamm LH, Wu O, Gonzalez RG, Yamada K, Sorensen GA, Koroshetz WJ. Normal diffusion-weighted MRI during stroke-like deficits. *Neurology* 1999; **52**: 1784-1792 [PMID: 10371524 DOI: 10.1212/WNL.52.9.1784]
29 **Sorensen AG**, Copen WA, Ostergaard L, Buonanno FS, Gonzalez RG, Rordorf G, Rosen BR, Schwamm LH, Weisskoff RM, Koroshetz WJ. Hyperacute stroke: simultaneous measurement of relative cerebral blood volume, relative cerebral blood flow, and mean tissue transit time. *Radiology* 1999; **210**: 519-527 [PMID: 10207439]
30 **González RG**, Schaefer PW, Buonanno FS, Schwamm LH, Budzik RF, Rordorf G, Wang B, Sorensen AG, Koroshetz WJ. Diffusion-weighted MR imaging: diagnostic accuracy in patients imaged within 6 hours of stroke symptom onset. *Radiology* 1999; **210**: 155-162 [PMID: 9885601]
31 **Schwamm LH**, Koroshetz WJ, Sorensen AG, Wang B, Copen WA, Budzik R, Rordorf G, Buonanno FS, Schaefer PW, Gonzalez RG. Time course of lesion development in patients with acute stroke: serial diffusion- and hemodynamic-weighted magnetic resonance imaging. *Stroke* 1998; **29**: 2268-2276 [PMID: 9804633 DOI: 10.1161/01.STR.29.11.2268]
32 **Rordorf G**, Koroshetz WJ, Copen WA, Cramer SC, Schaefer PW, Budzik RF, Schwamm LH, Buonanno F, Sorensen

AG, Gonzalez G. Regional ischemia and ischemic injury in patients with acute middle cerebral artery stroke as defined by early diffusion-weighted and perfusion-weighted MRI. *Stroke* 1998; **29**: 939-943 [PMID: 9596239 DOI: 10.1161/01.STR.29.5.939]

33 **Sorensen AG**, Buonanno FS, Gonzalez RG, Schwamm LH, Lev MH, Huang-Hellinger FR, Reese TG, Weisskoff RM, Davis TL, Suwanwela N, Can U, Moreira JA, Copen WA, Look RB, Finklestein SP, Rosen BR, Koroshetz WJ. Hyperacute stroke: evaluation with combined multisection diffusion-weighted and hemodynamically weighted echo-planar MR imaging. *Radiology* 1996; **199**: 391-401 [PMID: 8668784]

34 **Warach S**, Dashe JF, Edelman RR. Clinical outcome in ischemic stroke predicted by early diffusion-weighted and perfusion magnetic resonance imaging: a preliminary analysis. *J Cereb Blood Flow Metab* 1996; **16**: 53-59 [PMID: 8530555 DOI: 10.1097/00004647-199601000-00006]

35 **Schellinger PD**, Bryan RN, Caplan LR, Detre JA, Edelman RR, Jaigobin C, Kidwell CS, Mohr JP, Sloan M, Sorensen AG, Warach S. Evidence-based guideline: The role of diffusion and perfusion MRI for the diagnosis of acute ischemic stroke: report of the Therapeutics and Technology Assessment Subcommittee of the American Academy of Neurology. *Neurology* 2010; **75**: 177-185 [PMID: 20625171 DOI: 10.1212/WNL.0b013e3181e7c9dd]

36 **Staroselskaya IA**, Chaves C, Silver B, Linfante I, Edelman RR, Caplan L, Warach S, Baird AE. Relationship between magnetic resonance arterial patency and perfusion-diffusion mismatch in acute ischemic stroke and its potential clinical use. *Arch Neurol* 2001; **58**: 1069-1074 [PMID: 11448295 DOI: 10.1001/archneur.58.7.1069]

37 **Kidwell CS**, Saver JL, Mattiello J, Starkman S, Vinuela F, Duckwiler G, Gobin YP, Jahan R, Vespa P, Kalafut M, Alger JR. Thrombolytic reversal of acute human cerebral ischemic injury shown by diffusion/perfusion magnetic resonance imaging. *Ann Neurol* 2000; **47**: 462-469 [PMID: 10762157]

38 **Röther J**. CT and MRI in the diagnosis of acute stroke and their role in thrombolysis. *Thromb Res* 2001; **103** Suppl 1: S125-S133 [PMID: 11567680 DOI: 10.1016/S0049-3848(01)00309-7]

39 **Wintermark M**, Reichhart M, Cuisenaire O, Maeder P, Thiran JP, Schnyder P, Bogousslavsky J, Meuli R. Comparison of admission perfusion computed tomography and qualitative diffusion- and perfusion-weighted magnetic resonance imaging in acute stroke patients. *Stroke* 2002; **33**: 2025-2031 [PMID: 12154257 DOI: 10.1161/01.STR.0000023579.61630.AC]

40 **Wintermark M**, Reichhart M, Thiran JP, Maeder P, Chalaron M, Schnyder P, Bogousslavsky J, Meuli R. Prognostic accuracy of cerebral blood flow measurement by perfusion computed tomography, at the time of emergency room admission, in acute stroke patients. *Ann Neurol* 2002; **51**: 417-432 [PMID: 11921048 DOI: 10.1002/ana.10136]

41 **Meuli RA**. Imaging viable brain tissue with CT scan during acute stroke. *Cerebrovasc Dis* 2004; **17** Suppl 3: 28-34 [PMID: 14730256 DOI: 10.1159/000075302]

42 **Michel P**, Reichhart M, Wintermark M, Meuli R, Bogousslavsky J. Perfusion-CT guided acute stroke management. *Rinsho Shinkeigaku* 2003; **43**: 728-731 [PMID: 15152451]

43 **Wintermark M**, Fischbein NJ, Smith WS, Ko NU, Quist M, Dillon WP. Accuracy of dynamic perfusion CT with deconvolution in detecting acute hemispheric stroke. *AJNR Am J Neuroradiol* 2005; **26**: 104-112 [PMID: 15661711]

44 **Wintermark M**. Brain perfusion-CT in acute stroke patients. *Eur Radiol* 2005; **15** Suppl 4: D28-D31 [PMID: 16479642 DOI: 10.1007/s10406-005-0112-y]

45 **Schaefer PW**, Roccatagliata L, Ledezma C, Hoh B, Schwamm LH, Koroshetz W, Gonzalez RG, Lev MH. First-pass quantitative CT perfusion identifies thresholds for salvageable penumbra in acute stroke patients treated with intra-arterial therapy. *AJNR Am J Neuroradiol* 2006; **27**: 20-25 [PMID: 16418350]

46 **Parsons MW**, Pepper EM, Bateman GA, Wang Y, Levi CR. Identification of the penumbra and infarct core on hyperacute noncontrast and perfusion CT. *Neurology* 2007; **68**: 730-736 [PMID: 17339580 DOI: 10.1212/01.wnl.0000256366.86353.ff]

47 **Wintermark M**, Meuli R, Browaeys P, Reichhart M, Bogousslavsky J, Schnyder P, Michel P. Comparison of CT perfusion and angiography and MRI in selecting stroke patients for acute treatment. *Neurology* 2007; **68**: 694-697 [PMID: 17325279 DOI: 10.1212/01.wnl.0000255959.30107.08]

48 **Sparacia G**, Iaia A, Assadi B, Lagalla R. Perfusion CT in acute stroke: predictive value of perfusion parameters in assessing tissue viability versus infarction. *Radiol Med* 2007; **112**: 113-122 [PMID: 17310286 DOI: 10.1007/s11547-007-0125-9]

49 **Abels B**, Villablanca JP, Tomandl BF, Uder M, Lell MM. Acute stroke: a comparison of different CT perfusion algorithms and validation of ischaemic lesions by follow-up imaging. *Eur Radiol* 2012; **22**: 2559-2567 [PMID: 22717727 DOI: 10.1007/s00330-012-2529-8]

50 **Soares BP**, Dankbaar JW, Bredno J, Cheng S, Bhogal S, Dillon WP, Wintermark M. Automated versus manual post-processing of perfusion-CT data in patients with acute cerebral ischemia: influence on interobserver variability. *Neuroradiology* 2009; **51**: 445-451 [PMID: 19274457 DOI: 10.1007/s00234-009-0516-9]

51 **Hand PJ**, Kwan J, Lindley RI, Dennis MS, Wardlaw JM. Distinguishing between stroke and mimic at the bedside: the brain attack study. *Stroke* 2006; **37**: 769-775 [PMID: 16484610]

52 **Gupta R**, Horev A, Nguyen T, Gandhi D, Wisco D, Glenn BA, Tayal AH, Ludwig B, Terry JB, Gershon RY, Jovin T, Clemmons PF, Frankel MR, Cronin CA, Anderson AM, Hussain MS, Sheth KN, Belagaje SR, Tian M, Nogueira RG. Higher volume endovascular stroke centers have faster times to treatment, higher reperfusion rates and higher rates of good clinical outcomes. *J Neurointerv Surg* 2013; **5**: 294-297 [PMID: 22581925 DOI: 10.1136/neurintsurg-2011-010245]

53 **Sun CH**, Nogueira RG, Glenn BA, Connelly K, Zimmermann S, Anda K, Camp D, Frankel MR, Belagaje SR, Anderson AM, Isakov AP, Gupta R. "Picture to puncture": a novel time metric to enhance outcomes in patients transferred for endovascular reperfusion in acute ischemic stroke. *Circulation* 2013; **127**: 1139-1148 [PMID: 23393011 DOI: 10.1161/CIRCULATIONAHA.112.000506]

54 **Donnan GA**, Davis SM. Neuroimaging, the ischaemic penumbra, and selection of patients for acute stroke therapy. *Lancet Neurol* 2002; **1**: 417-425 [PMID: 12849364]

55 **Baird AE**, Dambrosia J, Janket S, Eichbaum Q, Chaves C, Silver B, Barber PA, Parsons M, Darby D, Davis S, Caplan LR, Edelman RE, Warach S. A three-item scale for the early prediction of stroke recovery. *Lancet* 2001; **357**: 2095-2099 [PMID: 11445104]

P- Reviewer: Alexander MD **S- Editor**: Zhai HH
L- Editor: Roemmele A **E- Editor**: Liu SQ

World Journal of Radiology

Online Submissions: http://www.wjgnet.com/esps/
bpgoffice@wjgnet.com
doi:10.4329/wjr.v5.i12.455

World J Radiol 2013 December 28; 5(12): 455-459
ISSN 1949-8470 (online)

Magnetic resonance imaging of soft-tissue tumors of the extremities: A practical approach

Wing P Chan

Wing P Chan, Department of Radiology, Wan Fang Hospital, Taipei Medical University, Taipei 116, Taiwan
Wing P Chan, Department of Radiology, School of Medicine, College of Medicine, Taipei Medical University, Taipei 110, Taiwan
Author contributions: Chan WP designed the study and wrote the manuscript.
Correspondence to: Wing P Chan, MD, Professor, Chief, Department of Radiology, Wan Fang Hospital, Taipei Medical University, 111 Hsing-Long Road, Sec 3, Taipei 116, Taiwan. wingchan@tmu.edu.tw
Telephone: +886-2-29307930 Fax: +886-2-29316809
Received: August 13, 2013 Revised: September 22, 2013
Accepted: October 15, 2013
Published online: December 28, 2013

Abstract

Diagnosis of extremity soft-tissue tumors can be challenging. Characteristics of tumor margins can help precisely identify locally aggressive or non-aggressive behavior for surgical planning, but cannot differentiate benign from malignant lesions. Most malignant tumors can have inhomogeneous signals on T2-weighted images. Although a uniform signal on T2-weighted images can be a reliable indication of a benign lesion, a well-defined mass with homogeneous internal signal intensity does not definitively identify a benign lesion. Some common and distinctive soft-tissue lesions can have specific clinical and imaging features allowing a diagnosis without biopsy. These are known as determinate lesions. This illustrative report presents a diagnostic guide for extremity soft-tissue tumors based on tissue signal and morphological characteristics on magnetic resonance images. It is important for clinicians to be familiar with the imaging characteristics of common determinate lesions.

Key words: Extremity; Magnetic resonance imaging; Musculoskeletal neoplasm; Sarcoma; Soft-tissue tumors

Core tip: The aim of this illustrative report is to provide a diagnostic guide for soft-tissue tumors of the extremities based on tissue signal and morphological characteristics on magnetic resonance images.

Chan WP. Magnetic resonance imaging of soft-tissue tumors of the extremities: A practical approach. *World J Radiol* 2013; 5(12): 455-459 Available from: URL: http://www.wjgnet.com/1949-8470/full/v5/i12/455.htm DOI: http://dx.doi.org/10.4329/wjr.v5.i12.455

MAGNETIC RESONANCE IMAGING OF SOFT-TISSUE TUMORS OF THE EXTREMITIES: A PRACTICAL APPROACH

The functions of magnetic resonance (MR) imaging in evaluation of soft-tissue tumors of the extremities include detection, characterization, local staging, and detection of recurrence and complications after therapy.

MR imaging and computed tomography (CT) scanning can be equally accurate for detecting the size and extent of a tumor. MR imaging is more accurate than CT for evaluating individual muscle involvement and therefore can be the staging procedure of choice in patients with soft-tissue sarcoma of the extremities.

MR imaging is superior to CT in detecting recurrent soft-tissue sarcomas. A nodule or mass with a mass effect on surrounding tissue is highly indicative of recurrent tumors. However, both the tumor and organizing scar (or granulation tissue) can show marked gadolinium enhancement.

MRI determinate lesions

Some common and distinctive soft-tissue lesions have specific clinical and imaging features allowing a diagnosis with-

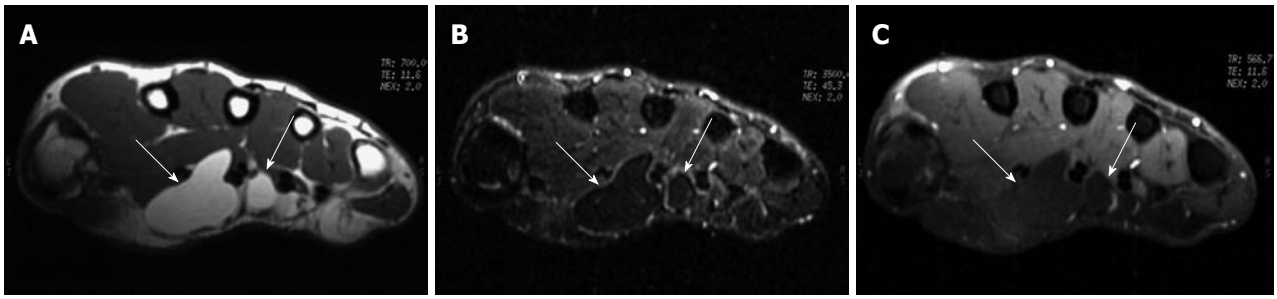

Figure 1 Lipoma of the tendon sheath. A: T1-weighted MR image of the right wrist shows a lobulated high-signal-intensity mass (arrows) located between the palmar muscles; B: Fat-saturated proton-density weighted MR image shows homogeneous low signal intensity of the tumor mass (arrows), suggestive of a fat component; C: There is no enhancement of the tumor mass (arrows) after gadolinium administration on fat-saturated T1-weighted image. MR: Magnetic resonance.

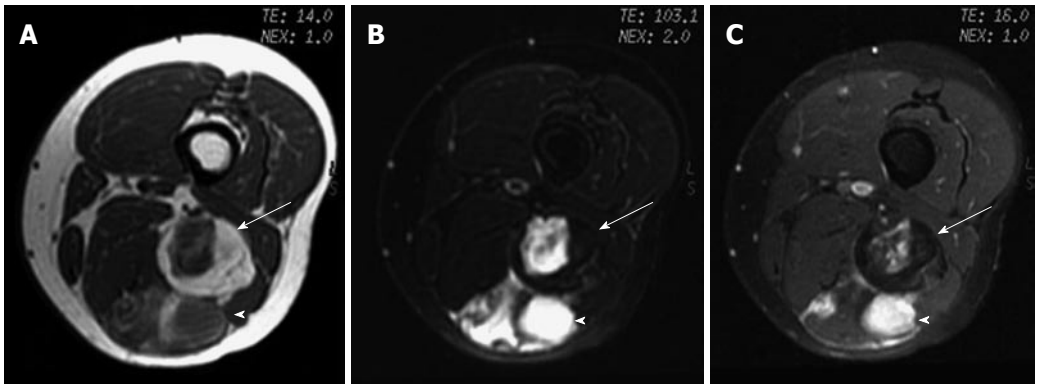

Figure 2 Myxoid liposarcoma. A: Axial T1-weighted image; B: Fat-saturated T2-weighted MR image; C: Fat saturated gadolinium-enhanced T1-weighted images of left thigh show a lobulated fat-containing mass (arrow) with an enhancing nonadipose mass-like area (arrowhead) on the left thigh, suggestive of myxoid stroma.

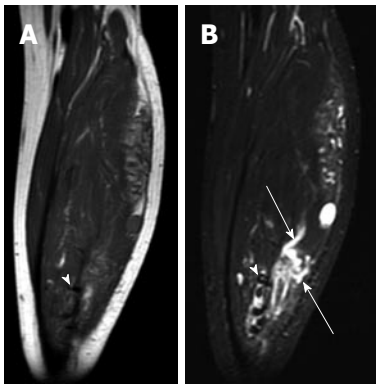

Figure 3 Cavernous hemangioma. A: Coronal T1-weighted image; B: Fat saturated T2-weighted MR image. The left calf shows a heterogeneous serpiginous high-signal-intensity lesion (arrows) on T2-weighted image, which is caused by dilated slow-flowing vessels with methemoglobin. Some low-signal-intensity pattern (arrowhead) indicates fast-flow blood or hemosiderin or calcification. MR: Magnetic resonance.

out biopsy[1,2]. These are known as determinate lesions[2]. Examples of lesions with specific signal characteristics on MR imaging are lipoma (Figure 1), liposarcoma (Figure 2), hemangioma (Figure 3), ganglion and Baker cysts (Figure 4), giant cell tumor (GCT) arising from the tendon sheath (Figure 5), peripheral nerve sheath tumor (PNST) and neurofibroma (Figures 6, 7 and 8), subungual glomus tumor (Figure 9), localized solitary synovitis (Figure 10), muscle tear and hematoma (Figure 11), abscess (Figure 12), myonecrosis, bursitis, and aneurysm.

MRI indeterminate lesions

An indeterminate lesion is one that must be biopsied to ensure an accurate diagnosis[2]. Examples of lesions are malignant fibrous histiocytoma (Figure 13), fibroma, fibrosarcoma, leiomyoma, leiomyosarcoma, angiosarcoma (hemangiosarcoma), rhabdomyoma, rhabdomyosarcoma, synovial sarcoma, synovioma, lymphangiosarcoma, malignant hemangiopericytoma, alveolar soft parts sarcoma, epithelioid sarcoma, and angiosarcoma. Diagnosis of a lesion suspicious for a malignant tumor should never be relied on imaging alone. All suspicious tumors should be biopsied (Figures 14 and 15).

Characteristics of tumor margins

A well-demarcated lesion or a tumor mass with a capsule can favor a benign diagnosis, whereas a less well-demarcated lesion or tumor mass with an infiltrative margin is most likely malignant. Margin characteristics can help precisely identify locally aggressive or non-aggressive behavior for surgical planning, but cannot differentiate benign from malignant lesions[3]. Clinical data always play an important role in evaluating the aggressiveness of tumors.

Characteristics of MRI signals

Fat, fibrous tissue, fluid or cyst, and protein can be characterized by specific signals on MR imaging. Most benign lesions

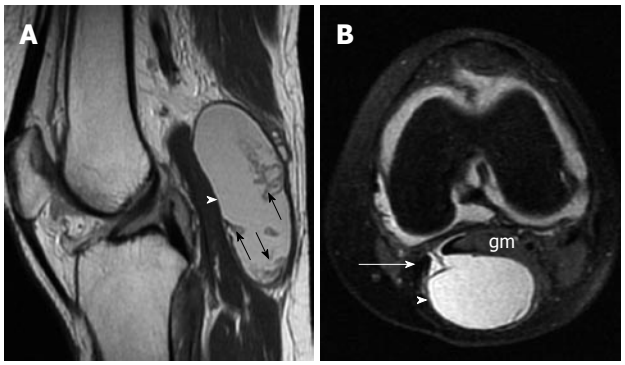

Figure 4 Baker cysts. A: Sagittal proton-density B: Axial gradient-echo images. The left knee shows a well-defined cystic lesion (arrowhead) connected to the knee joint by way of a narrow neck between the semimembranosus tendon (arrow) and the medial head of the gastrocnemius muscle (gm). Note that the Baker cyst contains debris (small arrows in A).

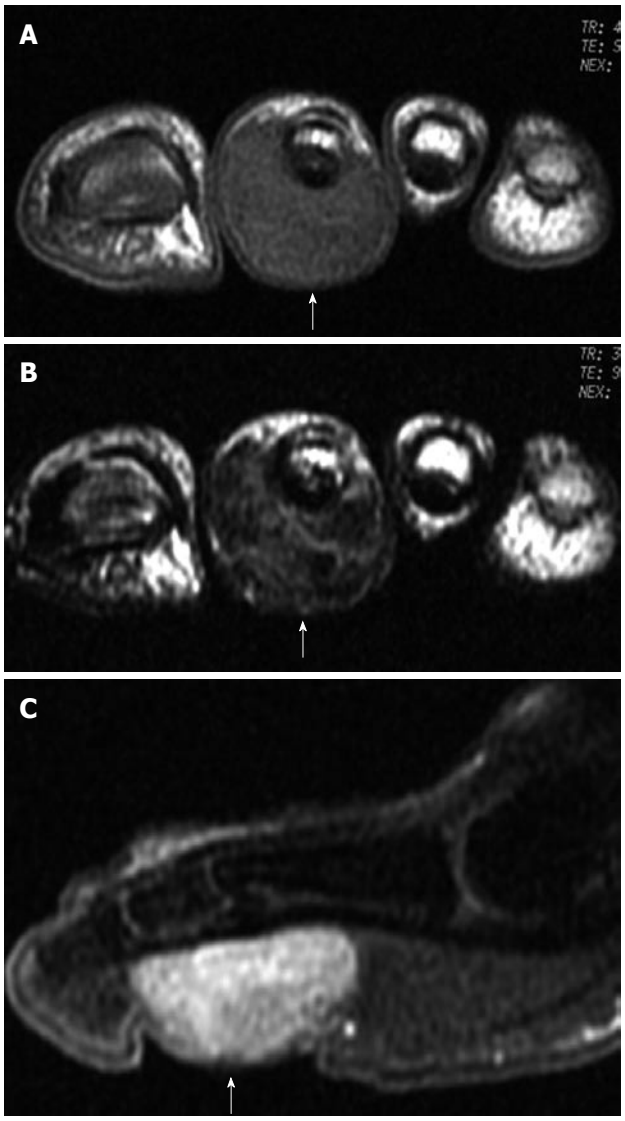

Figure 5 Giant cell tumor of the tendon sheath. A: T1-weighted image shows the tumor (arrow) on the plantar side; B: T2-weighted image shows heterogeneous low signal intensity of the tumor (arrow) due to hemosiderin deposition; C: Sagittal gadolinium-enhanced T1-weighted image with fat saturation shows obvious enhancement of the tumor mass (arrow).

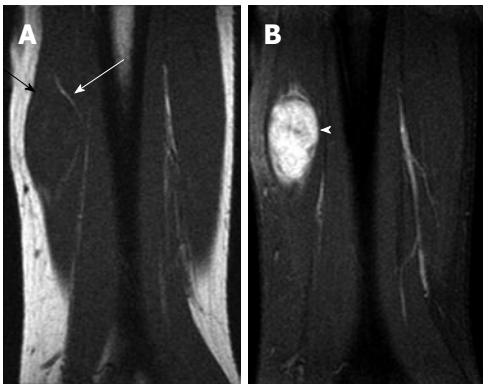

Figure 6 Neurofibroma of the left ulnar nerve (split-fat sign) in a 58-year-old man. A: Coronal T1-weighted image of the left forearm shows a spindle-shaped mass with isointensity relative to adjacent muscle. Note the presence of the split-fat sign (arrows). Because the neurovascular bundle is normally surrounded by fat, masses arising at this site maintain a rim of fat about them as they slowly enlarge; B: Coronal T1-weighted fat-saturated gadolinium-enhanced image shows heterogeneous enhancement of the mass (arrowhead). Recognition of the spindle shape of the tumor and contiguity of the tumor and adjacent nerve may suggest the diagnosis[6].

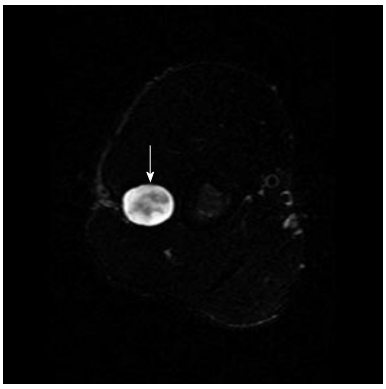

Figure 7 Neurofibroma of the right radial nerve (target sign) in a 35-year-old man. High signal intensity of myxoid Antoni type B (arrow)[6].

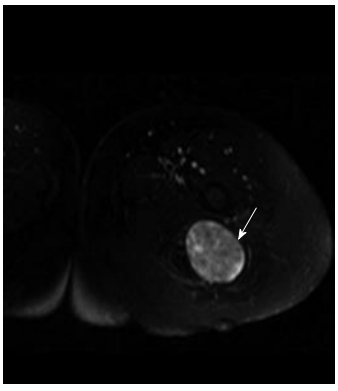

Figure 8 Neurofibroma of the left sciatic nerve (fascicular sign) in a 55-year-old woman. A hyperintense mass (arrow) with multiple small hypointense fascicle-like structures in the mass, representing the "fascicular sign"[6].

have a uniform signal on T1-weighted and T2-weighted images, with the exception, for example, of neurofibromas

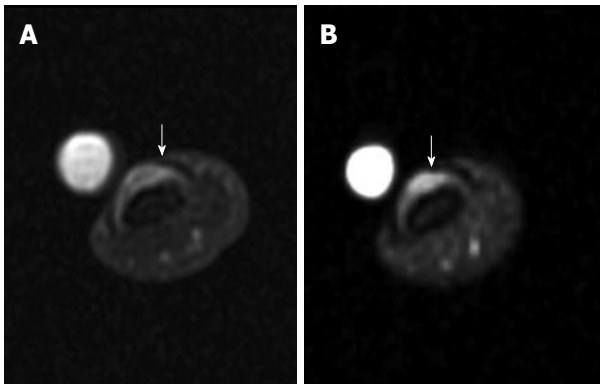

Figure 9 Subungual glomus tumor. A: Axial proton-density-weighted MR image of the left thumb shows a small subungual tumor (arrow); B: Fat-saturated gadolinium-enhanced T1-weighted image shows obvious enhancement of the tumor (arrow). MR: Magnetic resonance.

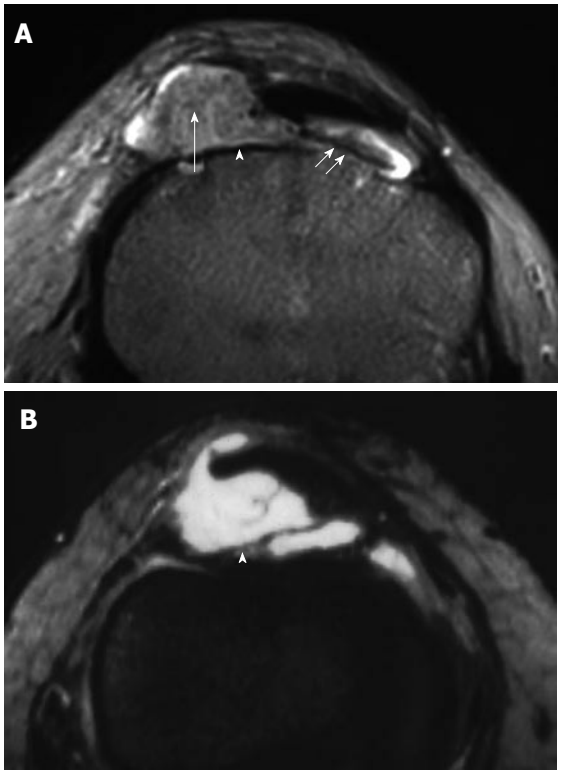

Figure 10 Localized nodular synovitis (solitary PVNS). A: Axial T2-weighted MR image of the knee shows a nodular mass (arrowhead), with a long pedicle (double short arrows) attaching the mass to the adjacent synovium, involving the infrapatellar fat pad. Note small circular foci of low signal intensity (arrow), corresponding to deposition of hemosiderin. B: Gadolinium-enhanced T1-weighted image with fat saturation shows obvious enhancement of the lesion (arrow) caused by capillary proliferation. (Photo courtesy of Dr. Guo-Shu Huang). MR: Magnetic resonance.

and hemangiomas, which exhibit inhomogeneous signals on T2-weighted images. Most malignant tumors can have a uniform signal on T1-weighted images but inhomogeneous signals on T2-weighted images. Although a uniform signal on T2-weighted images can be a reliable indication of a benign lesion, a well-defined mass with homogeneous internal signal intensity does not definitively identify a benign lesion.

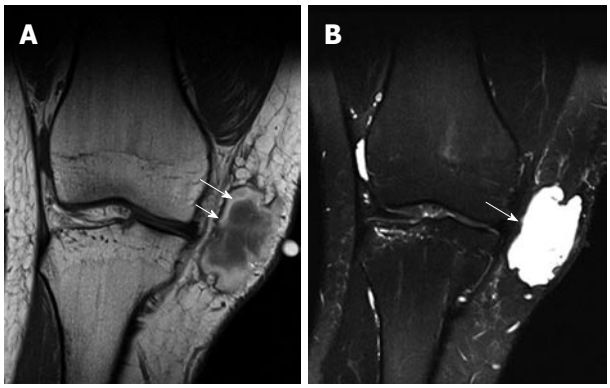

Figure 11 Early subacute hematoma. A: Coronal T1-weighted; B: T2-weighted MR image of the knee. On T1-weighted image, there is a hyperintensity of extracellular methemoglobin at the periphery (long arrow) of the hematoma (which is seen 2-7 d after injury). Note a very thin low-signal-intensity rim at the outermost layer of the hematoma, indicating hemosiderin (short arrow). B: Coronal T2-weighted MR image shows overall hyperintensity of the hematoma (arrow), exception made for a very thin low-signal-intensity peripheral rim caused by hemosiderin.

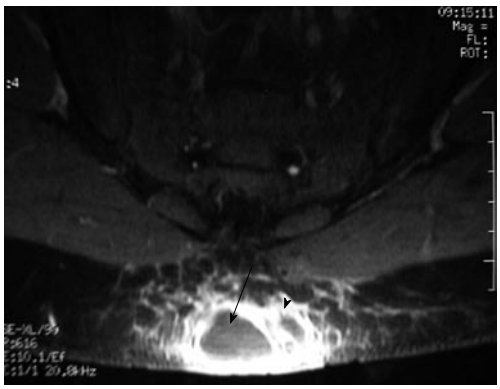

Figure 12 Abscess. Axial gadolinium-enhanced T1-weighted image with fat saturation shows a mass lesion within the subcutaneous fat of the buttock, with a pronounced rim of enhancement (arrowhead), corresponding to large amounts of granulation tissue. The unenhanced central area is a fluid-debris cavity (arrow).

Lack of uniformity does not reliably indicate malignancy[3]. Low-grade liposarcomas (Figure 14) and leiomyosarcoma, for example, are malignant lesions with misleading benign appearances. Soft-tissue lesions arising from trauma (*e.g.*, hematoma) can mimic malignancy.

On dynamic gadolinium-enhanced MR imaging, measurement of relaxation times cannot guide evaluation, as the T1- and T2-relaxation times of benign and malignant lesions overlap significantly[4]. Whether the time-intensity-curve (TIC) shape analysis alone can differentiate malignant from benign soft-tissue tumors, or differentiate between tumor grades, remains controversial[5].

The aim of this illustrative report is to provide a diagnostic guide for soft-tissue tumors of the extremities based on tissue signal and morphological characteristics on MR images. Examples of common determinate lesions are illustrated, except that one indeterminate lesion (malignant fibrous histiocytoma) is shown as an example for com-

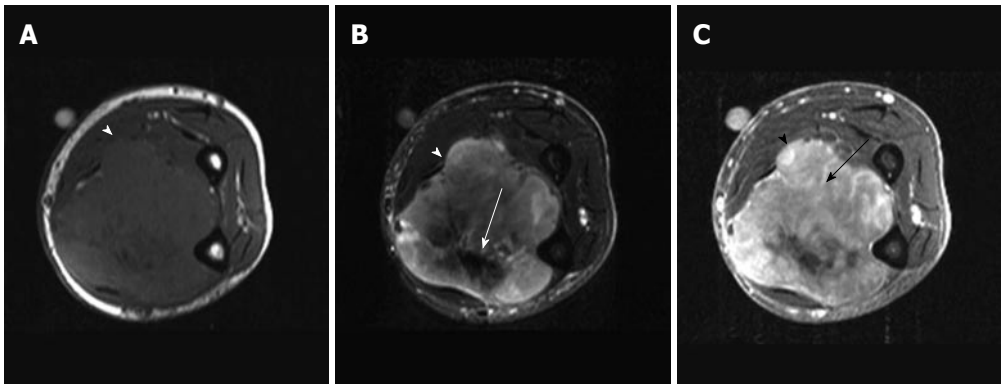

Figure 13 Malignant fibrous histiocytoma. A: Axial T1-weighted MR image of the forearm shows a soft-tissue tumor (arrowhead) with a relatively well-defined margin. No invasion to the adjacent radius or ulna was noted; B: Axial T2-weighted MR image shows heterogeneous signal intensity of the tumor mass (arrowhead), with an area of low signal intensity (arrow), suggesting fibrosis; C: Axial gadolinium-enhanced T1-weighted image with fat saturation shows enhancement of the parenchymal tissue (arrow) of the tumor mass (arrowhead), corresponding to the hypervascular part of the tumor. MR: Magnetic resonance.

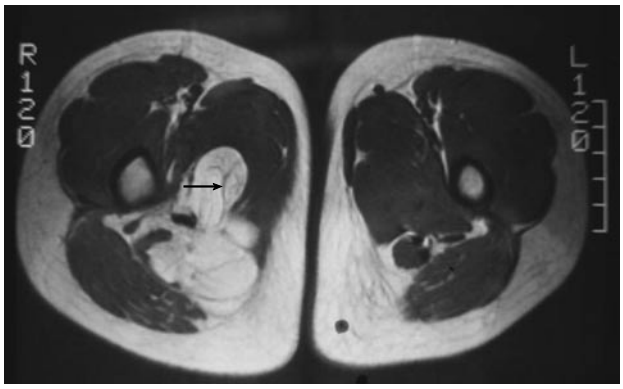

Figure 14 Low-grade liposarcoma. Axial T1-weighted MR image of bilateral thighs shows a lobulated high-signal-intensity mass with uneven or focal thickening septa (arrow) within the tumor on the right thigh, which can be a finding for low-grade liposarcoma. MR: Magnetic resonance.

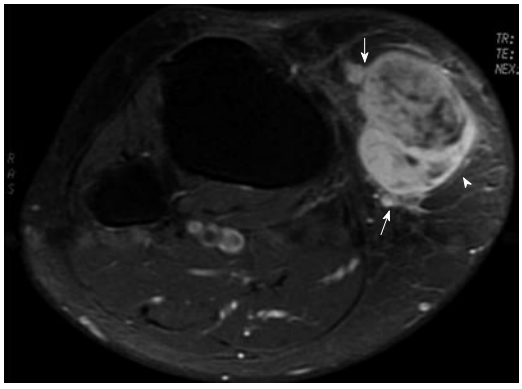

Figure 15 Malignant peripheral nerve sheath tumor involving the subcutis of the right knee in a 65-year-old woman. Tumor mass (arrowhead) is located in the subcutaneous area of the right knee. The mass has an ill-defined margin (arrows) with a fascicular appearance centrally.

parison.

In summary, MR imaging can be helpful in evaluating soft-tissue tumors of the extremities, but it can also be misleading. The combination of signal and morphological characteristics on MR images allows radiologists to categorize many lesions as benign or malignant, although a significant proportion of the images are not specific. It is important for clinicians to be familiar with the imaging characteristics of common determinate lesions. Biopsy is needed to define the histological nature of an indeterminate soft-tissue neoplasm.

REFERENCES

1 **Wu JS**, Hochman MG. Soft-tissue tumors and tumorlike lesions: a systematic imaging approach. *Radiology* 2009; **253**: 297-316 [PMID: 19864525 DOI: 10.1148/radiol.2532081199]
2 **Papp DF**, Khanna AJ, McCarthy EF, Carrino JA, Farber AJ, Frassica FJ. Magnetic resonance imaging of soft-tissue tumors: determinate and indeterminate lesions. *J Bone Joint Surg Am* 2007; **89** Suppl 3: 103-115 [PMID: 17908876 DOI: 10.2106/JBJS.G.00711]
3 **Lang P**, Genant HK, Johnston JO, Honda G. Musculoskeletal neoplasm. In Chan WP, Lang P, Genant HK (eds). MRI of the Musculoskeletal System. Philadelphia: W.B. Saunders, 1994, 401-443
4 **Mirowitz SA**, Totty WG, Lee JK. Characterization of musculoskeletal masses using dynamic Gd-DTPA enhanced spin-echo MRI. *J Comput Assist Tomogr* 1992; **16**: 120-125 [PMID: 1729290]
5 **Lavini C**, Buiter MS, Maas M. Use of dynamic contrast enhanced time intensity curve shape analysis in MRI: theory and practice. *Reports Med Imaging* 2013; **6**: 71-82 [DOI: 10.2147/RMI.S35088]
6 **Li CS**, Huang GS, Wu HD, Chen WT, Shih LS, Lii JM, Duh SJ, Chen RC, Tu HY, Chan WP. Differentiation of soft tissue benign and malignant peripheral nerve sheath tumors with magnetic resonance imaging. *Clin Imaging* 2008; **32**: 121-127 [PMID: 18313576 DOI: 10.1016/j.clinimag.2007.05.006]

P- Reviewers: Nouh MR, Plataniotis G
S- Editor: Qi Y **L- Editor**: Wang TQ **E- Editor**: Liu XM

World Journal of Radiology

Online Submissions: http://www.wjgnet.com/esps/
bpgoffice@wjgnet.com
doi:10.4329/wjr.v5.i12.460

World J Radiol 2013 December 28; 5(12): 460-467
ISSN 1949-8470 (online)

TOPIC HIGHLIGHT

WJR 6th Anniversary Special Issues (7): Positron emission tomography

Fluorodeoxyglucose uptake in absence of CT abnormality on PET-CT: What is it?

Yiyan Liu

Yiyan Liu, Nuclear Medicine Service, Department of Radiology, New Jersey Medical School, Newark, NJ 07103, United States
Author contributions: Liu Y solely contributed to this paper.
Correspondence to: Yiyan Liu, MD, PhD, Nuclear Medicine Service, Department of Radiology, University Hospital, H-141, 150 Bergen Street, Newark, NJ 07103, United States. liuyl@njms.rutgers.edu
Telephone: +1-973-9726022 Fax: +1-973-9726954
Received: September 17, 2013 Revised: October 29, 2013
Accepted: November 18, 2013
Published online: December 28, 2013

Key words: Fluorodeoxyglucose uptake; Positron emission tomography-computer tomography; ARTEF actual uptake; Mis-registration; Positron emission tomography interpretation

Core tip: Abnormal focal uptake without corresponding anatomic abnormality on the integrated computer tomography (CT) imaging poses a dilemma in interpretation of whole-body fluorodeoxyglucose positron emission tomography (PET)-CT imaging. Most of the PET hot spots with the absence of CT lesions or abnormalities are artefactual or secondary to benign etiologies, but some may represent early staged or small sized neoplasm or metastases especially in the gastrointestinal tract and skeletons. Caution should be exercised to simply diagnose a pathology based on the presence of the uptake only, or exclude the disease based on the absence of anatomic abnormality.

Liu Y. Fluorodeoxyglucose uptake in absence of CT abnormality on PET-CT: What is it? *World J Radiol* 2013; 5(12): 460-467 Available from: URL: http://www.wjgnet.com/1949-8470/full/v5/i12/460.htm DOI: http://dx.doi.org/10.4329/wjr.v5.i12.460

Abstract

The purpose of this article is to provide a pictorial review of the findings and interpretative pitfalls about focal fluorodeoxyglucose (FDG) uptake in the absence of corresponding computer tomography (CT) lesion or abnormality on an integrated positron emission tomography (PET)-CT. The integrated CT images in the PET-CT scanner allow correct co-registration and fused imaging of anatomical and functional data. On FDG PET-CT imaging, a real pathologic process often demonstrates abnormal uptake associated with a visible corresponding CT lesion or abnormality. When focal uptake is seen on PET imaging but no corresponding anatomic abnormality is visualized on the integrated CT, one should always be aware of possible mis-registration or mismatch of the PET and CT images due to the patient's respiratory or body motion. While most of the hot spots in the absence of corresponding anatomic abnormalities are artefactual or secondary to benign etiologies, some may represent small sized or early staged neoplasm or metastases, especially in the gastrointestinal tract and skeletons. Caution should be exercised to simply diagnose a pathology based on the presence of the uptake only, or exclude the disease based on the absence of anatomic abnormality.

INTRODUCTION

Today, most of clinical positron emission tomography (PET) scanners are sold as integrated PET-computer tomography (CT) units. The integrated CT data allow correct co-registration and fused imaging of anatomical and functional data. CT scan acquisition (transmission scan) is also used for attenuation correction of positron photon annihilation from radiotracer (^{18}F) fluorodeoxyglucose (FDG). CT imaging in an integrated PET-CT scanner significantly decreases false positive results and improves specificity of the study in PET interpretation[1-3]. The advantage of PET/CT over PET alone can be attributed

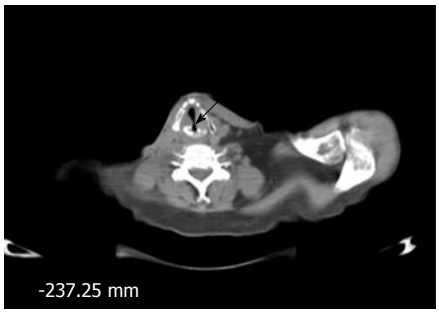

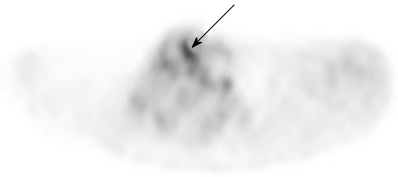

Figure 1 Unilateral vocal cord uptake. A 59-year-old man with history of transglottic squamous cell carcinoma had fluorodeoxyglucose positron emission tomography-computer tomography (PET-CT) for restaging. Axial PET image of the neck shows intense unilateral uptake without a visible lesion on CT in the left true vocal cord (arrows). Subsequent laryngoscopic examination revealed paralysis of the right vocal cord.

to the low anatomic resolution of PET and difficulty in lesion localization on PET[4,5].

Corresponding to abnormal FDG uptake on a whole body FDG PET/CT, a visible lesion or abnormality is often identified on the integrated CT in the same location. This co-registration of anatomic and functional imaging greatly increases confidence of nuclear radiologists in PET interpretation. Sometime, misalignment between PET and CT images may be present, usually resulting from either repositioning of the patient or the time interval between two scans for CT and PET[6]. The misalignment or mis-registration of PET and CT images is often noted in the lower thorax and upper abdomen, because of changes of organ positions during different breathing cycles between CT and PET acquisitions[7]. In general, this kind of PET/CT misalignment artifact can be solved without many difficulties in interpretation by checking adjacent upper and lower levels of the CT or PET slices when a FDG focus or CT lesion is identified.

It is not uncommon that markedly abnormal focal uptake is noted on FDG PET but no anatomic counterpart is visualized on the CT, which is bizarre and poses a dilemma in interpretation about the nature of uptake. Focal pattern and increased intensity of uptake can not be simply ignored or considered as an artifact in these cases. On the other hand, a diagnosis of the pathologic finding cannot be made with a lack of corresponding CT abnormality. What is this kind of hot spot? In this paper, we outline some common locations of abnormal focal uptake with the absence of corresponding CT finding on a whole body FDG PET-CT imaging. We also briefly discuss the interpretative pitfalls.

MOST COMMONLY SEEN FOCAL FLUORODEOXYGLUCOSE UPTAKE WITHOUT COMPUTER TOMOGRAPHY ABNORMALITY

Vocal cord uptake

Physiologic uptake in the vocal cords is mostly seen as symmetric. In some patients with known primary or metastatic malignancy of the head and neck, focal intense uptake may be noted in the unilateral true vocal cord, with no lesion or abnormality on CT images. In general, this uptake is secondary to the increased compensatory metabolic activity of the muscle in a normal true vocal cord responsible for the contralateral vocal cord paralysis as a result of damage or palsy of the recurrent laryngeal nerve (Figure 1). Lee *et al*[8] reported that all 15 patients with one-sided vocal cord uptake on FDG-PET had contralateral vocal cord paralysis on laryngoscopic examination. Therefore, when asymmetric intense uptake is seen in the unilateral vocal cord and no discrete lesion is appreciated on CT, clinical correlation including laryngoscopic examination is helpful to verify the nature of uptake.

Iatrogenic uptake in the lung

Unlike other tissues or organs, normal lung parenchyma does not demonstrate notable FDG uptake on PET. Sometimes mild vague uptake may be noted in the vascular structures of the lungs. Evident FDG uptake in the lungs is always associated with abnormalities on CT, for example, nodule or mass, opacity or density, infiltrate, consolidation, *etc*. Abnormal uptake in the lung bases with no lung abnormality on CT may actually represent a lesion in the upper abdomen, for example the liver or spleen, because of mis-registration of PET and CT images secondary to the patient's respiratory motion. But a real focus may be identified in any area of the lung without a visible corresponding abnormality on lung window of the CT (Figure 2).

There are a few case reports in recent years about iatrogenic focal FDG accumulation in lung parenchyma without abnormal CT findings[9-12]. Observed foci in the lung parenchyma were in different areas with variable intensity of uptake, but they were typically peripheral in the location and very intense in uptake. A common characteristic in the most cases was partial paravenous injection of the radiotracer. A possible and the most likely explanation for these iatrogenic foci in the lungs could be micro-emboli secondary to paravenous injection. The damage to the vein endothelium during paravenous injection causes the formation of blood clots at the site of injury, which in turn detach from the vein, enter the small pulmonary vasculature and are seen as hot spots in the distal lung.

Axillary uptake

Although less reported, it is relatively common that small ipsilateral axillary lymph nodes, draining the region of tracer extravasation in the antecubital injection, demonstrate significant uptake on FDG-PET due to extravasa-

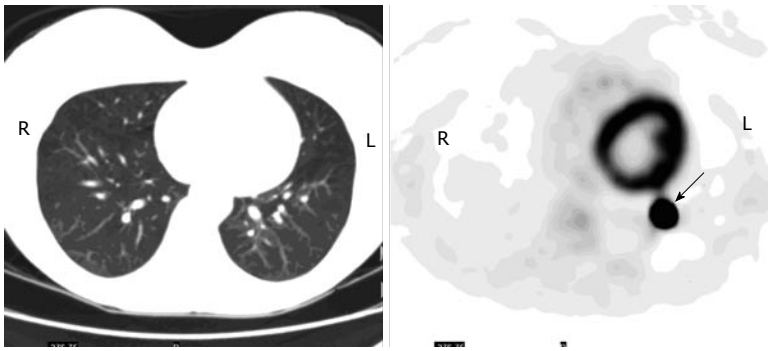

Figure 2 Iatrogenic uptake in the lung. A 35-year-old woman with history of low grade serous ovarian cancer had fluorodeoxyglucose positron emission tomography-computer tomography (PET-CT) for initial staging. Axial PET image of the lungs shows a focus of intense uptake in the left lower lobe (arrow), but no nodule or lesion is seen on CT. Subsequent diagnostic CT was negative as well for lung nodule. The uptake is likely secondary to microembolism due to a paravenous injection.

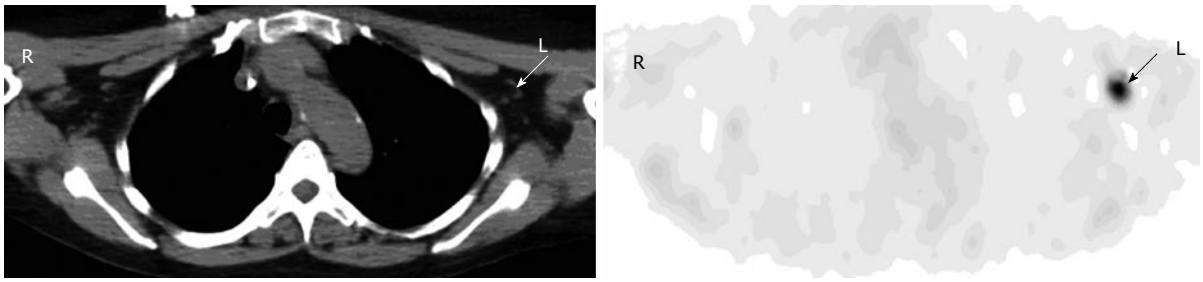

Figure 3 Axillary uptake. A 63-year-old man with history of bladder cancer had fluorodeoxyglucose (FDG) positron emission tomography-computer tomography (PET-CT) for restaging. Axial PET image of the upper chest shows focal uptake in the left axilla (arrow). Corresponding to this focus, there is a small benign lymph node with fat lumen on CT (arrow). The uptake is secondary to infiltration of injected FDG at the antecubital site.

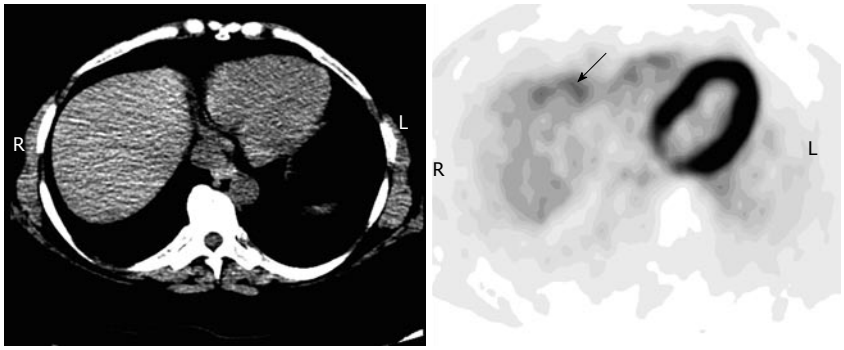

Figure 4 Noise artifact in the liver. A 42-year-old man with history of cervical cancer had fluorodeoxyglucose positron emission tomography-computer tomography (PET-CT) for initial staging. Axial PET image of the upper abdomen shows irregular uptake in the anterior margin (arrow) but without discrete lesions on an integrated CT, representing noise artifacts. Subsequent diagnostic CT was negative.

tion or partial subcutaneous injection[13]. The findings between PET and CT images are often discordant in the ipsilateral axilla following an infiltrated injection: small or no lymph node on CT, but intense uptake on PET (Figure 3). An interpretation of lymphadenopathy, especially metastasis, should be avoided in this situation when an infiltrated injection is present in the ipsilateral arm. In the most cases, the artefactual axillary lymph node uptake can be identified when linear superficial uptake in the ipsilateral arm is seen from the injection site to the axilla. To avoid confusion in interpretation of PET imaging for the breast, lung or chest wall lesion, the radiotracer should be always administered at the contralateral arm.

Noise uptake in the liver

Normal uptake of the liver is often inhomogeneous because of a relatively high and variable glucose-6-phosphatase activity. In our experience, so-called "noise artifact" in the liver on FDG-PET is not uncommon in a whole body imaging. Typically, this kind of noise artifact is displayed as ill defined, mildly increased uptake on PET without anatomic abnormality on CT (Figure 4). However, sometimes a discrete focus without corresponding CT abnormality may also represent the noise artifact in the liver. When a discrete focus is seen in the liver with the absence of a lesion on CT imaging of integrated PET/CT, a diagnosis can not be made about hepatic pathology; on the other hand, caution should also be exercised to exclude a lesion based on a negative finding on an integrated CT imaging only, because small hepatic lesions are often not well appreciated on the low dose, non-contrast CT. A diagnostic CT or magnetic resonance imaging (MRI) is necessary for correlation.

Increased hepatic uptake may be also seen on the anteromedial or posteromedial margin of the liver and adjacent to the hepatic flexure colon. If there is no corresponding hepatic lesion is identified on the CT, the uptake may represent colonic activity especially when the uptake is linear (Figure 5). Mal-location of the bowel uptake is due to patient's motion or respiratory effect. The coronal

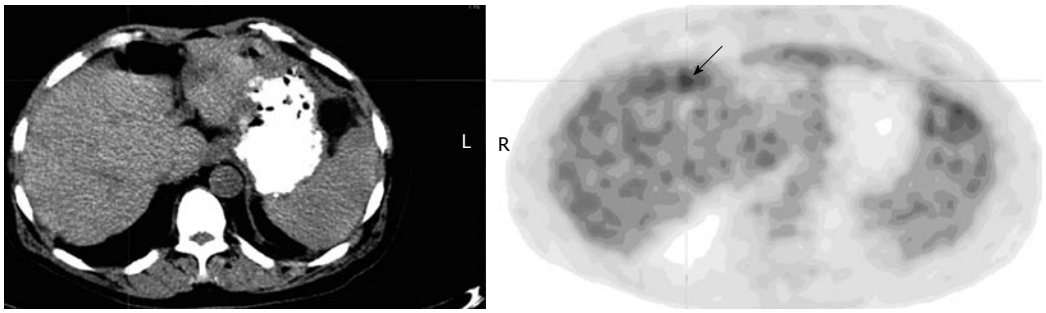

Figure 5 Colonic uptake abutting the margin of the liver. A 59-year-old man with newly diagnosed pancreatic cancer had fluorodeoxyglucose positron emission tomography-computer tomography (PET-CT) for staging. Axial PET image of the upper abdomen shows a small focus of increased uptake abutting the anterior margin of the liver (arrow). But there is no visible hepatic lesion on the integrated CT. A magnetic resonance imaging was also negative for any lesion in the liver. The uptake is from the adjacent transverse colon with slight motion artifact and mis-registration of PET and CT images.

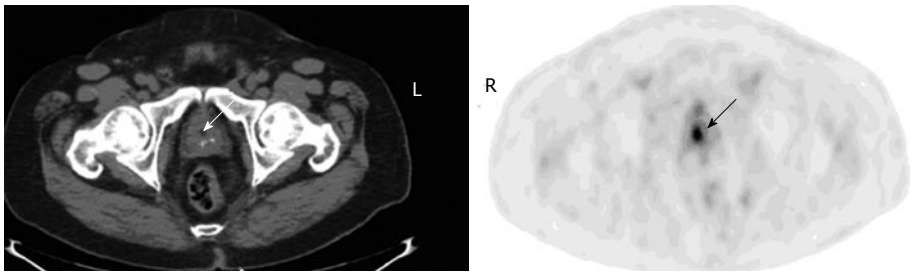

Figure 6 Urine activity in the prostatic urethra. A 65-year-old man with history of lung cancer had fluorodeoxyglucose positron emission tomography-computer tomography (PET-CT) for restaging. Axial PET image of the lower pelvis shows a focus at the midline of the prostate, corresponding to the dilated urethra on CT (arrows). The finding represents urine retention in the urethra of previous trans-urethral prostate resection site.

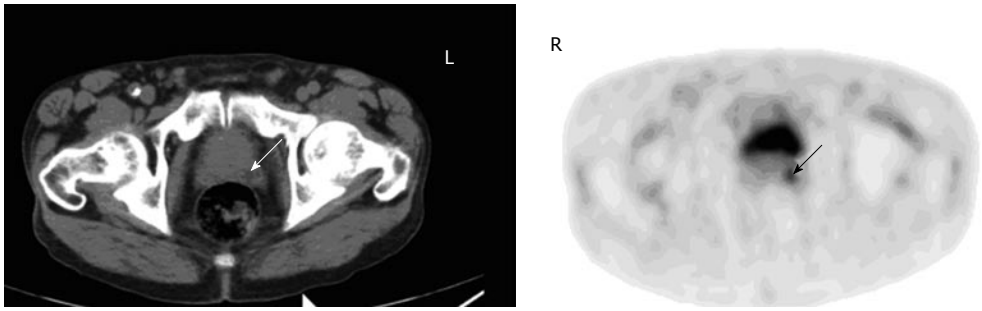

Figure 7 Uptake of prostate cancer. A 63-year-old man with history of laryngeal cancer had fluorodeoxyglucose positron emission tomography-computer tomography (PET-CT) for restaging Axial PET image of the lower pelvis shows a focus corresponding to a hypodensity lesion on the CT in the left peripheral prostate (arrows). Biopsy confirmed prostate cancer.

and sagittal views are helpful to confirm the findings.

Focal urine activity

Focal urine activity in the ureter is easily identified by identifying the ureter on the integrated CT. Although some authors recommended re-acquisition following furosemide administration[14,15], it is not necessary in our experience. A focus in the urethra is more challenging in interpretation, especially in the prostatic urethra. For patients with prior trans-urethral resection of prostate, a focus is often seen in the dilated prostatic urethra, representing urine activity (Figure 6). If a focus is noted inferior to the urinary bladder and at the midline of the prostate, and no corresponding lesion is identified on CT, it is most likely urine activity as well, even though low density urine can not be seen on CT. In contrast, a real prostate lesion is often seen as either calcified or low density area with focal uptake in the peripheral prostate, rather than at the midline and location of the prostatic urethra (Figure 7).

Atypical brown fat or muscle uptake

Brown fat uptake is well known on FDG-PET, and is easily identified in well-defined patterns in the most cases. The most common location for brown fat is the neck and supraclavicular area, which is usually bilateral, linear or curvilinear[16-18]. Focal uptake of brown fat is often seen in the mediastinum, axillae, paravertebral areas and intercostals spaces[17,18]. However, brown fat uptake may be encountered anywhere as a focus or separate foci[19]. When focal uptake is seen on PET corresponding to "dark" low

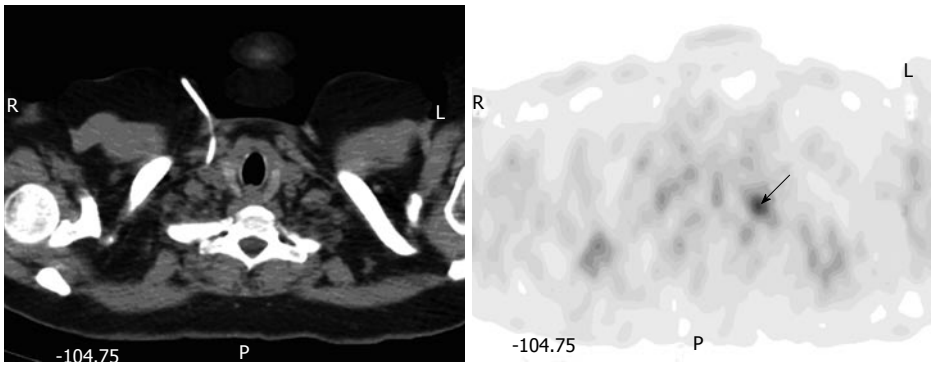

Figure 8 Focal brown fat uptake. A 50-year-old woman with history of metastatic breast cancer had fluorodeoxyglucose positron emission tomography-computer tomography (PET-CT) for restaging. Axial PET image shows a focus in the left supraclavicular region (arrow). On the integrated CT, there is no node or lesion except for fat tissue in this location. The uptake is from the brown fat.

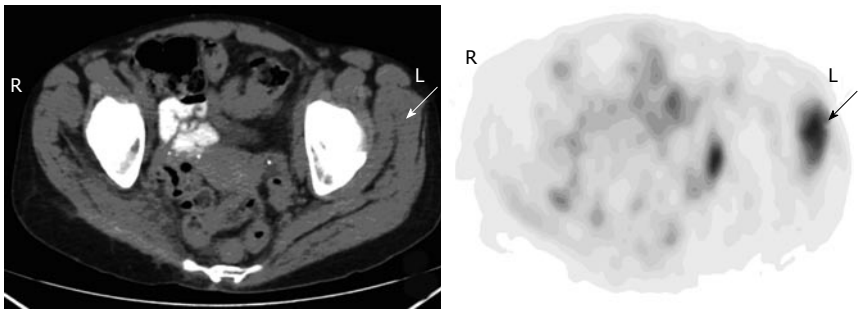

Figure 9 Muscular uptake. A 45-year-old woman with history of leiomyosarcoma had fluorodeoxyglucose positron emission tomography-computer tomography (PET-CT) for restaging. Axial PET-CT images of the pelvis show intense focal muscular uptake in the left gluteus maximus, gluteus minimus and obturator intermus, with no corresponding lesions on the CT (arrows). Two subsequent magnetic resonance images were unremarkable of the muscles.

density rather than soft tissue on the integrated CT, it represents brown fat (Figure 8). HU measurement can be confirmative, fat tissue usually ranges -50 to -150 HU. A pitfall to identify brown fat uptake is to be aware of motion artifact or mismatch of PET and CT images. When a focus of uptake corresponds to low density fat on CT, it is always a good practice to carefully check the adjacent structures or tissues and exclude a real lesion on the CT images.

Muscular uptake is often seen in anxious patients or due to stress induced muscle tension or secondary to motion after the FDG injection. Usually benign muscular uptake can be distinguished from malignant or metastatic disease due to its mostly symmetric pattern that matches the anatomy of the muscular groups, and the absence of a lesion on the integrated CT images. However, focal intense muscular uptake may be also seen with no corresponding CT lesion or abnormality (Figure 9). Whereas the uptake is mostly benign, further correlation with a MRI may be necessary because of limited value of the integrated CT for muscular pathology.

Real lesion not seen on CT

Focal FDG uptake without a visible corresponding lesion on CT does not always indicate benign nature or an artifact. Caution should be exercised in some structures or tissues for example the gastrointestinal tract. The pattern rather than the intensity of uptake is more important in interpretation of the gastrointestinal tract. Physiologic or inflammatory uptake of the gastrointestinal tract is often diffuse and linear. Focal increased uptake may be frequently seen and mostly benign in some areas such as the gastroesophageal junction (Figure 10), the gastric wall, the rectal ampulla or the anal canal[20]. Less commonly seen focal uptake without a lesion on CT in the colon is most likely benign in nature as well, but a neoplasm should be excluded with colonoscopy since a small or superficial lesion may be not well appreciated on CT. Compared to that in the stomach and colon, focal uptake in the esophagus more likely represents a neoplastic process because physiologic esophageal uptake is very mild and linear, even though the integrated or diagnostic CT does not demonstrate discrete lesion or wall thickening (Figure 11). Endoscopic examination and biopsy may be warranted to diagnose or exclude an esophageal lesion if a discrete focus is noted on the esophageal wall. The false negative CT may be resulted from a small size of the tumor, lack of a discrete mass or mass effect and suboptimal sensitivity of CT for esophageal pathology due to poor distensibility of the esophagus[21].

Focal osseous uptake is often seen on PET imaging with the absence of CT abnormality on bone window. Although a sclerotic or lytic bone lesion demonstrating abnormal FDG uptake is almost certainly diagnosed as a neoplasm or metastasis in an oncologic patient, focal uptake without a visible lesion on the integrated CT is potentially problematic in PET interpretation. Taira *et al*[22] reported that discordant findings between the PET and CT occurred in more than half of the bone lesions. While a CT noted osseous lesion lacking FDG uptake is most likely a benign or treated disease, abnormal osseous uptake with the absence of a lesion on CT more likely represents a metastasis[22,23]. When the examinations are discordant, PET is far more accurate than CT in the characterization of bone lesions[22,24]. In our experience, mild vague uptake may be secondary to some benign etiologies for example degenerative disease, but significant focal uptake in the bone is highly suspicious for metastatic disease in a patient with known malignancy even though the CT is negative (Figure 12). In addition, positive pre-

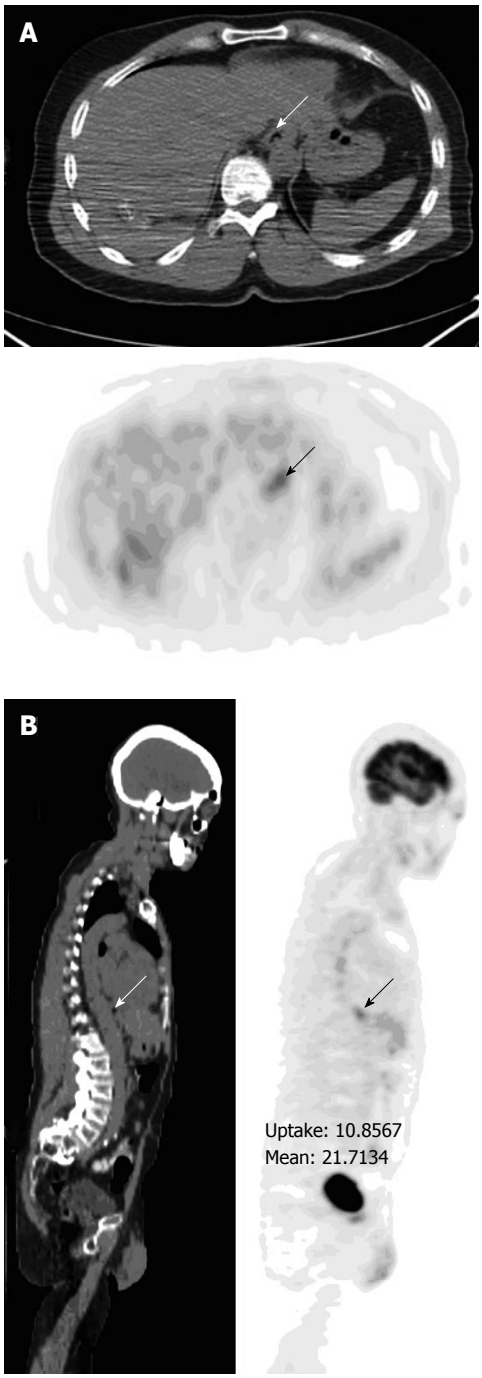

Figure 10 Prominent uptake in the gastroesophageal junction. A 57-year-old man with history of osteosarcoma had fluorodeoxyglucose positron emission tomography-computer tomography (PET-CT) for initial staging. Axial (A) and sagittal (B) PET-CT images show focal uptake in the gastroesophageal junction (arrows), with no lesion on CT and stable over two years on follow-ups.

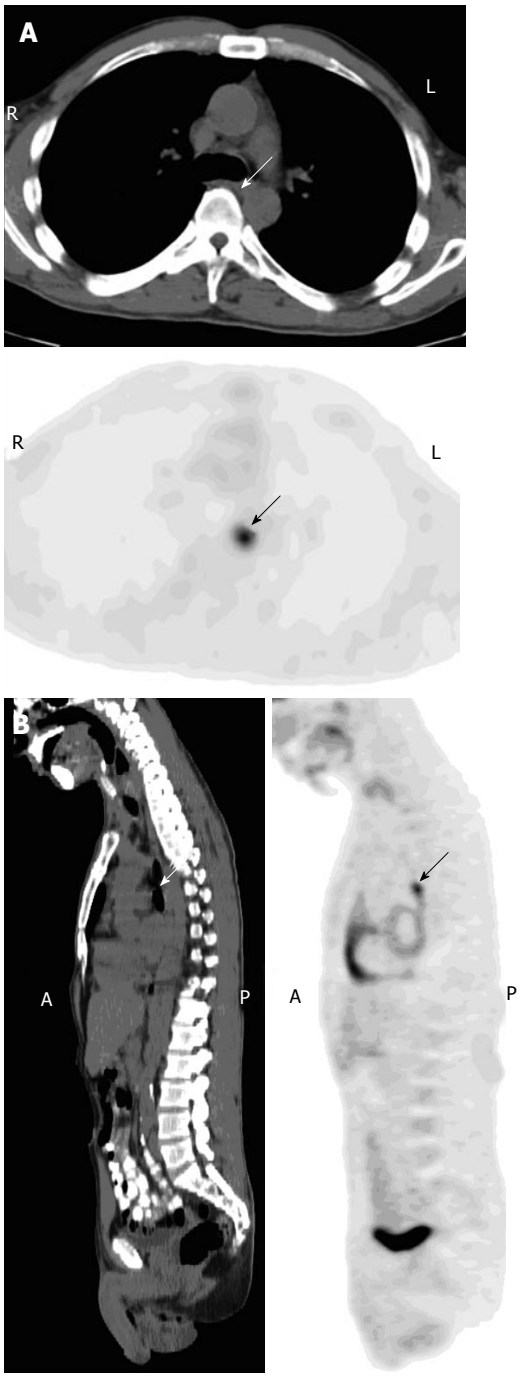

Figure 11 Uptake representing esophageal cancer. A 49-year-old man with history of retromolar carcinoma had fluorodeoxyglucose positron emission tomography-computer tomography (PET-CT) for restaging. Axial (A) and sagittal (B) PET-CT images show a focus in the mid esophagus at the subcarinal level (arrows), without a visible lesion or evident wall thickening on the integrated CT. Subsequent contrast CT was negative as well. An endoscopic biopsy revealed squamous cell carcinoma.

dictive value is significantly greater when multiple foci are seen in the bones compared to one solitary focus. It is not uncommon that in the cases with multiple osseous metastases, many foci of uptake have no discrete lesions on the integrated CT, because the metabolic change often precedes the anatomic change.

In lymphomatous disease of the bones, PET and CT findings may be discordant: intense FDG uptake but without significant CT abnormality on bone window (Figure 13). On CT, Bone lymphoma often demonstrates a permeative pattern with periosteal reaction, sequestra and absence of cortical destruction[25,26]. Therefore, early lymphomatous bone involvement or small bone lesions without marked bone destruction may only be visualized as increased FDG uptake on PET imaging only. In disseminated lymphomatous disease, FDG PET often

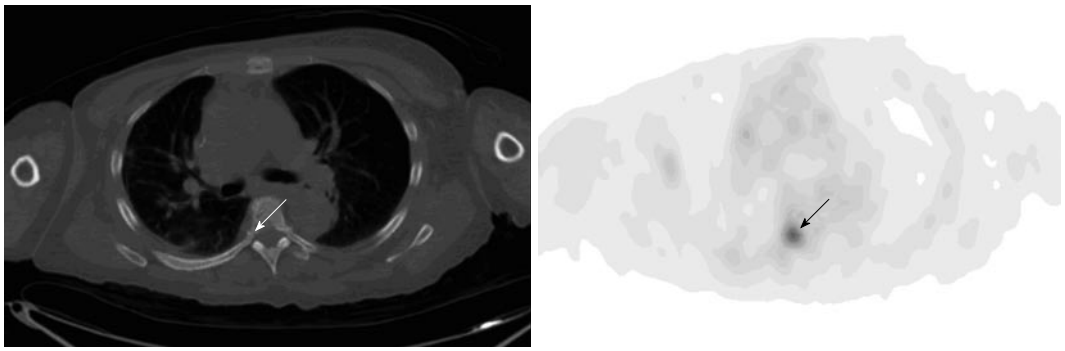

Figure 12 Osseous uptake. A 55-year-old woman with history of metastatic breast cancer had fluorodeoxyglucose positron emission tomography-computer tomography (PET-CT) for restaging. Axial PET image of the chest shows focal uptake at the right pedicle of the T6 (arrow). There is no visible corresponding bone lesion on the integrated CT (arrow). Repeat PET-CT three months after shows multiple bone metastases including worsening uptake in the right-sided T6.

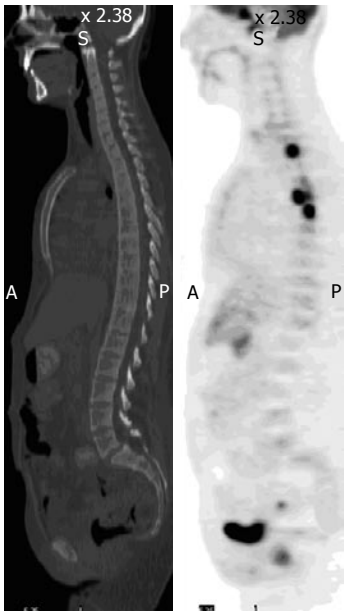

Figure 13 Lymphomatous disease of bone. A 28-year-old man with disseminated B-cell lymphoma had fluorodeoxyglucose positron emission tomography-computer tomography (PET-CT) for initial staging. Sagittal PET image shows foci of intense uptake in the vertebral bodies of the upper thoracic spine, but the CT is unremarkable in the corresponding sites. Repeated scan 3 mo after chemotherapy demonstrate resolution of uptake in the bones as well as lungs and lymph nodes.

reveals more osseous lesions than CT imaging.

CONCLUSION

On FDG PET-CT imaging, a real pathologic process often demonstrates abnormal uptake associated with a visible corresponding CT lesion or abnormality. It is a dilemma of interpretation that evident focal uptake is seen on PET but without corresponding anatomic abnormality on CT. Before exploring the nature of abnormal uptake, one should always be aware of possible misregistration or mismatch of the PET and CT images due to patient's respiratory or body motion. Most of the PET hot spots with the absence of CT lesions or abnormalities are artefactual or secondary to benign etiologies, but some may represent early staged or small sized neoplasm or metastases especially in the gastrointestinal tract and skeletons. Because of poor resolution of the low dose, non-contrast integrated CT imaging in some organ or tissue such as the liver, a diagnostic anatomic imaging is often necessary for further evaluation of abnormal uptake.

REFERENCES

1 **Antoch G**, Saoudi N, Kuehl H, Dahmen G, Mueller SP, Beyer T, Bockisch A, Debatin JF, Freudenberg LS. Accuracy of whole-body dual-modality fluorine-18-2-fluoro-2-deoxy-D-glucose positron emission tomography and computed tomography (FDG-PET/CT) for tumor staging in solid tumors: comparison with CT and PET. *J Clin Oncol* 2004; **22**: 4357-4368 [PMID: 15514377 DOI: 10.1200/JCO.2004.08.120]

2 **Pelosi E**, Messa C, Sironi S, Picchio M, Landoni C, Bettinardi V, Gianolli L, Del Maschio A, Gilardi MC, Fazio F. Value of integrated PET/CT for lesion localisation in cancer patients: a comparative study. *Eur J Nucl Med Mol Imaging* 2004; **31**: 932-939 [PMID: 14991245 DOI: 10.1007/s00259-004-1483-3]

3 **Reinartz P**, Wieres FJ, Schneider W, Schur A, Buell U. Side-by-side reading of PET and CT scans in oncology: which patients might profit from integrated PET/CT? *Eur J Nucl Med Mol Imaging* 2004; **31**: 1456-1461 [PMID: 15248033 DOI: 10.1007/s00259-004-1593-y]

4 **Metser U**, Miller E, Lerman H, Even-Sapir E. Benign non-physiologic lesions with increased 18F-FDG uptake on PET/CT: characterization and incidence. *AJR Am J Roentgenol* 2007; **189**: 1203-1210 [PMID: 17954662 DOI: 10.2214/AJR.07.2083]

5 **Gorospe L**, Raman S, Echeveste J, Avril N, Herrero Y, Herna Ndez S. Whole-body PET/CT: spectrum of physiological variants, artifacts and interpretative pitfalls in cancer patients. *Nucl Med Commun* 2005; **26**: 671-687 [PMID: 16000985 DOI: 10.1097/01.mnm.0000171779.65284.eb]

6 **Cohade C**, Wahl RL. Applications of positron emission tomography/computed tomography image fusion in clinical positron emission tomography-clinical use, interpretation methods, diagnostic improvements. *Semin Nucl Med* 2003; **33**: 228-237 [PMID: 12931324 DOI: 10.1053/snuc.2003.127312]

7 **Wang X**, Koch S. Positron emission tomography/computed tomography potential pitfalls and artifacts. *Curr Probl Diagn Radiol* 2009; **38**: 156-169 [PMID: 19464586 DOI: 10.1067/j.cpradiol.2008.01.001]

8 **Lee M**, Ramaswamy MR, Lilien DL, Nathan CO. Unilateral vocal cord paralysis causes contralateral false-positive positron emission tomography scans of the larynx. *Ann Otol Rhinol Laryngol* 2005; **114**: 202-206 [PMID: 15825569]

9 **Hany TF**, Heuberger J, von Schulthess GK. Iatrogenic FDG foci in the lungs: a pitfall of PET image interpretation. *Eur*

Radiol 2003; **13**: 2122-2127 [PMID: 12928963 DOI: 10.1007/s00330-002-1681-y]
10 **Farsad M**, Ambrosini V, Nanni C, Castellucci P, Boschi S, Rubello D, Fabbri M, Franchi R, Fanti S. Focal lung uptake of 18F-fluorodeoxyglucose (18F-FDG) without computed tomography findings. *Nucl Med Commun* 2005; **26**: 827-830 [PMID: 16096587 DOI: 10.1097/01.mnm.0000175786.27423.42]
11 **Karantanis D**, Subramaniam RM, Mullan BP, Peller PJ, Wiseman GA. Focal F-18 fluoro-deoxy-glucose accumulation in the lung parenchyma in the absence of CT abnormality in PET/CT. *J Comput Assist Tomogr* 2007; **31**: 800-805 [PMID: 17895795 DOI: 10.1097/RCT.0b013e3180340376]
12 **Ha JM**, Jeong SY, Seo YS, Kwon SY, Chong A, Oh JR, Song HC, Bom HS, Min JJ. Incidental focal F-18 FDG accumulation in lung parenchyma without abnormal CT findings. *Ann Nucl Med* 2009; **23**: 599-603 [PMID: 19452248 DOI: 10.1007/s12149-009-0262-4]
13 **Alibazoglu H**, Megremis D, Ali A, LaMonica G. Injection artifact on FDG PET imaging. *Clin Nucl Med* 1998; **23**: 264-265 [PMID: 9554212 DOI: 10.1097/00003072-199804000-00026]
14 **López-Gandul S**, Pérez-Moure G, García-Garzón JR, Soler-Peter M, Simó-Perdigó M, Lomeña F. Intravenous furosemide injection during 18F-FDG PET acquisition. *J Nucl Med Technol* 2006; **34**: 228-231 [PMID: 17146112]
15 **Kamel EM**, Jichlinski P, Prior JO, Meuwly JY, Delaloye JF, Vaucher L, Malterre J, Castaldo S, Leisinger HJ, Delaloye AB. Forced diuresis improves the diagnostic accuracy of 18F-FDG PET in abdominopelvic malignancies. *J Nucl Med* 2006; **47**: 1803-1807 [PMID: 17079813]
16 **Rosenbaum SJ**, Lind T, Antoch G, Bockisch A. False-positive FDG PET uptake--the role of PET/CT. *Eur Radiol* 2006; **16**: 1054-1065 [PMID: 16365730 DOI: 10.1007/s00330-005-0088-y]
17 **Yeung HW**, Grewal RK, Gonen M, Schöder H, Larson SM. Patterns of (18)F-FDG uptake in adipose tissue and muscle: a potential source of false-positives for PET. *J Nucl Med* 2003; **44**: 1789-1796 [PMID: 14602861]
18 **Nedergaard J**, Bengtsson T, Cannon B. Unexpected evidence for active brown adipose tissue in adult humans. *Am J Physiol Endocrinol Metab* 2007; **293**: E444-E452 [PMID: 17473055 DOI: 10.1152/ajpendo.00691.2006]
19 **Paidisetty S**, Blodgett TM. Brown fat: atypical locations and appearances encountered in PET/CT. *AJR Am J Roentgenol* 2009; **193**: 359-366 [PMID: 19620432 DOI: 10.2214/AJR.08.2081]
20 **Heusner TA**, Hahn S, Hamami ME, Kim UH, Baumeister R, Forsting M, Stahl A, Bockisch A, Antoch G. Gastrointestinal 18F-FDG accumulation on PET without a corresponding CT abnormality is not an early indicator of cancer development. *Eur Radiol* 2009; **19**: 2171-2179 [PMID: 19415294 DOI: 10.1007/s00330-009-1405-7]
21 **Ba-Ssalamah A**, Zacherl J, Noebauer-Huhmann IM, Uffmann M, Matzek WK, Pinker K, Herold C, Schima W. Dedicated multi-detector CT of the esophagus: spectrum of diseases. *Abdom Imaging* 2009; **34**: 3-18 [PMID: 17653787 DOI: 10.1007/s00261-007-9290-5]
22 **Taira AV**, Herfkens RJ, Gambhir SS, Quon A. Detection of bone metastases: assessment of integrated FDG PET/CT imaging. *Radiology* 2007; **243**: 204-211 [PMID: 17392254 DOI: 10.1148/radiol.2431052104]
23 **Nakamoto Y**, Cohade C, Tatsumi M, Hammoud D, Wahl RL. CT appearance of bone metastases detected with FDG PET as part of the same PET/CT examination. *Radiology* 2005; **237**: 627-634 [PMID: 16244271 DOI: 10.1148/radiol.2372031994]
24 **Liu NB**, Zhu L, Li MH, Sun XR, Hu M, Huo ZW, Xu WG, Yu JM. Diagnostic value of 18F-FDG PET/CT in comparison to bone scintigraphy, CT and 18F-FDG PET for the detection of bone metastasis. *Asian Pac J Cancer Prev* 2013; **14**: 3647-3652 [PMID: 23886160]
25 **Ilica AT**, Kocacelebi K, Savas R, Ayan A. Imaging of extranodal lymphoma with PET/CT. *Clin Nucl Med* 2011; **36**: e127-e138 [PMID: 21892025 DOI: 10.1097/RLU.0b013e31821c99cd]
26 **Kim SH**, Smith SE, Mulligan ME. Hematopoietic tumors and metastases involving bone. *Radiol Clin North Am* 2011; **49**: 1163-183, vi [PMID: 22024293 DOI: 10.1016/j.rcl.2011.07.004]

P- Reviewers: Bartalena T, Seo JB **S- Editor**: Zhai HH
L- Editor: A **E- Editor**: Liu SQ

World Journal of Radiology

Online Submissions: http://www.wjgnet.com/esps/
bpgoffice@wjgnet.com
doi:10.4329/wjr.v5.i12.468

World J Radiol 2013 December 28; 5(12): 468-471
ISSN 1949-8470 (online)

MINIREVIEWS

Nano/microparticles and ultrasound contrast agents

Shu-Guang Zheng, Hui-Xiong Xu, Hang-Rong Chen

Shu-Guang Zheng, Hui-Xiong Xu, Department of Medical Ultrasound, Shanghai Tenth People's Hospital, Tenth People's Hospital of Tongji University, Shanghai 200072, China
Hang-Rong Chen, State Key Laboratory of High Performance Ceramic and Superfine Microstructures, Shanghai Institute of Ceramic Chinese Academy of Science, Shanghai 200050, China
Author contributions: Zheng SG, Xu HX and Chen HR conducted the literature research; Zheng SG wrote the paper; Xu HX edited and revised the paper.
Supported by National Natural Science Foundation of China, No. 81371570; Key Project from Shanghai Health Bureau, No. 20114003; Shanghai Talent Development Project from Shanghai Human Resource and Social Security Bureau, No. 2012045
Correspondence to: Hui-Xiong Xu, MD, PhD, Department of Medical Ultrasound, Shanghai Tenth People's Hospital, Tenth People's Hospital of Tongji University, No. 301 Yanchangzhong Road, Shanghai 200072, China. xuhuixiong@hotmail.com
Telephone: +86-21-66301031 Fax: +86-21-66301031
Received: July 17, 2013 Revised: October 31, 2013
Accepted: November 15, 2013
Published online: December 28, 2013

Abstract

Microbubbles have been used for many years now in clinical practice as contrast agents in ultrasound imaging. Recently, their therapeutic applications have also attracted more attention. However, the short circulation time (minutes) and relatively large size (two to ten micrometers) of currently used commercial microbubbles do not allow effective extravasation into tumor tissue, preventing efficient tumor targeting. Fortunately, more multifunctional and theranostic nanoparticles with some special advantages over the traditional microbubbles have been widely investigated and explored for biomedical applications. The way to synthesize an ideal ultrasound contrast agent based on nanoparticles in order to achieve an expected effect on contrast imaging is a key technique. Currently a number of nanomaterials, including liposomes, polymers, micelles, dendrimers, emulsions, quantum dots, solid nanoparticles *etc.*, have already been applied to pre or clinical trials. Multifunctional and theranostic nanoparticles with some special advantages, such as the tumor-targeted (passive or active), multi-mode contrast agents (magnetic resonance imaging, ultrasonography or fluorescence), carrier or enhancer of drug delivery, and combined chemo or thermal therapy *etc.*, are rapidly gaining popularity and have shown a promising application in the field of cancer treatment. In this mini review, the trends and the advances of multifunctional and theranostic nanoparticles are briefly discussed.

Key words: Ultrasound contrast agent; Microbubble; Nanoparticle; Imaging; Nanomaterial

Core tip: The theranostic nanoparticles are defined as nanoparticles with double functions (for both therapeutic and diagnostic purposes) and are commonly applied to simultaneous drug delivery and molecular imaging.

Zheng SG, Xu HX, Chen HR. Nano/microparticles and ultrasound contrast agents. *World J Radiol* 2013; 5(12): 468-471 Available from: URL: http://www.wjgnet.com/1949-8470/full/v5/i12/468.htm DOI: http://dx.doi.org/10.4329/wjr.v5.i12.468

MICROBUBBLES

Conventionally, the ultrasound contrast agents (UCAs) commercially used are microbubbles with sizes in the micrometer range, such as SonoVue®, Definity®, Luminity®, Sonazoid® *etc.*, which are mainly composed of insoluble gas (perfluorocarbons or sulfur hexafluoride) and an encapsulating shell (lipids, proteins or polymers)[1-5]. During the past decades, these UCAs were mainly used for imaging in clinical practice[2-11]. Recently, microbubbles and their associated cavitation are playing an increasingly significant role in both diagnostic and therapeutic applications of ultrasound[12]. Besides that, microbubbles have also attracted more attention as carriers and enhancers of

drug and gene delivery and have been widely investigated for these applications (especially in the area of anticancer research)[13]. However, short circulation time (minutes) and relatively large size (two to ten micrometers) of currently used commercial microbubbles do not allow effective extravasation into tumor tissue (pore size of tumor endothelium is typically in the range 380-780 nm), preventing efficient tumor targeting[14,15].

NANOMATERIALS

Fortunately, with the development of nanotechnology, nanomaterials have also evolved and now are widely recognized as a novel type of biomaterial, with very promising applications in the field of drug delivery[13,16-21]. Currently, a number of nanomaterials, including liposomes, polymers, micelles, dendrimers, emulsions, quantum dots, solid nanoparticles *etc*., have already been applied to pre or clinical trials[22-30]. In theory, nanomaterials can overcome the aforementioned shortcomings of microbubbles due to their smaller sizes (in the nanometer range)[29,31,32]. The National Cancer Institute has defined the nanoparticle as any particle with at least one dimension under 100 nm, while in many articles, some sub-micrometer particles have also been regarded as nanoparticles[1].

The way to synthesize an ideal ultrasound contrast agent based on nanoparticles in order to achieve an expected effect on contrast imaging is a key technique. According to some recently published articles, most researchers were able to enhance the acoustic backscatter by using nanomaterial equipped with gas (perfluorocarbon), although the nanoparticle-based contrast agents for the imaging modalities discussed were in various stages of development[25-27,33-35].

The use of nanomaterials as carriers for drug delivery represents the mainstream in the field of biomedical research[29,31,36-39]. However, recently, multifunctional and theranostic nanoparticles with some special advantages, such as the tumor-targeted (passive or active), multimode contrast agents [magnetic resonance imaging (MRI), ultrasonography (US) or fluorescence], carrier or enhancer of drug delivery, and combined chemo or thermal therapy, *etc*., are rapidly gaining popularity and have shown a promising application in the field of cancer treatment[13,18-20,29,38-42].

For instance, Lammers *et al*[31] discussed the principles, pitfalls and (pre) clinical progress of drugs (including those with nanoparticles) used for tumor-targeting. Most nanoparticles can be easily functionalized with a wide variety of biomolecules or antibodies and could be used for the targeted recognition or imaging of specific tissue/organs[19,43-47]. Besides, regarding its multifunction and multimode imaging, Malvindi *et al*[48] reported a magnetic/silica nanocomposite as a dual-mode contrast agent for combined MRI and US which enables non-invasive detection of the molecular components of pathological processes through multiple-mode imaging techniques[14,48]. Wang *et al*[35] proposed that Au nanoparticle coated mesoporous silica nanocapsule-based enhancement agents can be used as an inorganic theranostic platform for contrast-intensified US imaging, combined chemotherapy and efficient high intensity focused ultrasound tumor ablation[42,45,49].

Nowadays, these kinds of nanoparticles with more novel functions are still the research focus of biomaterials and are being explored for further biomedical applications[1,14,18,20,35,43,48,50].

We hope that the information presented in this mini review will stimulate the readers' interest regarding the field of nano/microparticles and UCAs.

REFERENCES

1 **Mullin LB**, Phillips LC, Dayton PA. Nanoparticle delivery enhancement with acoustically activated microbubbles. *IEEE Trans Ultrason Ferroelectr Freq Control* 2013; **60**: 65-77 [PMID: 23287914 DOI: 10.1109/TUFFC.2013.2538]

2 **Claudon M**, Cosgrove D, Albrecht T, Bolondi L, Bosio M, Calliada F, Correas JM, Darge K, Dietrich C, D'Onofrio M, Evans DH, Filice C, Greiner L, Jäger K, Jong Nd, Leen E, Lencioni R, Lindsell D, Martegani A, Meairs S, Nolsøe C, Piscaglia F, Ricci P, Seidel G, Skjoldbye B, Solbiati L, Thorelius L, Tranquart F, Weskott HP, Whittingham T. Guidelines and good clinical practice recommendations for contrast enhanced ultrasound (CEUS) - update 2008. *Ultraschall Med* 2008; **29**: 28-44 [PMID: 18270887 DOI: 10.1055/s-2007-963785]

3 **Claudon M**, Dietrich CF, Choi BI, Cosgrove DO, Kudo M, Nolsøe CP, Piscaglia F, Wilson SR, Barr RG, Chammas MC, Chaubal NG, Chen MH, Clevert DA, Correas JM, Ding H, Forsberg F, Fowlkes JB, Gibson RN, Goldberg BB, Lassau N, Leen EL, Mattrey RF, Moriyasu F, Solbiati L, Weskott HP, Xu HX. Guidelines and good clinical practice recommendations for Contrast Enhanced Ultrasound (CEUS) in the liver - update 2012: A WFUMB-EFSUMB initiative in cooperation with representatives of AFSUMB, AIUM, ASUM, FLAUS and ICUS. *Ultrasound Med Biol* 2013; **39**: 187-210 [PMID: 23137926 DOI: 10.1016/j.ultrasmedbio.2012.09.002]

4 **Xu HX**. Contrast-enhanced ultrasound: The evolving applications. *World J Radiol* 2009; **1**: 15-24 [PMID: 21160717 DOI: 10.4329/wjr.v1.i1.15]

5 **Quaia E**. Microbubble ultrasound contrast agents: an update. *Eur Radiol* 2007; **17**: 1995-2008 [PMID: 17351779 DOI: 10.1007/s00330-007-0623-0]

6 **Xu HX**. Contrast-enhanced ultrasound in the biliary system: Potential uses and indications. *World J Radiol* 2009; **1**: 37-44 [PMID: 21160719 DOI: 10.4329/wjr.v1.i1.37]

7 **Xu HX**. Era of diagnostic and interventional ultrasound. *World J Radiol* 2011; **3**: 141-146 [PMID: 21666820 DOI: 10.4329/wjr.v3.i5.141]

8 **Xu HX**, Lu MD. The current status of contrast-enhanced ultrasound in China. *J Med Ultrason* 2010; **37**: 97-106 [DOI: 10.1007/s10396-010-0264-9]

9 **Liu GJ**, Lu MD. Diagnosis of liver cirrhosis with contrast-enhanced ultrasound. *World J Radiol* 2010; **2**: 32-36 [PMID: 21160737 DOI: 10.4329/wjr.v2.i1.32]

10 **Ignee A**, Straub B, Schuessler G, Dietrich CF. Contrast enhanced ultrasound of renal masses. *World J Radiol* 2010; **2**: 15-31 [PMID: 21160736 DOI: 10.4329/wjr.v2.i1.15]

11 **Molins IG**, Font JM, Alvaro JC, Navarro JL, Gil MF, Rodríguez CM. Contrast-enhanced ultrasound in diagnosis and characterization of focal hepatic lesions. *World J Radiol* 2010; **2**: 455-462 [PMID: 21225000 DOI: 10.4329/wjr.v2.i12.455]

12 **Stride EP**, Coussios CC. Cavitation and contrast: the use of bubbles in ultrasound imaging and therapy. *Proc Inst Mech Eng H* 2010; **224**: 171-191 [PMID: 20349814]

13 **Mohan P**, Rapoport N. Doxorubicin as a molecular nanotheranostic agent: effect of doxorubicin encapsulation in micelles or nanoemulsions on the ultrasound-mediated in-

tracellular delivery and nuclear trafficking. *Mol Pharm* 2010; **7**: 1959-1973 [PMID: 20957997 DOI: 10.1021/mp100269f]
14 **Casciaro S**, Soloperto G, Greco A, Casciaro E, Franchini R, Conversano F. Effectiveness of functionalized nanosystems for multimodal molecular sensing and imaging in medicine. *IEEE Sens J* 2013; **6**: 2305-2312 [DOI: 10.1109/JSEN.2013.2252164]
15 **Maeda H**, Wu J, Sawa T, Matsumura Y, Hori K. Tumor vascular permeability and the EPR effect in macromolecular therapeutics: a review. *J Control Release* 2000; **65**: 271-284 [PMID: 10699287]
16 **Suzuki R**, Oda Y, Utoguchi N, Namai E, Taira Y, Okada N, Kadowaki N, Kodama T, Tachibana K, Maruyama K. A novel strategy utilizing ultrasound for antigen delivery in dendritic cell-based cancer immunotherapy. *J Control Release* 2009; **133**: 198-205 [PMID: 19000727 DOI: 10.1016/j.jconrel.2008.10.015]
17 **Petros RA**, DeSimone JM. Strategies in the design of nanoparticles for therapeutic applications. *Nat Rev Drug Discov* 2010; **9**: 615-627 [PMID: 20616808 DOI: 10.1038/nrd2591]
18 **Janib SM**, Moses AS, MacKay JA. Imaging and drug delivery using theranostic nanoparticles. *Adv Drug Deliv Rev* 2010; **62**: 1052-1063 [PMID: 20709124 DOI: 10.1016/j.addr.2010.08.004]
19 **Byrne JD**, Betancourt T, Brannon-Peppas L. Active targeting schemes for nanoparticle systems in cancer therapeutics. *Adv Drug Deliv Rev* 2008; **60**: 1615-1626 [PMID: 18840489 DOI: 10.1016/j.addr.2008.08.005]
20 **Chen Y**, Chen H, Zeng D, Tian Y, Chen F, Feng J, Shi J. Core/shell structured hollow mesoporous nanocapsules: a potential platform for simultaneous cell imaging and anticancer drug delivery. *ACS Nano* 2010; **4**: 6001-6013 [PMID: 20815402 DOI: 10.1021/nn1015117]
21 **De Jong WH**, Borm PJ. Drug delivery and nanoparticles: applications and hazards. *Int J Nanomedicine* 2008; **3**: 133-149 [PMID: 18686775]
22 **Nie S**, Xing Y, Kim GJ, Simons JW. Nanotechnology applications in cancer. *Annu Rev Biomed Eng* 2007; **9**: 257-288 [PMID: 17439359 DOI: 10.1146/annurev.bioeng.9.060906.152025]
23 **Kratz F**. Albumin as a drug carrier: design of prodrugs, drug conjugates and nanoparticles. *J Control Release* 2008; **132**: 171-183 [PMID: 18582981 DOI: 10.1016/j.jconrel.2008.05.010]
24 **Torchilin VP**. Recent advances with liposomes as pharmaceutical carriers. *Nat Rev Drug Discov* 2005; **4**: 145-160 [PMID: 15688077 DOI: 10.1038/nrd1632]
25 **Chung MF**, Chen KJ, Liang HF, Liao ZX, Chia WT, Xia Y, Sung HW. A liposomal system capable of generating CO2 bubbles to induce transient cavitation, lysosomal rupturing, and cell necrosis. *Angew Chem Int Ed Engl* 2012; **51**: 10089-10093 [PMID: 22952023 DOI: 10.1002/anie.201205482]
26 **Wang X**, Chen H, Chen Y, Ma M, Zhang K, Li F, Zheng Y, Zeng D, Wang Q, Shi J. Perfluorohexane-encapsulated mesoporous silica nanocapsules as enhancement agents for highly efficient high intensity focused ultrasound (HIFU). *Adv Mater* 2012; **24**: 785-791 [PMID: 22223403 DOI: 10.1002/adma.201104033]
27 **Kang E**, Min HS, Lee J, Han MH, Ahn HJ, Yoon IC, Choi K, Kim K, Park K, Kwon IC. Nanobubbles from gas-generating polymeric nanoparticles: ultrasound imaging of living subjects. *Angew Chem Int Ed Engl* 2010; **49**: 524-528 [PMID: 20013828 DOI: 10.1002/anie.200903841]
28 **Wang L**, Shi J, Zhang H, Li H, Gao Y, Wang Z, Wang H, Li L, Zhang C, Chen C, Zhang Z, Zhang Y. Synergistic anticancer effect of RNAi and photothermal therapy mediated by functionalized single-walled carbon nanotubes. *Biomaterials* 2013; **34**: 262-274 [PMID: 23046752 DOI: 10.1016/j.biomaterials.2012.09.037]
29 **Eifler AC**, Thaxton CS. Nanoparticle therapeutics: FDA approval, clinical trials, regulatory pathways, and case study. *Methods Mol Biol* 2011; **726**: 325-338 [PMID: 21424459 DOI: 10.1007/978-1-61779-052-2_21]
30 **Chen H**, Li B, Ren X, Li S, Ma Y, Cui S, Gu Y. Multifunctional near-infrared-emitting nano-conjugates based on gold clusters for tumor imaging and therapy. *Biomaterials* 2012; **33**: 8461-8476 [PMID: 22951103 DOI: 10.1016/j.biomaterials.2012.08.034]
31 **Lammers T**, Kiessling F, Hennink WE, Storm G. Drug targeting to tumors: principles, pitfalls and (pre-) clinical progress. *J Control Release* 2012; **161**: 175-187 [PMID: 21945285 DOI: 10.1016/j.jconrel.2011.09.063]
32 **Allen TM**, Cullis PR. Drug delivery systems: entering the mainstream. *Science* 2004; **303**: 1818-1822 [PMID: 15031496 DOI: 10.1126/science.1095833]
33 **Liberman A**, Martinez HP, Ta CN, Barback CV, Mattrey RF, Kono Y, Blair SL, Trogler WC, Kummel AC, Wu Z. Hollow silica and silica-boron nano/microparticles for contrast-enhanced ultrasound to detect small tumors. *Biomaterials* 2012; **33**: 5124-5129 [PMID: 22498299 DOI: 10.1016/j.biomaterials.2012.03.066]
34 **Yang F**, Chen P, He W, Gu N, Zhang X, Fang K, Zhang Y, Sun J, Tong J. Bubble microreactors triggered by an alternating magnetic field as diagnostic and therapeutic delivery devices. *Small* 2010; **6**: 1300-1305 [PMID: 20486225 DOI: 10.1002/smll.201000173]
35 **Wang X**, Chen H, Zheng Y, Ma M, Chen Y, Zhang K, Zeng D, Shi J. Au-nanoparticle coated mesoporous silica nanocapsule-based multifunctional platform for ultrasound mediated imaging, cytoclasis and tumor ablation. *Biomaterials* 2013; **34**: 2057-2068 [PMID: 23246067 DOI: 10.1016/j.biomaterials.2012.11.044]
36 **Wang AZ**, Langer R, Farokhzad OC. Nanoparticle delivery of cancer drugs. *Annu Rev Med* 2012; **63**: 185-198 [PMID: 21888516 DOI: 10.1146/annurev-med-040210-162544]
37 **Egusquiaguirre SP**, Igartua M, Hernández RM, Pedraz JL. Nanoparticle delivery systems for cancer therapy: advances in clinical and preclinical research. *Clin Transl Oncol* 2012; **14**: 83-93 [PMID: 22301396 DOI: 10.1007/s12094-012-0766-6]
38 **Chen Y**, Chen H, Guo L, He Q, Chen F, Zhou J, Feng J, Shi J. Hollow/rattle-type mesoporous nanostructures by a structural difference-based selective etching strategy. *ACS Nano* 2010; **4**: 529-539 [PMID: 20041633 DOI: 10.1021/nn901398j]
39 **Chen Y**, Chen H, Zhang S, Chen F, Zhang L, Zhang J, Zhu M, Wu H, Guo L, Feng J, Shi J. Multifunctional Mesoporous Nanoellipsoids for Biological Bimodal Imaging and Magnetically Targeted Delivery of Anticancer Drugs. *Adv Funct Mater* 2011; **21**: 270-278 [DOI: 10.1002/adfm.201001495]
40 **Rapoport N**, Gao Z, Kennedy A. Multifunctional nanoparticles for combining ultrasonic tumor imaging and targeted chemotherapy. *J Natl Cancer Inst* 2007; **99**: 1095-1106 [PMID: 17623798]
41 **Popović Z**, Liu W, Chauhan VP, Lee J, Wong C, Greytak AB, Insin N, Nocera DG, Fukumura D, Jain RK, Bawendi MG. A nanoparticle size series for in vivo fluorescence imaging. *Angew Chem Int Ed Engl* 2010; **49**: 8649-8652 [PMID: 20886481 DOI: 10.1002/anie.201003142]
42 **Wang ZY**, Song J, Zhang DS. Nanosized As2O3/Fe2O3 complexes combined with magnetic fluid hyperthermia selectively target liver cancer cells. *World J Gastroenterol* 2009; **15**: 2995-3002 [PMID: 19554652]
43 **Behnke T**, Mathejczyk JE, Brehm R, Würth C, Gomes FR, Dullin C, Napp J, Alves F, Resch-Genger U. Target-specific nanoparticles containing a broad band emissive NIR dye for the sensitive detection and characterization of tumor development. *Biomaterials* 2013; **34**: 160-170 [PMID: 23072943 DOI: 10.1016/j.biomaterials.2012.09.028]
44 **Liu J**, Li J, Rosol TJ, Pan X, Voorhees JL. Biodegradable nanoparticles for targeted ultrasound imaging of breast cancer cells in vitro. *Phys Med Biol* 2007; **52**: 4739-4747 [PMID: 17671332]
45 **Sheeran PS**, Luois SH, Mullin LB, Matsunaga TO, Dayton

PA. Design of ultrasonically-activatable nanoparticles using low boiling point perfluorocarbons. *Biomaterials* 2012; **33**: 3262-3269 [PMID: 22289265 DOI: 10.1016/j.biomaterials.2012.01.021]

46 **Brannon-Peppas L**, Blanchette JO. Nanoparticle and targeted systems for cancer therapy. *Adv Drug Deliv Rev* 2004; **56**: 1649-1659 [PMID: 15350294]

47 **Veiseh O**, Gunn JW, Zhang M. Design and fabrication of magnetic nanoparticles for targeted drug delivery and imaging. *Adv Drug Deliv Rev* 2010; **62**: 284-304 [PMID: 19909778 DOI: 10.1016/j.addr.2009.11.002]

48 **Malvindi MA**, Greco A, Conversano F, Figuerola A, Corti M, Bonora M, Lascialfari A, Doumari HA, Moscardini M, Cingolani R, Gigli G, Casciaro S, Pellegrino T, Ragusa A. Magnetic/Silica Nanocomposites as Dual-Mode Contrast Agents for Combined Magnetic Resonance Imaging and Ultrasonography. *Adv Funct Mater* 2011; **21**: 2548-2555 [DOI: 10.1002/adfm.201100031]

49 **Wei H**, Huang J, Yang J, Zhang X, Lin L, Xue E, Chen Z. Ultrasound exposure improves the targeted therapy effects of galactosylated docetaxel nanoparticles on hepatocellular carcinoma xenografts. *PLoS One* 2013; **8**: e58133 [PMID: 23469265 DOI: 10.1371/journal.pone.0058133]

50 **Dai LC**, Yao X, Wang X, Niu SQ, Zhou LF, Fu FF, Yang SX, Ping JL. In vitro and in vivo suppression of hepatocellular carcinoma growth by midkine-antisense oligonucleotide-loaded nanoparticles. *World J Gastroenterol* 2009; **15**: 1966-1972 [PMID: 19399928]

P- Reviewers: Martins WP, Tsalafoutas I **S- Editor**: Wen LL
L- Editor: Roemmele A **E- Editor**: Liu SQ

World Journal of Radiology

Online Submissions: http://www.wjgnet.com/esps/
bpgoffice@wjgnet.com
doi:10.4329/wjr.v5.i12.472

World J Radiol 2013 December 28; 5(12): 472-483
ISSN 1949-8470 (online)

ORIGINAL ARTICLE

Magnetic resonance imaging characterization of circumferential and longitudinal strain under various coronary interventions in swine

Mohammed SA Suhail, Mark W Wilson, Steven W Hetts, Maythem Saeed

Mohammed SA Suhail, Mark W Wilson, Steven W Hetts, Maythem Saeed, Department of Radiology and Biomedical Imaging, School of Medicine, University of California San Francisco, CA 94107-5705, United States
Mohammed SA Suhail, School of Medicine, University of California San Diego, CA 94107-5705, United States
Author contributions: Suhail MSA achieved and analyzed the images, prepared the figures and drafted the manuscript; Wilson MW and Hetts SW provided vital advices and were also involved in the editing; Saeed M designed the study, performed the experiments and wrote the final version of the manuscript.
Correspondence to: Maythem Saeed, PhD, Professor, Department of Radiology and Biomedical Imaging, School of Medicine, University of California San Francisco, 185 Berry Street, Suite 350, Campus Box 0946, San Francisco, CA 94107-5705, United States. msaeed@ucsf.edu
Telephone: +1-415-5146221 Fax: +1-415-3539423
Received: July 26, 2013 Revised: October 18, 2013
Accepted: December 9, 2013
Published online: December 28, 2013

Abstract

AIM: To compare the acute changes in circumferential and longitudinal strain after exposing a coronary artery to various interventions in swine.

METHODS: Percutaneous balloon angioplasty catheter was guided to location aid device (LAD) under X-ray fluoroscopy to create different patterns of ischemic insults. Pigs (n = 32) were equally divided into 4 groups: controls, 90 min LAD occlusion/reperfusion, LAD microembolization, and combined LAD occlusion/microembolization/reperfusion. Three days after interventions, cine, tagged and viability magnetic resonance imaging (MRI) were acquired to measure and compare left and right circumferential strain, longitudinal strain and myocardial viability, respectively. Measurements were obtained using HARP and semi-automated threshold method and statistically analyzed using unpaired t-test. Myocardial and vascular damage was characterized microscopically.

RESULTS: Coronary microemboli caused greater impairment in l left ventricular (LV) circumferential strain and dyssynchrony than LAD occlusion/reperfusion despite the significant difference in the extent of myocardial damage. Microemboli also caused significant decrease in peak systolic strain rate of remote myocardium and LV dyssynchrony. Cine MRI demonstrated the interaction between LV and right ventricular (RV) at 3 d after interventions. Compensatory increase in RV free wall longitudinal strain was seen in response to all interventions. Viability MRI, histochemical staining and microscopy revealed different patterns of myocardial damage and microvascular obstruction.

CONCLUSION: Cine MRI revealed subtle changes in LV strain caused by various ischemic insults. It also demonstrated the interaction between the right and left ventricles after coronary interventions. Coronary microemboli with and without acute myocardial infarction (AMI) cause complex myocardial injury and ventricular dysfunction that is not replicated in solely AMI.

Key words: Magnetic resonance imaging; Percutaneous coronary interventions; Acute myocardial infarct; Microembolization; Myocardial strain

Core tip: Cine and tagging magnetic resonance imaging showed that segments in pre-existing acute myocardial superimposed with microemboli have the most severe impairment in both longitudinal and circumferential strain, while segments subjected to solely microembolization or location aid device (LAD) occlusion/reperfusion showed only circumferential impairment. The

interaction between right and left ventricles after LAD interventions is clearly demonstrated by the increase in right ventricular (RV) free wall strain, suggesting that both left ventricular and RV need assessment in ischemic heart disease.

Suhail MSA, Wilson MW, Hetts SW, Saeed M. Magnetic resonance imaging characterization of circumferential and longitudinal strain under various coronary interventions in swine. *World J Radiol* 2013; 5(12): 472-483 Available from: URL: http://www.wjgnet.com/1949-8470/full/v5/i12/472.htm DOI: http://dx.doi.org/10.4329/wjr.v5.i12.472

INTRODUCTION

Acute myocardial infarction (AMI) remains a leading cause of morbidity and mortality worldwide. It has been classified into subtypes based on clinical scenario; namely ischemia from a primary coronary event (*e.g.,* plaque rupture, thrombotic occlusion), ischemia from a supply-and-demand mismatch, and percutaneous/surgical coronary interventions[1]. Different procedures have been introduced to reperfused blocked major coronary artery. However, the effects of persistent microvascular blockage by dislodged microemboli are still a clinical problem, which has been acknowledged by multiple cardiac and interventional societies[2].

Echocardiography is the most commonly used clinical method for quantification of global and regional left ventricular (LV) function, where LV ejection fraction and wall motion score are measured[3]. Others used 2D speckle-tracking images for measuring regional strain and strain rate[4]. This method enables quantification of myocardial deformation[5], but associated with limitations, such as the inability of peak velocity to differentiate dyskinetic from hypokinetic myocardium[6]. Unlike other modalities, magnetic resonance imaging (MRI) provides quantitative prognostic functional and structural information[7,8]. Clinical MRI studies demonstrated the impairment in radial, circumferential and longitudinal strain in ischemic myocardium[9-11]. Investigators found that these MRI indices have higher sensitivity and specificity than 2D strain echocardiography in patients with AMI[12] and scar[13]. Furthermore, contrast enhanced MRI has the capability to delineate patchy myocardial infarct in patients[14] and animals[15-17]. However, the magnitude and mechanical effects of microemboli in pre-existing reperfused AMI on circumferential and longitudinal strain have not been characterized or compared to solely reperfused AMI using MRI. We hypothesized that coronary microemboli in pre-existing AMI cause complex ventricular dysfunction that is not replicated in solely AMI. Thus, this experimental investigation aimed at simulating 3 interventional clinical scenarios, namely location aid device (LAD) occlusion/reperfusion, LAD microembolization, and combined LAD occlusion/microembolization/reperfusion.

MATERIALS AND METHODS

Coronary intervention

This study was performed in accordance with the Guide for the Care and Use of Laboratory Animals and approval from IACUC. Farm pigs (30-32 kg) were sedated and anesthetized using isoflurane/oxygen 2%-5%/2-3 L/min. Small volume and size of microemboli (32 mm^3 volume, average diameter 80 μm) were tested in the current study because previous autopsy study in humans showed that the sizes of these microemboli were less than 120 μm and most of microemboli (89%) were located in the LAD territory[18]. Accordingly, a 3F balloon catheter was advanced under X-ray fluoroscopy to the LAD coronary artery in swine model. The balloon catheter was used to (1) occlude (90 min) LAD coronary artery (n = 8), (2) delivery of microemboli (32 mm^3 volume, about 120 microemboli with an average diameter of 80 μm (Embosphere®, Biosphere Med, Rockland, MA (n = 8), and (3) combine 90 min LAD occlusion and delivery of microemboli (32 mm^3 volume, n = 8) followed by reperfusion. The occlusion or microemboli delivery was in the LAD at the middle of LV and the second diagonal branch was used as a land mark. Intravenous heparin and lidocaine were administered prior to coronary catheterization. ECG, heart rate, blood pressure, O_2-sat, PCO_2 and body temperature was monitored during the interventions. All animals were imaged 3 d after the interventions. Another 8 animals with matching body weight (30-32 kg) served as controls (no intervention).

Cardiac MRI

MRI was performed using 1.5-T scanner (GE Medical Systems, Milwaukee, WI, United States). For circumferential strain of the LV, a tagged turbo-field echo-planar sequence was used. The tagging technique used complementary spatial modulation of magnetization for horizontal and vertical tag orientation images obtained in one breath-hold. Imaging parameters were: TR/TE = 35/6.1 ms, flip = 25°, NEX = 1, section thickness = 8 mm, FOV = 24 cm × 24 cm, matrix = 128 × 45, pixel size = 1.875 × 5.333 mm^2, temporal resolution = 35 ms, EPI factor = 11, bandwidth = 185 Hz, echo length = 1, tag spacing = 5 mm, temporal resolution = 35 ms and cardiac phases = 16. Images were acquired in the short axis plane of the entire LV[19]. For quantitative analysis, two apical slices within the area of infarction (2.4 and 3.2 cm from the apex of the heart) were used. The tagging technique used complementary spatial modulation of magnetization for horizontal and vertical tag orientation images obtained in breath-hold and for longitudinal strain, multiple cine MR images in the long-axis view were acquired using a steady-state free precession sequence. Imaging parameters were: TR/TE/flip angle = 3.5 ms/1.75 ms/70°, slice thickness = 8 mm, no slice gap, FOV = 25 cm × 25 cm, matrix size = 160 × 152 and cardiac phases = 16.

For viability imaging, inversion-recovery gradient-echo DE-MRI images were acquired in the short and

long axis views of the heart. The imaging parameters were: TR/TE/flip angle = 5/2 ms/15°, interval = 2RR-intervals, slice thickness = 8 mm, no slice gap, FOV = 26 cm × 26 cm, matrix size = 256 × 162. Viability images were acquired 10-15 min after intravenous administration of 0.15 mmol/kg Gd-DTPA using inversion time of 220-230 ms to null remote myocardium. For quantitative measurement of large and patchy infarct a semi-automatic threshold method (3SD) was used. At the conclusion of the imaging sessions, the animals were sacrificed by intravenous injection of saturated KCl (1 mL/kg). The hearts were excised, sliced and incubated in 2% triphenyltetrazolium chloride (TTC) at 37 ℃. Digital images of TTC-stained slices were acquired, converted to black and white images using Adobe Photoshop CS2. The same semi-automatic method (3SD) used above was used to measure infarct size on TTC.

Image and statistical analysis

Phasic and peak longitudinal strain and circumferential strain were analyzed from complex raw data circumferential strain was obtained by manual outline of the endocardium and epicardium of the LV in multiple tagged images, which was automatically propagated by HARP tagged CMRI analysis software. The segmentation on HARP we done as follow: First, in a given timeframe, 2D HARP images were unwrapped in each slice[19]. Displacement measurements from the phase-unwrapped images were then used to compute a 3D displacement field from which strain was computed. This procedure was repeated for each imaged timeframe[20]. In each animal, two defined apical slices (2.4 and 3.2 cm from the apex of the heart) with infarct were analyzed. HARP software automatically provided strain at each point in the cardiac cycle, peak strain, time to peak strain (TTPS), and provided strain rate by obtaining a strain curve and differentiating the curve with respect to time[21]. Peak systolic and diastolic strain rate and TTP systolic and diastolic strain rates were obtained from these curves.

Peak systolic longitudinal strain was obtained from a 4 chamber view of cine MR images after delineating endocardial length of LV and right ventricular (RV) during systole and diastole using an echocardiographic method[22,23]. Figure 1 shows the semi-automated traced myocardium throughout the cardiac cycle. Longitudinal strain was determined in LV free wall (LVFW), RV free wall (RVFW), and interventricular septum (IVS). This method has been recently validated against spatial modulation of magnetization tissue tagging method[24]. Semi-automatic threshold method (+3SD), ImageJ was also used to measure large infarct and patchy microinfarct on contrast enhanced MRI and histochemical TTC staining. Paired and unpaired nonparametric Student *t*-tests and nonparametric ANOVA with Dunn's multiple comparison tests were used. A $P < 0.05$ was considered significant.

Postmortem staining

At the conclusion of the imaging protocol, the hearts were excised, sliced and incubated in 2% TTC at 37 ℃ for 30 min. Digital images of TTC stained short-axis slices were acquired and converted to black-and-white images. For confirmation of structural changes caused by coronary interventions, 3 LV rings from each animal were fixed in 10% buffered formalin, processed, sectioned and stained with hematoxylin/eosin. Microscopically, the stained sections were magnified (× 40 to × 100), photographed under light microscopy using NIS Elements-F (Nikon, Melville, NY, United States) and studied.

RESULTS

Myocardial viability

Control animals revealed no evidence of infarction on DE-MRI and TTC staining or differential strain between LAD territory and remote myocardium (Figure 2A, $P = 0.72$). The different interventions produced continuous, patchy or combined pattern of enhancement of myocardial damage on DE-MRI. Furthermore, myocardial damage was significantly smaller (8.8% ± 0.5% LV mass) in solely microembolized animals compared with animals subjected to occlusion/reperfusion (12.4% ± 1.2%, $P < 0.01$) or the combination of the two insults (15.7% ± 1.1%, $P < 0.05$).

Circumferential strain

All animals subjected to coronary interventions demonstrated decline in peak circumferential strain compared with remote myocardium (Figure 2A, all $P < 0.001$) or LAD territory of control animals (Figure 2B). However, peak circumferential strain showed no difference between interventions, suggesting disproportion between myocardial damage and regional strain. At 3 d, remote myocardium of animals subjected to interventions showed decreased TTPS without increase in circumferential strain compared with controls (Figure 2B). In contrast, the LAD territory demonstrated increased TTPS (Figure 2C), suggesting LV dyssynchrony.

All interventions caused significant decrease in peak strain rate of LAD territory compared with remote myocardium and controls (Figure 3A and B, all $P < 0.001$). Microembolized and combined intervention animals had significantly decreased systolic strain rate compared to LAD occluded/reperfused animals. In remote myocardium, peak systolic strain rate was significantly decreased in microembolized and combined insult animals, but not in occluded/reperfused animals, compared with controls. Additionally, all interventions caused decreased peak diastolic strain rate in the LAD territory compared with controls (Figure 3C). Similar to peak systolic strain rate, peak diastolic strain rate in remote myocardium was significantly decreased in animals subjected to microembolization or combined interventions, but not in LAD occluded/reperfused animals, compared with controls. Remote myocardium also showed significantly decreased TTP systolic and diastolic circumferential strain rates in animals subjected to microembolization or combined intervention (Figure 4), but not in LAD occluded/reperfused animals.

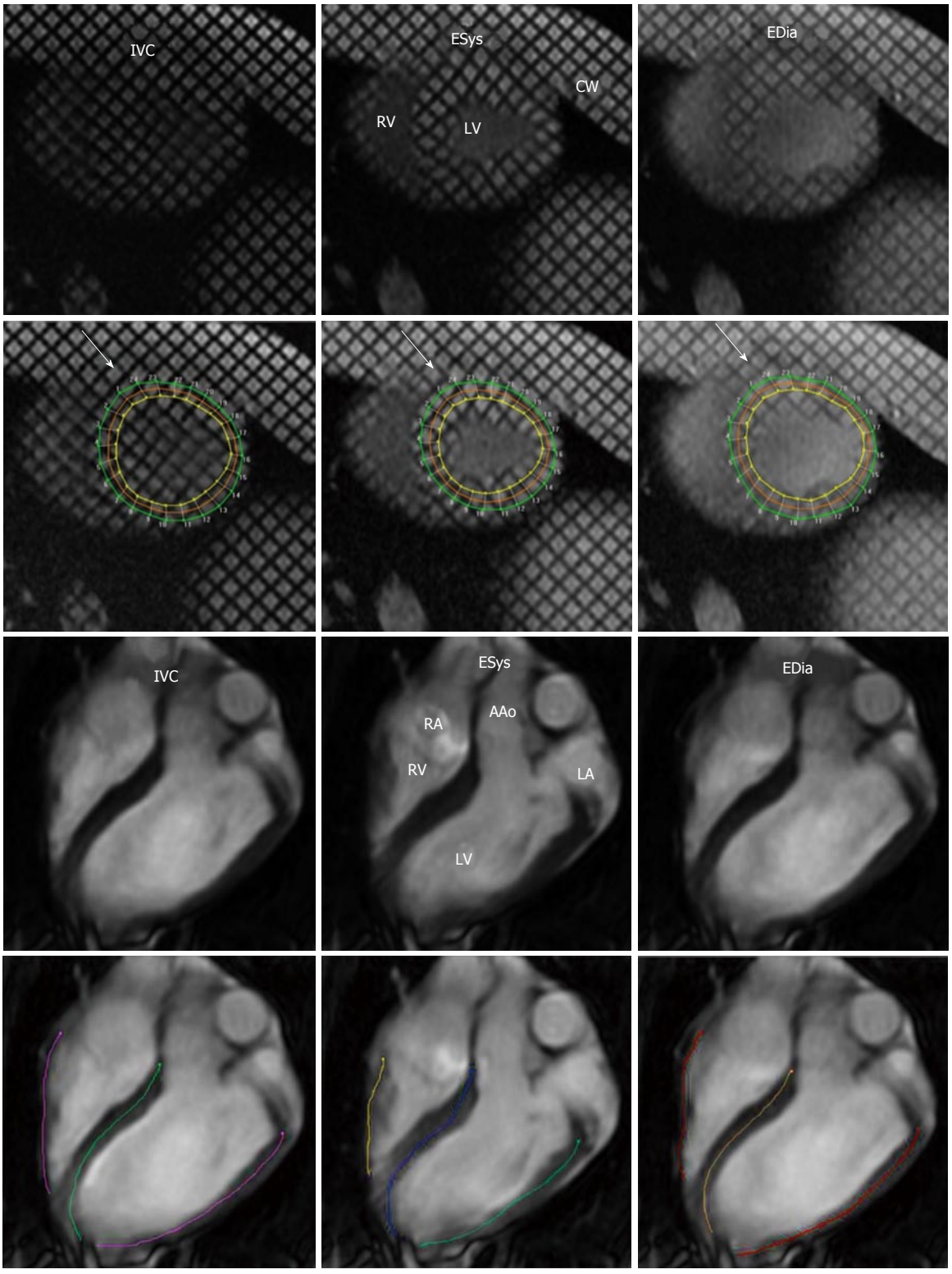

Figure 1 Representative tagged and cine magnetic resonance images with tracing method. Top row demonstrates short-axis and long-axis magnetic resonance images (MRI) images, while bottom row demonstrates images after tracing of the myocardium using HARP. Left three columns are cine tagged MRI and right three columns are cine MRI. IVC: Isovolumetric contraction; ESys: End systole; EDia: End diastole; LV: Left ventricle; RV: Right ventricle; CW: Chest wall; RA: Right atrium; LA: Left atrium; AAo: Ascending aorta.

Longitudinal strain

Figure 5 demonstrates strain curves during the cardiac cycle for each cohort. No significant change in longitudinal strain was observed in both LVFW and IVS of animals subjected microembolization or LAD occlusion/reperfusion compared with controls (Figure 5). In contrast, animals subjected LAD occlusion/microembolization/reperfusion showed significant compensatory increased peak longitudinal strain in the RVFW. Unlike other groups, animals subjected to LAD occlusion/mi-

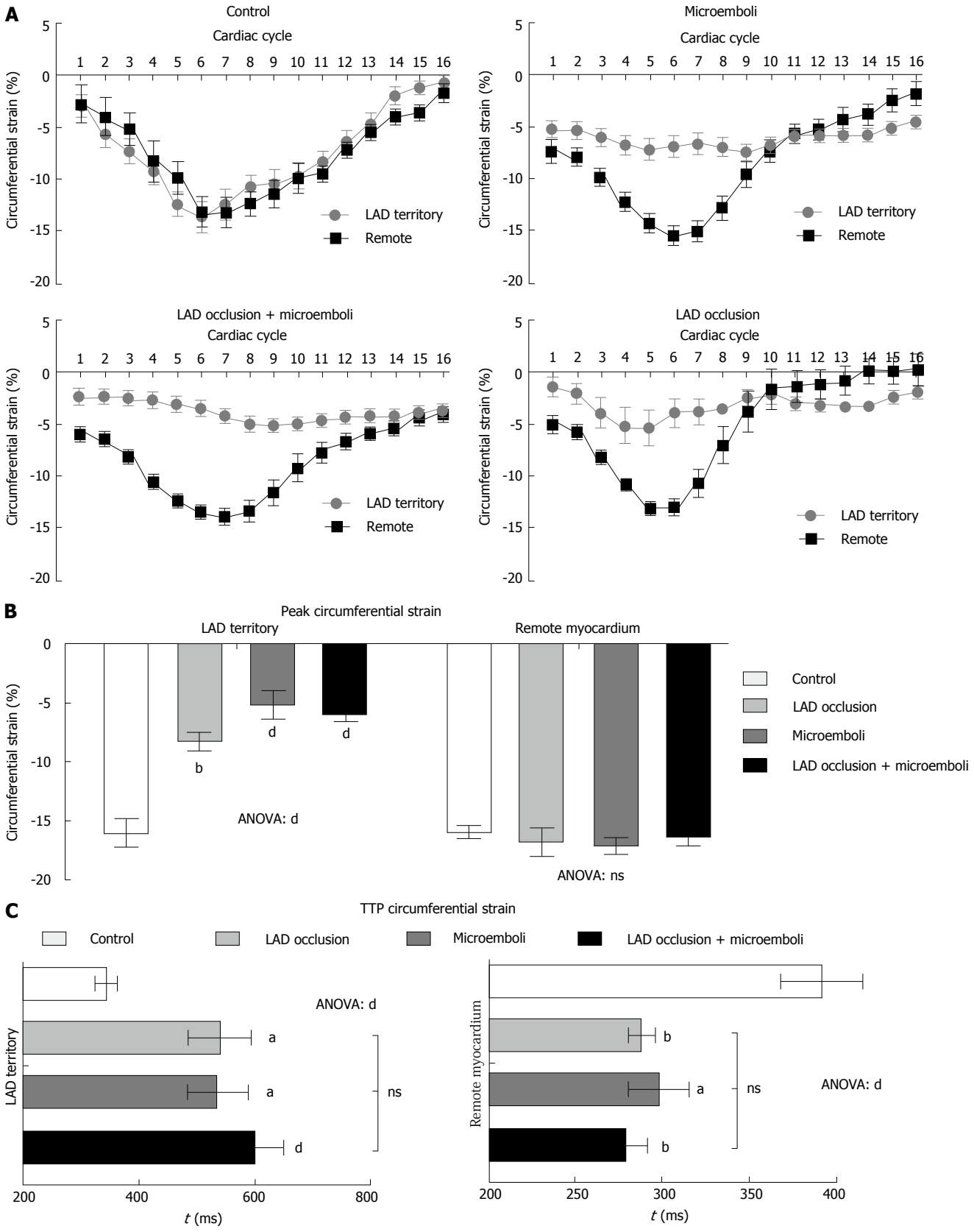

Figure 2 Circumferential strain analysis: phasic, peak, and territory time to peak strain. A: Phasic circumferential strain peak and rate during one R-R interval in LAD territory and remote myocardium of the 4 groups. Data are presented as means ± SEM. A significantly decreased peak circumferential strain was observed in the LAD territory compared with remote myocardium in all coronary interventions ($P < 0.001$); B: Bars show average peak circumferential strain. ANOVA showed significant decrease in strain of the LAD territory 3 d after interventions compared with controls. Remote myocardium showed no significant difference between interventions and control; C: shows significant variation in time to peak circumferential strain between remote and the LAD territory time to peak strain (TTPS). Remote myocardium showed decreased TTPS for all interventions, while the LAD territory demonstrated increased TTPS. Control *vs* LAD, $^{a}P < 0.05$; Control *vs* Microemboli, $^{b}P < 0.01$; Control *vs* ANOVA $^{d}P < 0.001$. LAD: Location aid device.

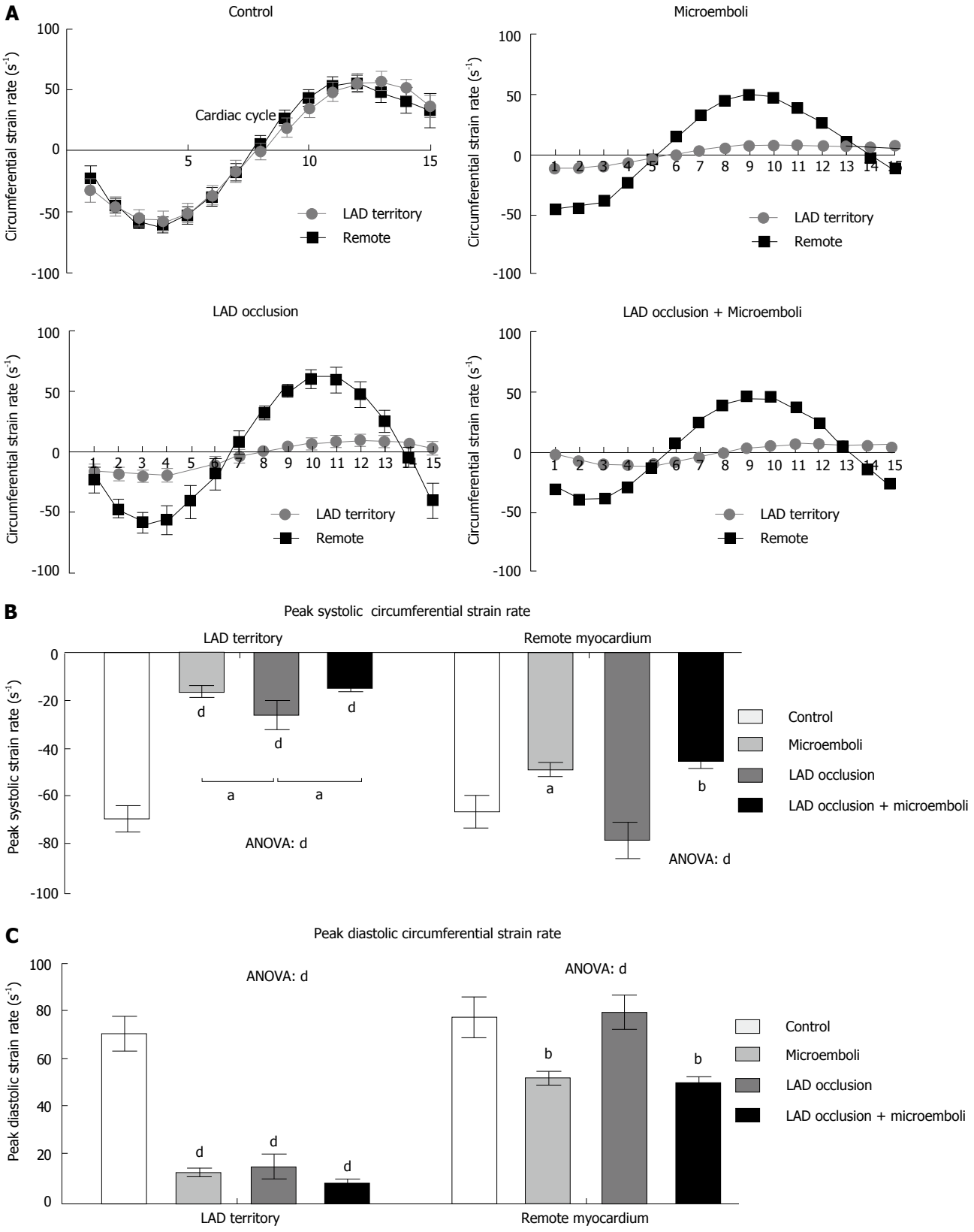

Figure 3 Circumferential strain rate analysis: phasic, peak, and territory time to peak systolic and diastolic strain rate. A: Circumferential strain rate curves. Data are presented as means ± SEM. In control animals, remote myocardium and location aid device (LAD) territory have identical curves, while remote *vs* LAD territory in all interventions were significantly different ($P < 0.001$); B: The LAD territory showed significantly decreased systolic strain rate in LAD territory for all interventions, with microembolized and combined groups significantly less than solely LAD occlusion. Remote myocardium showed only a decrease in microembolized and combined groups; C: The LAD territory demonstrated significantly decreased diastolic strain rate in LAD territory for all interventions. Remote myocardium again showed only significant decrease in microembolized and combined groups. Control *vs* LAD, $^{a}P < 0.05$; Control *vs* Microemboli, $^{b}P < 0.01$; Control *vs* ANOVA $^{d}P < 0.001$.

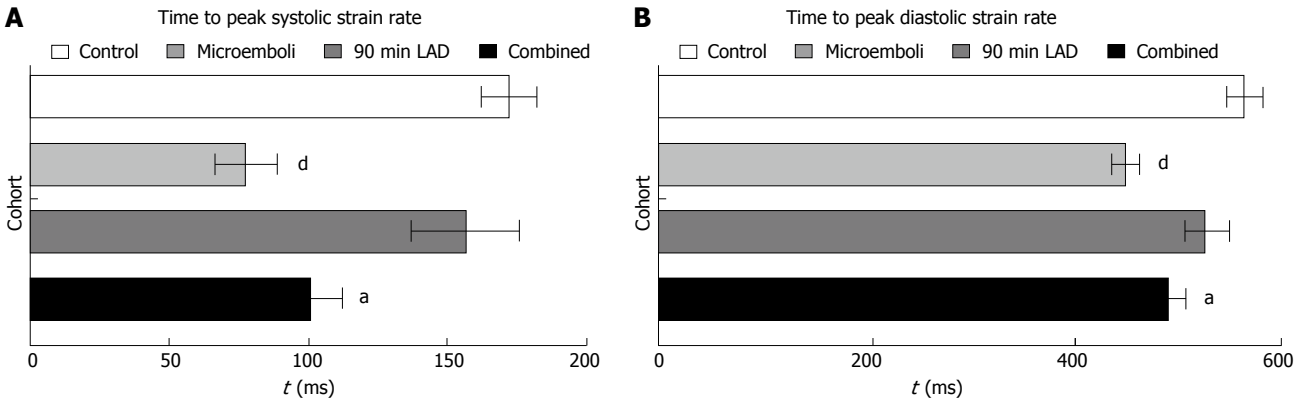

Figure 4 Time to peak systolic and diastolic strain rate in remote myocardium. Remote myocardium peak systolic (left) and diastolic strain rate (right) in controls and animals subjected to interventions. Only animals subjected to microembolization or combined ischemic insults showed significantly earlier systolic and diastolic strain rates. Data are presented as means ± SEM. Control *vs* Combined, [a]$P < 0.05$; Control *vs* Microemboli, [d]$P < 0.001$. LAD: Location aid device.

croembolization/reperfusion showed severe reduction in IVS longitudinal strain compared with controls (Figure 5).

Microscopic examination

Microscopic examinations revealed both patchy and homogeneous myocardial damage (depending on the type of the insult), microvascular damage and obstruction in all animals subjected to coronary interventions, but not controls. The microemboli were settled either individually or in clusters in the intravascular compartment (Figure 6). LAD occlusion/reperfusion animals showed contiguous myocardial damage associated with severe interstitial edema, intramyocardial hemorrhage and inflammation, while animals subjected to LAD occlusion/microembolization/reperfusion showed contiguous infarct containing severe intramyocardial hemorrhage, edema, deposited calcium in the core and patchy microinfarct at the border zone.

DISCUSSION

The major findings of this study are that (1) there was disproportion between the decline in circumferential strain, dyssynchrony and myocardial damage of animals subjected to microembolization and LAD occlusion/reperfusion; (2) microemboli caused unique effect on remote myocardial strain rates not seen in LAD occlusion/reperfusion group; (3) unlike LAD occlusion/reperfusion group, microemboli produced persistent microvascular obstruction, which may explain the difference in strain and dyssynchrony between the groups; and (4) MRI demonstrated the interaction between LV and RV, where compensatory longitudinal strain increase in the RVFW was evident in all coronary interventions.

Microvascular obstruction

Clinical studies have demonstrated that patients with CMR-defined microvascular obstruction have significantly increase cardiovascular events in follow up[25]. Galiuto[26] has recently classified microvascular damage to structural (irreversible) or functional (reversible), where the structural damage is related damage of microvascular walls; conversely, the functional damage is related to edema and cellular plugging. This MR study focused on the effects of persistent MVO caused by LAD microembolization, with and without pre-existing AMI and compared it with reperfused infarct (reperfusion injury). Our histologic examination revealed that the microvascular are patent, but modeled, in LAD occlusion/reperfusion group, but persistently obstructed in microembolized groups. Funaro *et al*[27] indicated that coronary microvascular obstruction is the strongest predictor of post-ischemic myocardial dysfunction and strongly associated with increased morbidity and mortality.

Circumferential strain

The contraction pattern is an important measure of LV function and independent of EF, wall motion abnormalities or MVO_2[19]. Early methods for measuring LV strain had limitations in resolution and subjectivity[28]. Echocardiography showed that visual tracking is insufficient to assess strain[29] and peak velocity cannot differentiate dyskinetic from hypokinetic myocardium[6]. Other used Doppler-based imaging or speckle tracking.for strain and dyssynchrony measurement, but this approach has other limitation, such as 2D, intersegmental tethering, cardiac motion, dependence of measurements upon the angle and low image quality[6,29,30].

Recent studies showed that the complex contraction pattern of the heart and alterations to this pattern due to various cardiac pathologies could be determined using tagged cine MRI[9-11]. Therefore, tagged cine MRI has been used in patients with corrected Tetralogy of Fallot and near-normal EF. Investigators found decreased circumferential strain in the basal and apical LV slices and dyssynchronous basal rotation[11]. While previous occlusion/reperfusion studies have shown correlation between infarct size and measurements of contraction pattern (such as circumferential strain and TTPS)[12,13]. This MR study demonstrated that peak strain and TTPS are early predictors of dysfunction. Surprisingly, 4/8 animals at 3 d with transmural infarcts on contrast enhanced MRI

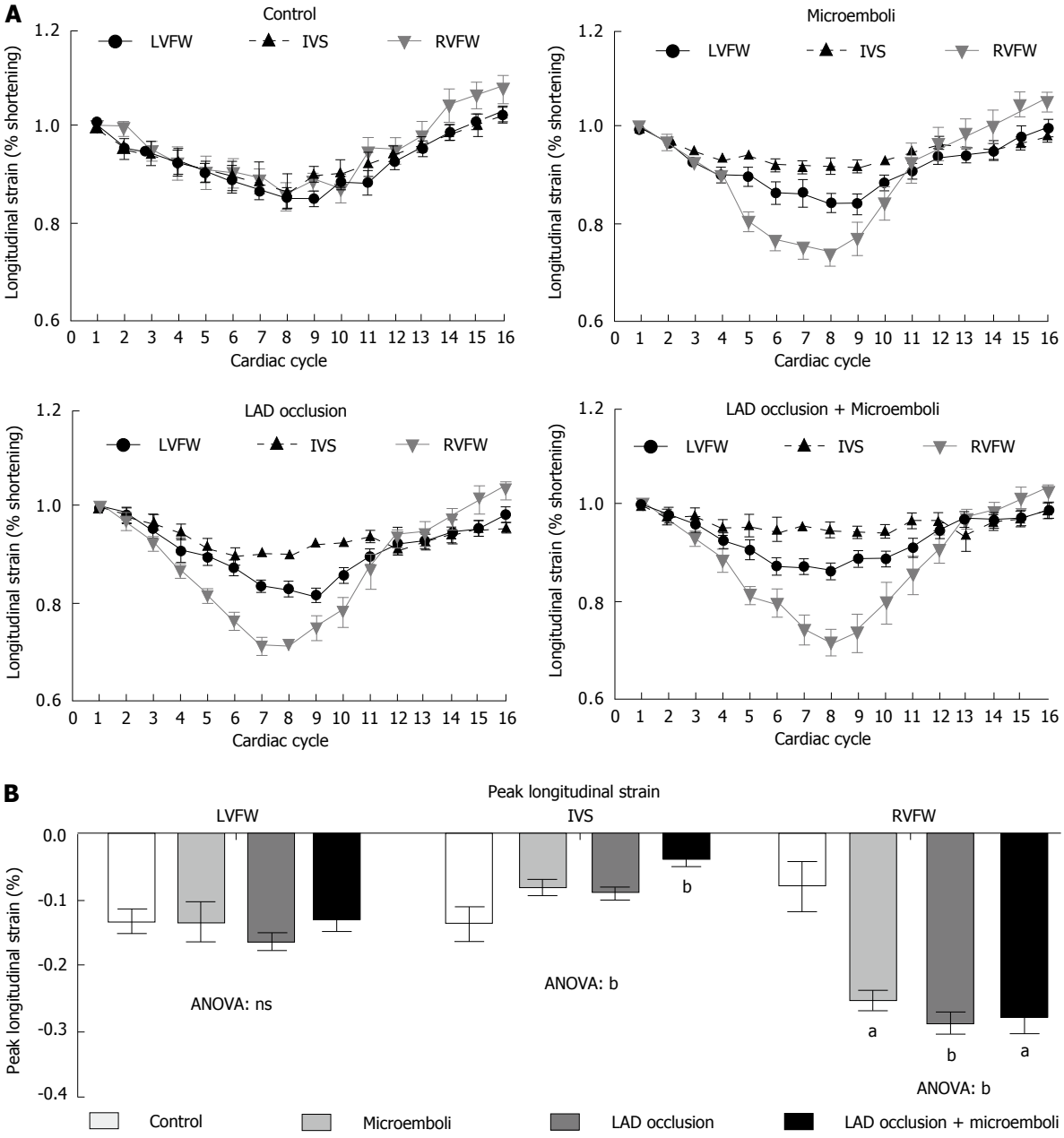

Figure 5 Longitudinal strain analysis: phasic and peak. A: Phasic longitudinal strain rate curves quantitatively show increased strain in right ventricular free wall (RVFW) and decreased strain in interventricular septum (IVS); B: Peak longitudinal strain. All interventions showed compensatory increase in peak strain in RVFW, while significantly decreased longitudinal peak strain was only seen in the IVS of combined insult animals. Data are presented as means ± SEM. Control *vs* Microemboli, [a]$P < 0.05$; Control *vs* LAD Occlusion, [b]$P < 0.01$. LAD: Location aid device; LVFW: Left ventricular free wall.

demonstrated circumferential strain, confirming previous findings that systolic and diastolic strain of an infarcted segment is complex interaction[31].

Investigators have found that interventricular dyssynchrony is another measure of prognosis[32]. Our data showed LV dyssynchrony in all interventions, as evidenced by increased TTPS in LAD territory and decreased TTPS in remote myocardium. It has been shown that patients with dyssynchrony are much more likely to develop LV remodeling than those without dyssynchrony (91% *vs* 2%)[33], because the pathophysiological remodeling process likely begins with a disorganized pattern of contraction[34]. In the current study, all interventions caused significant dyssynchrony and underscored the disproportion of infarct size to functional myocardial damage. We also found unique strain rate changes in remote myocardium related to microembolization only. These measurements may yield valuable information on the pathogenesis of ischemic cardiomyopathy, which seems to have similar remodeling and is still poorly understood[30].

Longitudinal strain

It has been shown that RV has greater longitudinal pumping component than the LV[8]. Our study showed that all coronary interventions caused significant increase in peak systolic longitudinal strain of the RVFW. The changes

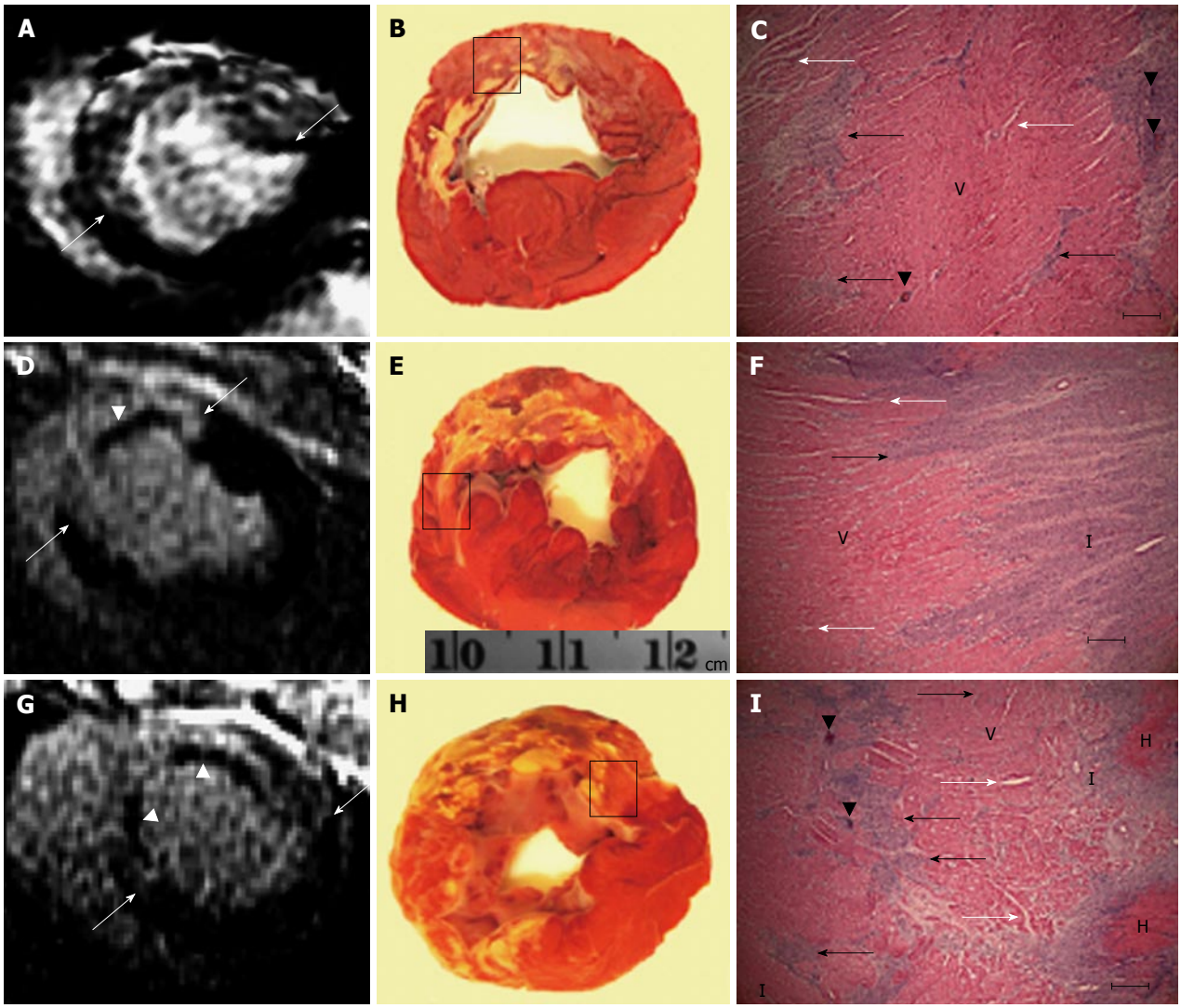

Figure 6 Viability contrast enhanced magnetic resonance images postmortem histochemical triphenyltetrazolium chloride stain and microscopy in animals subjected to soley microinfarction (top), soley location aid device occlusion/reperfusion (middle) and combined location aid device occlusion/reperfusion and microembolization (bottom). A: MR image and TTC stain show patchy microinfarct in the LAD territory; B: Postmortem histochemical TTC stain; C: Shows necrotic small islands (black arrows), interstitial edema (white arrow) and microemboli (black arrowhead); D: MR image shows the large infarct (white arrows) with hypoenhanced microvascular obstruction zone (white arrowhead); E: TTC section shows transmural infarct; F: Microinfarct tethering (black arrows) and interstial edema (white arrows) at the edge of the infarct; G: MR image shows the large infarct with patchy hyperenhanced microinfarct in the peri-infarct region (white arrows) with very large hypoenhanced microvascular obstruction zones (white arrowhead); H: TTC section shows hemorrhagic transmural infarct with patchy microinfarct in the peri-infarct region; I: Necrotic small islands (black arrows), interstitial edema (white arrow) and microemboli (black arrowhead). V: Viable myocardium, H: Hemorrhage; I: Large infarct. TTC: Triphenyltetrazolium chloride; MRI: Magnetic resonance imaging; LAD: Location aid device.

in the RVFW function after LV insult clearly indicate interventricular interaction and stressing the importance of evaluating both ventricles in cases of myocardial infarction. Previous studies have shown that longitudinal strain correlates to infarct size[35], Combined intervention impaired longitudinal strain in IVS that is not detectable in LAD occlusion/reperfusion group. It should be noted that our method for measuring peak systolic longitudinal strain is easy and quick enough to be applied in clinical practice. Furthermore, the acquired steady state free precession cine MR images can be used without the need to perform additional tagging imaging and it has been recently validated against spatial modulation of magnetization tissue tagging method[24]. We propose that the improvement in strain is an index of myocardial viability and is associated with global LV l improvement and may reverse remodeling, which is an important predictor of a favorable long-term outcome[26].

Study limitations

The synthetic microemboli used in this study may exhibit no inflammatory reaction, but previous enzymatic assay[36] and microscopy[16] demonstrated inflammatory reactions. Another limitation is that the longitudinal strain rate was not measured manually. A semi-automatic feature-tracking software has been recently used for assessing strain rate (TomTec Imaging Systems, Munich, Germany)[24].

In conclusion, this MRI study suggests that circum-

ferential and longitudinal strain and strain rate are sensitive and noninvasive indices of ventricular dysfunction. Patchy microinfarction is a complex ischemic injury, which features disproportionate functional impairment in the LV, including unique and dominant effects on global LV function that is not replicated by LAD occlusion/reperfusion, which represents "classic" acute MI. All interventions showed dynamic interaction between left and right ventricles. Furthermore, MRI has the potential to grade the severity of myocardial injury in various ischemic insults and identifies left and right ventricular dysfunction associated with myocardial damage.

ACKNOWLEDGMENTS

We would like to thank Loi Do and Carol Stillson for their technical support in the experimentation and archiving the images.

COMMENTS

Background

The use of percutaneous coronary intervention (PCI) has been a mainstay of treatment in acute myocardial infarctions in the past few decades. While these interventions are life-saving, they have been recently found to cause their own kinds of long term damage to the heart. Breaking of large clots into smaller ones causes these smaller microemboli to lodge in small blood vessels and damage the heart. Cardiac magnetic resonance imaging (MRI) is being used more frequently to study cardiac morphology and function, which was previously ascertained with less exact and operator-dependent methods, such as echocardiography. Cardiac MRI is thus an excellent imaging modality to assess damage after PCI.

Research frontiers

Research into the insidious effects of PCI has been improved with the use of cardiac MRI. While cardiac MRI has historically been used mostly in the imaging and follow up of congenital heart diseases, it is more frequently being used in routine clinical care and in the research settings of cardiac pathology that was once difficult to image precisely.

Innovations and breakthroughs

This article suggests that the effects of microemboli from PCI may be causing unique damage that has not previously been reported. Certain measurements of strain and strain rate, which are available only from cardiac MRI, demonstrated changes in the group of animals that had microemboli but not in those that simply had an occluded coronary without treatment. This suggests that the effects of PCI need to be more adequately studied. This paper also demonstrated and further validated a PCI model in swine.

Applications

This research should be taken into the context of the massive amount of literature in regards to percutaneous coronary intervention. While PCI may have risks, it is often a life-saving procedure and clinical practice should not change based on the results of this research. However, more research into the effects of PCI, especially the long term effects of microemboli, should be undertaken in order to adequately assess PCI risk and help to improve the procedure itself to prevent or alleviate these sequelae.

Terminology

Percutaneous coronary intervention: an intervention done by a cardiologist during AMIs, or "heart attacks" to relieve a blockage, usually from a clot, in the arteries that feed the heart. The most important of these arteries is the Left Anterior Descending artery, or location aid device. MRI is a form of imaging that utilizes a large magnet and radiofrequency pulses which does not cause any harmful radiation.

Peer review

This is a good study of the effects of microembolization from PCI on the cardiac function of swine. The results are interesting and suggest that PCI may have harmful effects that were not previously known. The long term changes in these effects needs to be further researched.

REFERENCES

1 **Thygesen K**, Alpert JS, White HD. Universal definition of myocardial infarction. *Eur Heart J* 2007; **28**: 2525-2538 [PMID: 17951287 DOI: 10.1093/eurheartj/ehm355]

2 **Anderson JL**, Adams CD, Antman EM, Bridges CR, Califf RM, Casey DE Jr, Chavey WE 2nd, Fesmire FM, Hochman JS, Levin TN, Lincoff AM, Peterson ED, Theroux P, Wenger NK, Wright RS, Smith SC Jr, Jacobs AK, Adams CD, Anderson JL, Antman EM, Halperin JL, Hunt SA, Krumholz HM, Kushner FG, Lytle BW, Nishimura R, Ornato JP, Page RL, Riegel B; American College of Cardiology; American Heart Association Task Force on Practice Guidelines (Writing Committee to Revise the 2002 Guidelines for the Management of Patients With Unstable Angina/Non-ST-Elevation Myocardial Infarction); American College of Emergency Physicians; Society for Cardiovascular Angiography and Interventions; Society of Thoracic Surgeons; American Association of Cardiovascular and Pulmonary Rehabilitation; Society for Academic Emergency Medicine. ACC/AHA 2007 guidelines for the management of patients with unstable angina/non-ST-Elevation myocardial infarction: a report of the American College of Cardiology/American Heart Association Task Force on Practice Guidelines (Writing Committee to Revise the 2002 Guidelines for the Management of Patients With Unstable Angina/Non-ST-Elevation Myocardial Infarction) developed in collaboration with the American College of Emergency Physicians, the Society for Cardiovascular Angiography and Interventions, and the Society of Thoracic Surgeons endorsed by the American Association of Cardiovascular and Pulmonary Rehabilitation and the Society for Academic Emergency Medicine. *J Am Coll Cardiol* 2007; **50**: e1-e157 [PMID: 17692738 DOI: 10.1016/j.jacc.2007.02.013]

3 **Lang RM**, Bierig M, Devereux RB, Flachskampf FA, Foster E, Pellikka PA, Picard MH, Roman MJ, Seward J, Shanewise JS, Solomon SD, Spencer KT, Sutton MS, Stewart WJ. Recommendations for chamber quantification: a report from the American Society of Echocardiography's Guidelines and Standards Committee and the Chamber Quantification Writing Group, developed in conjunction with the European Association of Echocardiography, a branch of the European Society of Cardiology. *J Am Soc Echocardiogr* 2005; **18**: 1440-1463 [PMID: 16376782 DOI: 10.1016/j.echo.2005.10.005]

4 **Møller JE**, Hillis GS, Oh JK, Reeder GS, Gersh BJ, Pellikka PA. Wall motion score index and ejection fraction for risk stratification after acute myocardial infarction. *Am Heart J* 2006; **151**: 419-425 [PMID: 16442909 DOI: 10.1016/j.ahj.2005.03.042]

5 **Reisner SA**, Lysyansky P, Agmon Y, Mutlak D, Lessick J, Friedman Z. Global longitudinal strain: a novel index of left ventricular systolic function. *J Am Soc Echocardiogr* 2004; **17**: 630-633 [PMID: 15163933 DOI: 10.1016/j.echo.2004.02.011]

6 **Thibault H**, Derumeaux G. Assessment of myocardial ischemia and viability using tissue Doppler and deformation imaging: the lessons from the experimental studies. *Arch Cardiovasc Dis* 2008; **101**: 61-68 [PMID: 18391875 DOI: 10.1016/S1875-2136(08)70257-2]

7 **Dicks DL**, Carlsson M, Heiberg E, Martin A, Saloner D, Arheden H, Saeed M. Persistent decline in longitudinal and radial strain after coronary microembolization detected on velocity encoded phase contrast magnetic resonance imaging. *J Magn Reson Imaging* 2009; **30**: 69-76 [PMID: 19557848 DOI: 10.1002/jmri.21773]

8 **Carlsson M**, Osman NF, Ursell PC, Martin AJ, Saeed M. Quantitative MR measurements of regional and global left ventricular function and strain after intramyocardial transfer of VM202 into infarcted swine myocardium. *Am J Physiol Heart Circ Physiol* 2008; **295**: H522-H532 [PMID: 18539758

DOI: 10.1152/ajpheart.00280.2008]
9 **Croisille P**, Moore CC, Judd RM, Lima JA, Arai M, McVeigh ER, Becker LC, Zerhouni EA. Differentiation of viable and nonviable myocardium by the use of three-dimensional tagged MRI in 2-day-old reperfused canine infarcts. *Circulation* 1999; **99**: 284-291 [PMID: 9892596 DOI: 10.1161/01.CIR.99.2.284]
10 **Götte MJ**, van Rossum AC, Twisk JWR JT, Visser CA. Quantification of regional contractile function after infarction: strain analysis superior to wall thickening analysis in discriminating infarct from remote myocardium. *J Am Coll Cardiol* 2001; **37**: 808-817 [PMID: 11693756 DOI: 10.1016/S0735-1097(00)01186-4]
11 **Marcus JT**, Götte MJ, Van Rossum AC, Kuijer JP, Heethaar RM, Axel L, Visser CA. Myocardial function in infarcted and remote regions early after infarction in man: assessment by magnetic resonance tagging and strain analysis. *Magn Reson Med* 1997; **38**: 803-810 [PMID: 9358455 DOI: 10.1002/mrm.1910380517]
12 **Migrino RQ**, Zhu X, Pajewski N, Brahmbhatt T, Hoffmann R, Zhao M. Assessment of segmental myocardial viability using regional 2-dimensional strain echocardiography. *J Am Soc Echocardiogr* 2007; **20**: 342-351 [PMID: 17400112 DOI: 10.1016/j.echo.2006.09.011]
13 **Rosendahl L**, Blomstrand P, Brudin L, Tödt T, Engvall JE. Longitudinal peak strain detects a smaller risk area than visual assessment of wall motion in acute myocardial infarction. *Cardiovasc Ultrasound* 2010; **8**: 2 [PMID: 20064264 DOI: 10.1186/1476-7120-8-2]
14 **Choi JW**, Gibson CM, Murphy SA, Davidson CJ, Kim RJ, Ricciardi MJ. Myonecrosis following stent placement: association between impaired TIMI myocardial perfusion grade and MRI visualization of microinfarction. *Catheter Cardiovasc Interv* 2004; **61**: 472-476 [PMID: 15065140 DOI: 10.1002/ccd.20024]
15 **Breuckmann F**, Nassenstein K, Bucher C, Konietzka I, Kaiser G, Konorza T, Naber C, Skyschally A, Gres P, Heusch G, Erbel R, Barkhausen J. Systematic analysis of functional and structural changes after coronary microembolization: a cardiac magnetic resonance imaging study. *JACC Cardiovasc Imaging* 2009; **2**: 121-130 [PMID: 19356544 DOI: 10.1016/j.jcmg.2008.10.011]
16 **Saeed M**, Hetts SW, Ursell PC, Do L, Kolli KP, Wilson MW. Evaluation of the acute effects of distal coronary microembolization using multidetector computed tomography and magnetic resonance imaging. *Magn Reson Med* 2012; **67**: 1747-1757 [PMID: 21956356 DOI: 10.1002/mrm.23149]
17 **Carlsson M**, Saloner D, Martin AJ, Ursell PC, Saeed M. Heterogeneous microinfarcts caused by coronary microemboli: evaluation with multidetector CT and MR imaging in a swine model. *Radiology* 2010; **254**: 718-728 [PMID: 20177087 DOI: 10.1148/radiol.09090527]
18 **Schwartz RS**, Burke A, Farb A, Kaye D, Lesser JR, Henry TD, Virmani R. Microemboli and microvascular obstruction in acute coronary thrombosis and sudden coronary death: relation to epicardial plaque histopathology. *J Am Coll Cardiol* 2009; **54**: 2167-2173 [PMID: 19942088 DOI: 10.1016/j.jacc.2009.07.042]
19 **Ordovas KG**, Carlsson M, Lease KE, Foster E, Meadows AK, Martin AJ, Hope M, Do L, Higgins CB, Saeed M. Impaired regional left ventricular strain after repair of tetralogy of Fallot. *J Magn Reson Imaging* 2012; **35**: 79-85 [PMID: 22002841 DOI: 10.1002/jmri.22686]
20 **Venkatesh BA**, Schiros CG, Gupta H, Lloyd SG, Dell'Italia L, Denney TS. Three-dimensional plus time biventricular strain from tagged MR images by phase-unwrapped harmonic phase. *J Magn Reson Imaging* 2011; **34**: 799-810 [PMID: 21769965 DOI: 10.1002/jmri.22665]
21 **Khalil M**, Fahmy A, Osman N. Correction of Left Ventricle Strain Signals Estimated from Tagged MR Images. *Int J Future Generation Commun and Net* 2010; **3**: 21
22 **Suffoletto MS**, Dohi K, Cannesson M, Saba S, Gorcsan J. Novel speckle-tracking radial strain from routine black-and-white echocardiographic images to quantify dyssynchrony and predict response to cardiac resynchronization therapy. *Circulation* 2006; **113**: 960-968 [PMID: 16476850 DOI: 10.1161/CIRCULATIONAHA.105.571455]
23 **Lim P**, Buakhamsri A, Popovic ZB, Greenberg NL, Patel D, Thomas JD, Grimm RA. Longitudinal strain delay index by speckle tracking imaging: a new marker of response to cardiac resynchronization therapy. *Circulation* 2008; **118**: 1130-1137 [PMID: 18725491 DOI: 10.1161/CIRCULATIONAHA.107.750190]
24 **Augustine D**, Lewandowski AJ, Lazdam M, Rai A, Francis J, Myerson S, Noble A, Becher H, Neubauer S, Petersen SE, Leeson P. Global and regional left ventricular myocardial deformation measures by magnetic resonance feature tracking in healthy volunteers: comparison with tagging and relevance of gender. *J Cardiovasc Magn Reson* 2013; **15**: 8 [PMID: 23331550 DOI: 10.1186/1532-429X-15-8]
25 **Wu KC**, Zerhouni EA, Judd RM, Lugo-Olivieri CH, Barouch LA, Schulman SP, Blumenthal RS, Lima JA. Prognostic significance of microvascular obstruction by magnetic resonance imaging in patients with acute myocardial infarction. *Circulation* 1998; **97**: 765-772 [PMID: 9498540 DOI: 10.1161/01.CIR.97.8.765]
26 **Galiuto L**. Optimal therapeutic strategies in the setting of post-infarct no reflow: the need for a pathogenetic classification. *Heart* 2004; **90**: 123-125 [PMID: 14729769 DOI: 10.1136/hrt.2003.020800]
27 **Funaro S**, Galiuto L, Boccalini F, Cimino S, Canali E, Evangelio F, DeLuca L, Paraggio L, Mattatelli A, Gnessi L, Agati L. Determinants of microvascular damage recovery after acute myocardial infarction: results from the acute myocardial infarction contrast imaging (AMICI) multi-centre study. *Eur J Echocardiogr* 2011; **12**: 306-312 [PMID: 21367810 DOI: 10.1093/ejechocard/jer009]
28 **Lorenz CH**, Pastorek JS, Bundy JM. Delineation of normal human left ventricular twist throughout systole by tagged cine magnetic resonance imaging. *J Cardiovasc Magn Reson* 2000; **2**: 97-108 [PMID: 11545133 DOI: 10.3109/10976640009148678]
29 **Voigt JU**, Arnold MF, Karlsson M, Hübbert L, Kukulski T, Hatle L, Sutherland GR. Assessment of regional longitudinal myocardial strain rate derived from doppler myocardial imaging indexes in normal and infarcted myocardium. *J Am Soc Echocardiogr* 2000; **13**: 588-598 [PMID: 10849513]
30 **Migrino RQ**, Zhu X, Morker M, Brahmbhatt T, Bright M, Zhao M. Myocardial dysfunction in the periinfarct and remote regions following anterior infarction in rats quantified by 2D radial strain echocardiography: an observational cohort study. *Cardiovasc Ultrasound* 2008; **6**: 17 [PMID: 18445286 DOI: 10.1186/1476-7120-6-17]
31 **Dang AB**, Guccione JM, Mishell JM, Zhang P, Wallace AW, Gorman RC, Gorman JH, Ratcliffe MB. Akinetic myocardial infarcts must contain contracting myocytes: finite-element model study. *Am J Physiol Heart Circ Physiol* 2005; **288**: H1844-H1850 [PMID: 15604126 DOI: 10.1152/ajpheart.00961.2003]
32 **Shin SH**, Hung CL, Uno H, Hassanein AH, Verma A, Bourgoun M, Køber L, Ghali JK, Velazquez EJ, Califf RM, Pfeffer MA, Solomon SD. Mechanical dyssynchrony after myocardial infarction in patients with left ventricular dysfunction, heart failure, or both. *Circulation* 2010; **121**: 1096-1103 [PMID: 20176989 DOI: 10.1161/CIRCULATIONAHA.109.863795]
33 **Mollema SA**, Bleeker GB, Liem SS, Boersma E, van der Hoeven BL, Holman ER, van der Wall EE, Schalij MJ, Bax JJ. Does left ventricular dyssynchrony immediately after acute myocardial infarction result in left ventricular dilatation? *Heart Rhythm* 2007; **4**: 1144-1148 [PMID: 17765611 DOI: 10.1016/j.hrthm.2007.05.018]
34 **Bilchick KC**, Helm RH, Kass DA. Physiology of biven-

tricular pacing. *Curr Cardiol Rep* 2007; **9**: 358-365 [PMID: 17877930]

35 **Cimino S**, Canali E, Petronilli V, Cicogna F, De Luca L, Francone M, Sardella G, Iacoboni C, Agati L. Global and regional longitudinal strain assessed by two-dimensional speckle tracking echocardiography identifies early myocardial dysfunction and transmural extent of myocardial scar in patients with acute ST elevation myocardial infarction and relatively preserved LV function. *Eur Heart J Cardiovasc Imaging* 2013; **14**: 805-811 [PMID: 23258316 DOI: 10.1093/ehjci/jes295]

36 **Charron T**, Jaffe R, Segev A, Bang KW, Qiang B, Sparkes JD, Butany J, Dick AJ, Freedman J, Strauss BH. Effects of distal embolization on the timing of platelet and inflammatory cell activation in interventional coronary no-reflow. *Thromb Res* 2010; **126**: 50-55 [PMID: 20541052 DOI: 10.1016/j.thromres.2010.03.012]

P- Reviewers: Razek AAKA, Sheehan JP
S- Editor: Qi Y **L- Editor**: A **E- Editor**: Liu SQ

World Journal of Radiology

Online Submissions: http://www.wjgnet.com/esps/
bpgoffice@wjgnet.com
doi:10.4329/wjr.v5.i12.484

World J Radiol 2013 December 28; 5(12): 484-490
ISSN 1949-8470 (online)

BRIEF ARTICLE

2-[18F]-fluoro-2-desoxy-D-glucose positron emission tomography initial staging impacts on survival in Hodgkin lymphoma

Juliano J Cerci, Camila C G Linardi, Luís F Pracchia, José Soares Junior, Evelinda Trindade, Dominique Delbeke, Rodrigo J Cerci, Robert Carr, José C Meneghetti, Valeria Buccheri

Juliano J Cerci, José Soares Junior, José C Meneghetti, Department of Nuclear Medicine, Heart Institute (InCor), University of São Paulo Medical School, São Paulo 05403-900, Brazil
Juliano J Cerci, Rodrigo J Cerci, Division of PET/CT, Quanta – Diagnóstico Nuclear, Curitiba 80045-170, Brazil
Camila C G Linardi, Luís F Pracchia, Valeria Buccheri, Division of Hematology, Clinical Hospital of the University of São Paulo Medical School, São Paulo 05403-900, Brazil
Evelinda Trindade, Health Technology Assessment/Executive Direction, Heart Institute (InCor), University of São Paulo Medical School, São Paulo 05403-900, Brazil
Dominique Delbeke, Department of Radiology and Radiological Sciences, Vanderbilt University Medical Center, Nashville, TN 37232, United States
Robert Carr, Department of Haematology, St Thomas' Hospital, London SE1 7EH, United Kingdom
Author contributions: Cerci JJ, Linardi CCG, Pracchia LF and Buccheri V contributed equally to this work performing research, study design, results analysis and writing the paper; Soares Junior J, Trindade E, Cerci RJ, Carr R, Delbeke D and Meneghetti JC contributed to design, analyze and write the paper.
Supported by The Brazilian Ministry of Health
Correspondence to: Juliano Julio Cerci, MD, PhD, Division of PET/CT, Quanta-Diagnóstico Nuclear, R. Almirante Tamandaré, 1000. Curitiba (PR), 80045-170, Brazil. cercijuliano@hotmail.com
Telephone: +55-41-33629778 Fax: +55-41-33629778
Received: September 4, 2013 Revised: October 17, 2013
Accepted: December 9, 2013
Published online: December 28, 2013

Abstract

AIM: To assess the prognostic value and risk classification improvement of metabolic staging (MS) with Initial 2-[18F]-fluoro-2-desoxy-D-glucose positron emission tomography (FDG-PET) in initial staging of Hodgkin's Lymphoma (HL) patients to predict 5 years overall survival (5y-OS) and event free survival (EFS).

METHODS: A total of 275 patients were included in this retrospective study, 155 patients were staged with conventional anatomical staging (AS), and 120 also submitted to MS (FDG-PET). Prognostic analysis compared 5y-OS and 5y-EFS of patients staged with AS and MS. Risk-adjusted models incorporated clinical risk factors, computed tomography and FDG-PET staging.

RESULTS: During the follow up of 267 evaluated patients, 220 (122 AS and 98 MS) achieved complete remission after first-line therapy (median follow-up: 70 ± 29 mo), treatment failure occurred in 79 patients and 34 died. The 5y-EFS for early *vs* advanced disease in AS patients was 79.3% and 66.7%, and 85.6% and 53.6% in MS patients, respectively ($P < 0.01$). The 5y-OS for early and advanced disease with AS was 91.3% and 81.5%, and 97.5% and 80.7% for patients staged with MS, respectively. Cox proportional hazards analysis demonstrated that FDG-PET added significant prognostic information and improved risk prediction ($P = 0.02$).

CONCLUSION: Initial staging FDG-PET could be used as an accurate and independent predictor of OS and EFS in HL, with impact in 5y-EFS and OS.

Key words: Hodgkin disease; Positron-emission tomography; 2-[18F]-fluoro-2-desoxy-D-glucose positron emission tomography; Neoplasm staging; Prognosis

Core tip: Initial 2-[18F]-fluoro-2-desoxy-D-glucose positron emission tomography (FDG-PET) has impact in

the determination of the event free survival and overall survival (OS) in Hodgkin's Lymphoma patients, also initial staging with FDG-PET was the strongest predictor of OS and event free survival of the evaluated variables analyzed. In the currently era of tailoring therapy to an individual level, initial staging might play an even more important role.

Cerci JJ, Linardi CCG, Pracchia LF, Soares Junior J, Trindade E, Delbeke D, Cerci RJ, Carr R, Meneghetti JC, Buccheri V. 2-[18F]-fluoro-2-desoxy-D-glucose positron emission tomography initial staging impacts on survival in Hodgkin lymphoma. *World J Radiol* 2013; 5(12): 484-490 Available from: URL: http://www.wjgnet.com/1949-8470/full/v5/i12/484.htm DOI: http://dx.doi.org/10.4329/wjr.v5.i12.484

INTRODUCTION

The anatomical extent, or stage, of disease is an important predictor of prognosis in Hodgkin's Lymphoma (HL). The method to determine disease stage at diagnosis has evolved over time. During the 1970s establishing the clinical extent of disease was based on clinical examination and laparotomy to assess abdominal disease[1]. During the 1980s computed tomography (CT) allowed more accurate assessment of the presence of enlarged visceral lymph nodes, increasing the staging precision, and then combining disease stage with other clinical signs to increase the accuracy of prognosis prediction at the time of diagnosis[2,3]. The Ann Arbor staging system, modified in Cotswolds in 1988 is used in the initial staging of Hodgkin lymphoma patients. Stage I indicates involvement of one lymph node chain, stage II indicates involvement of at least two lymph node chains, confined to one side of the diaphragm, stage III indicates involvement of lymph nodes from both sides of the diaphragm and stage IV indicates involvement at least one extra-lymphatic organ. The absence or presence of constitutional symptoms, like fever, weight loss or night sweating are denoted by adding "A" or "B" to the stage; respectively, and the presence of a large tumoral mass with at least 10 cm in the largest diameter is classified as bulky disease[2].

Since the 1990s, the introduction of positron emission tomography with 2-[18F]-fluoro-2-desoxy-D-glucose (FDG-PET) has enabled the detection of metabolically active tumors cells within anatomically normal lymph nodes and extranodal sites. A number of publications demonstrated the increased sensitivity of pre-treatment staging by PET compared to CT[4-8]. At that time, standard treatment for HL was based on the ABVD regimen irrespective of disease stage at diagnosis.

Subsequently, attention has focused on the use of PET to assess response to of treatment assessing the reduction of FDG after 2 or 3 cycles of chemotherapy[9-11]. Clinical interest has been directed to exploring the potential of early "metabolic" response assessment to reduce treatment, and therefore toxicity in rapid responders, or intensify treatment in slow responders to increase cure rates.

More recently, attempts to personalize treatment and increase cure has shifted the emphasis earlier, to focus on disease assessment at diagnosis and stratifying primary treatment intensity to match the better prognosis of early stage, and worse prognosis of late stage disease[12]. Initial treatment stratification is based on the premise that accurate staging, alone or as part of a prognostic index, predicts response to treatment and cure.

The availability of PET remains limited to major referral centers. Scarce evidence demonstrating the increased accuracy of metabolic staging by PET in comparison to anatomical staging by CT has been published. This increased accuracy would translate into greater discrimination between favorable and poor risk HL at the time of diagnosis. Therefore the aim of the current study was to establish whether PET staging translates into more accurate prediction of outcome. This information is not only clinically important, but also relevant to future planning of clinical PET indications.

MATERIALS AND METHODS

Patients

Patients presenting at the Hematology Division of the São Paulo University Clinics Hospital with newly diagnosed, biopsy proven, classical HL, between July 1999 and December 2007 were included in a this retrospective study comparing disease staging by CT or by PET. Patients included between 1999 and 2003 (Era 1) were imaged by CT, and from 2003 to the end of 2007 (Era 2) by PET in addition to CT. The Ethical Board of the Clinical Hospital of the University of São Paulo approved the study.

Staging by CT (Era 1)

All patients underwent clinical staging procedures including physical examination, complete blood cell counts and blood chemistry, CT scans (cervical, thoracic, abdomen and pelvic), and bilateral iliac crest bone marrow biopsy. CT scans were sectioned at a thickness of 1 mm, and oral and intravenous contrast agents were administered to all patients. Conventional anatomical staging (AS) of each patient was assigned according to the Ann Arbor staging system[1] modified during the Cotswold meeting based on CT imaging and results of bone marrow biopsy.

Staging by FDG-PET (Era 2)

Whole-body PET imaging was acquired after a 60 min uptake period following the intravenous administration of 296-444 MBq (8-12 mCi) of FDG. Imaging was performed using 2-D acquisition in a GE Advance PET scanner (GE Advance; GE Healthcare, Waukesha, Wisconsin, United States). Attenuation correction was performed using ^{68}Ge sources. Two experienced board-certified nuclear medicine physicians interpreted FDG-PET scan. Areas of non-physiological abnormalities

Table 1 Clinical characteristics of 267 patients with newly diagnosed hodgkin lymphoma *n* (%)

Characteristics	Era 1 150 patients AS	Era 2 117 patients MS	*P*
Gender			
Male	82 (54.7)	63 (52.5)	0.89
Age, median ± SD	33.4 ± 15.1	34.1 ± 16.1	0.25
Pathological subtype			
Nodular sclerosis	88 (58.7)	71 (59.2)	
Non classified	17 (11.3)	22 (18.3)	
Mixed cellularity	31 (20.7)	12 (10.0)	0.53
Lymphocyte predominance	12 (8.0)	9 (7.5)	
Lymphocyte depleted	2 (1.3)	6 (5.0)	
B symptoms	99 (66.0)	76 (65.0)	0.85
Bulky disease (> 7 cm)	91 (60.3)	67 (57.3)	0.74
Clinical stage			0.12
I	12 (8.0)	9 (7.7)	
II	61 (40.7)	45 (38.5)	
III	35 (23.3)	27 (23.1)	
IV	42 (28.0)	36 (30.8)	
Treatment failure	43 (28.7)	36 (30.8)	0.70
Death	20 (13.3)	14 (12.0)	0.73

AS: Anatomical staging; MS: Metabolic staging.

with increased FDG uptake over the background were classified as positive for disease. Involvement was defined according to the criteria established by the Consensus of the Imaging Subcommittee of International Harmonization Project in Lymphoma[4].

During Era 2 patients underwent CT, PET imaging and bone marrow biopsy. The interval between CT and PET scan was never longer than two weeks. Final stage assignment was based on information from both CT and PET, Metabolic stage (MS).

Treatment planning and outcome analysis were based on assignment of disease stage as determined by conventional AS in Era 1 and metabolic staging in Era 2.

Treatment and follow-up

Early stage I and II patients were treated with four to six cycles of chemotherapy using ABVD (doxorubicin, bleomycin, vinblastine and dacarbazine). Advanced stage III patients were treated with six to eight cycles (varying according to anatomical treatment response) of ABVD and all stage IV patients were treated with eight cycles of ABVD. Radiotherapy on involved fields was included in early stage I and II cases, as part of the combined modality therapy, after four cycles of chemotherapy, or when bulky disease was present, regardless of the clinical stage.

This approach to treatment of HL was the same throughout all the period of study, and did not change following the introduction of PET. Treatment was not modified by results of mid treatment scanning during the PET era.

Statistical analysis

Differences in categorical variables among groups were compared by the χ^2 test and differences in continuous variables among groups were compared by the Mann-Whitney test. The overall survival (OS) was calculated from the time of diagnosis to death from any cause or time of censoring and the event free survival (EFS) was calculated from the time of diagnosis to refractory disease, relapse, and death from any cause or time of censoring using the Kaplan-Meyer method. For the purpose of survival analysis patients were divided into Early Stage (I, II) and Advance Stage (III, IV) and the survival curves were compared by log-rank test. The effect of MS and AS on 5-year incidence of treatment failure and mortality risk were also determined using Cox regression models. Patients of Era 1 (AS) were censored if reached a maximum follow up of 5 years for the purpose of comparative analysis with patients of Era 2 (MS).

All statistical analyses were done using Stata Statistical Software, Release 11 (College Station, TX: StataCorp LP). A *P* value of 0.05 was considered statistically significant.

RESULTS

Clinical characteristics

This study population included 275 patients. Eight (2.8%) patients lost follow-up, therefore 267 patients (5/155 of AS and 3/120 of MS), were included in the final study cohort.

Table 1 shows the baseline clinical characteristics of the MS and AS groups. Baseline and clinical characteristics of patients were similar in both groups, with no statistical differences (Table 1).

Twenty six of the 117 Era 2 patients had their disease upstaged by PET, in comparison with anatomical staging (I→II, 5 patients; I→III, 1 patient; I→IV, 1 patient; II→IV, 4 patients, III→IV, 8 patients) and 14 had their disease downstaged (II→I, 3 patients; III→II, 4 patient; IV→I, 1 patient; IV→II, 2 patients; IV→III, 4 patients).

Follow up

During the follow up, 29.6% (79/267) patients presented treatment failure (refractory disease or relapse), includ-

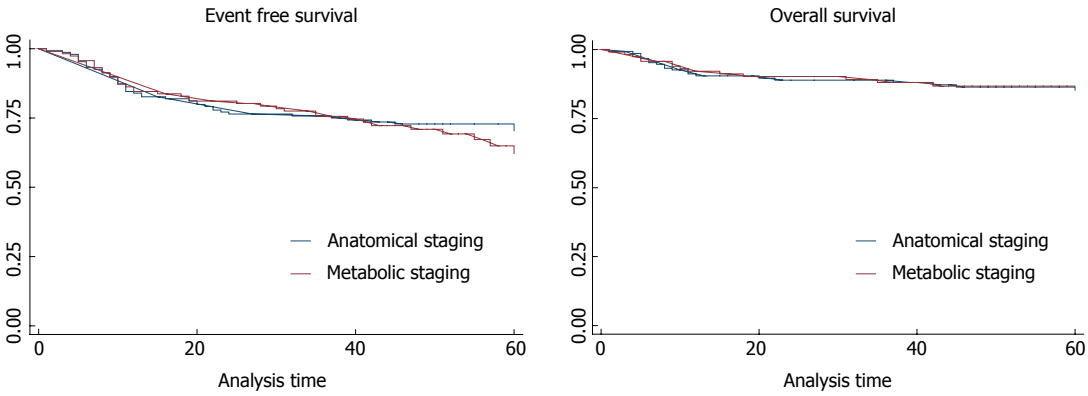

Figure 1 Kaplan-meier plot showing the overall survival and event free survival of conventional staging and metabolic staging in initial staging of Hodgkin lymphoma patients.

Table 2 Hazard ratio of clinical characteristics in the group of patients staged conventionally and with 2-[18F]-fluoro-2-desoxy-D-glucose positron emission tomography

	Five-year-EFS				Five-year-OS			
	AS		MS		CS		MS	
	HR (95%CI)	*P*	HR (95%CI)	*P*	HR (95%CI)	*P*	HR (95%CI)	*P*
Age (> 45, ≤ 45)	1.89 (0.95-3.76)	0.067	1.75 (0.86-3.57)	0.121	2.97 (1.18-7.47)	0.020	6.59 (2.20-19.68)	0.001
Gender	1.32 (0.72-2.44)	0.362	0.85 (0.44-1.63)	0.628	2.00 (0.76-5.20)	0.155	0.83 (0.29-2.38)	0.739
B symptoms	2.19 (1.05-4.57)	0.036	1.76 (0.82-3.76)	0.140	2.27 (0.76-6.81)	0.142	1.44 (0.45-4.61)	0.532
Bulky	0.94 (0.50-1.79)	0.868	0.94 (0.48-1.84)	0.869	1.06 (0.40-2.77)	0.899	0.41 (0.13-1.22)	0.111
Early vs advance clinical stage	2.05 (1.09-3.85)	0.024	2.73 (1.19-6.24)	0.017	2.51 (0.96-6.55)	0.059	8.09 (1.05-61.85)	0.044
Stage Ⅳ disease	2.42 (1.32-4.42)	0.004	2.33 (1.20-4.50)	0.012	3.67 (1.52-8.88)	0.004	6.54 (1.82-23.48)	0.004
Serum albumin	1.09 (.057-2.07)	0.775	1.52 (0.71-3.25)	0.273	2.12 (0.71-6.37)	0.178	1.91 (0.53-6.87)	0.318
Hemoglobin	1.50 (0.79-2.85)	0.206	1.35 (0.67-2.71)	0.399	2.47 (1.02-5.96)	0.044	1.43 (0.48-4.29)	0.514
White blood cell count	2.11 (1.03-4.30)	0.039	1.62 (0.62-4.18)	0.319	2.55 (1.84-8.2)	0.041	1.68 (0.37-7.54)	0.495
Lymphocyte count	1.81 (0.95-3.44)	0.067	2.61 (1.27-5.3)	0.009	2.44 (0.99-6.00)	0.050	2.84 (0.95-8.51)	0.061
IPI (0-2, ≥ 3)	3.41 (1.80-6.47)	0.000	2.08 (1.07-4.08)	0.031	3.74 (1.43-9.77)	0.007	4.98 (1.38-17.86)	0.014

IPI: International prognosis index; OS: Overall survival; EFS: Event free survival; AS: Anatomical staging; MS: Metabolic staging; CS: Conventional stage.

ing 28.6% (43/150) patients staged with AS and 30.7% (36/117) patients staged with MS. The median follow-up was 55 ± 16 mo; 45 ± 21 mo for patients staged with AS and 40 ± 18 mo for patients staged with MS. Moreover, 12.7% (34/267) patients died; 13.3% (20/150) patients staged with AS and 12% (14/117) patients staged with MS. All treatment failures were confirmed by biopsy. There were no statistical differences of treatment failure and mortality between the two groups (Table 1, Figure 1).

Staging and prognosis

The hazard ratios of clinical characteristics in the group of patients staged by CT and with FDG-PET are listed in Table 2. The evaluation with FDG-PET dividing patients with early and advance stage was the most important prognostic factor for EFS and OS in the MS group of patients, while international prognosis index was the most important in the AS group of patients.

The three- and five-year OS and EFS of AS and MS in initial staging of HL patients are shown in Table 3. The five-year EFS for early and advanced patients staged with AS was 79.3% and 66.7%, respectively; and 85.6% and 53.6% for patients staged with MS ($P < 0.01$). The five-year OS for early and advanced patients staged with AS was 91.3% and 81.5%, respectively; and 97.5% and 80.7% for patients staged with MS ($P = 0.04$). Figure 2 shows the Kaplan-Meier plot showing the OS and EFS for early and advance stage patients groups, staged with AS and MS.

When the EFS was evaluated in Era 2 patients according to their conventional staging, instead of their metabolic staging, the five-year EFS for early and advanced patients was 82.6% and 61.4%, respectively, instead of 85.6% and 53.6%. When the OS was evaluated in Era 2 patients according to their conventional staging, instead of their metabolic staging the five-year OS for early and advanced patients was 97.9% and 82.4%, respectively, instead of 97.5% and 80.7% (Figure 3).

DISCUSSION

The results of this single center study, with a standard-

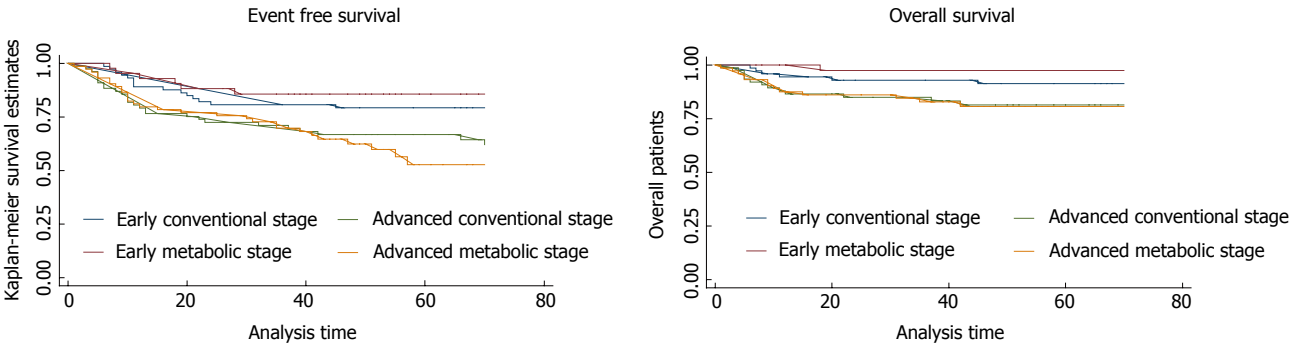

Figure 2 Kaplan-meier plot showing the overall survival and event free survival for early and advance stage patients groups, staged with anatomical staging and metabolic staging.

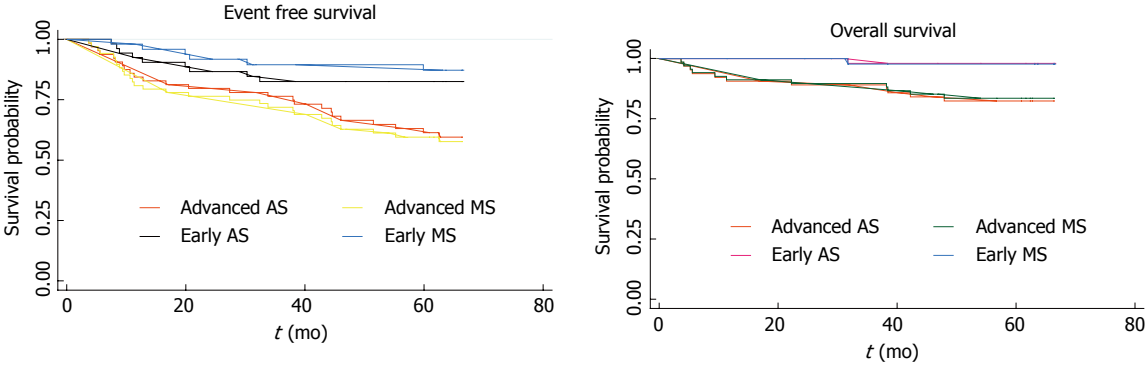

Figure 3 Kaplan-meier plot showing the overall survival and event free survival for early and advance stage Era 2 patients groups, staged with anatomical staging and metabolic staging. AS: Anatomical staging; MS: Metabolic staging.

ized protocol for treating early and advance stage disease, shows that the 5 years EFS for early and advanced patients staged with AS were 79.3% and 66.7%, and 85.6% and 53.6% for patients staged with MS, respectively ($P < 0.01$). The 5 years OS for early and advanced patients staged with AS was 91.3% and 81.5%, respectively; and 97.5% and 80.7% for patients staged with MS ($P = 0.04$). This demonstrates that MS has impact on EFS and OS.

In the last 20 years, FDG-PET has been shown to be more accurate then AS, changing clinical stage in about 30% of patients[5-8,13-16]. Although many studies compared CT and PET stage assignment, little data was presented on how this can be translated into outcomes. Munker *et al*[17], in a retrospective study evaluating 73 HL patients demonstrated a worse prognosis for the cases in which FDG-PET changed stage from I or II to III or IV. However, due to the limited time of follow-up, no difference in survival could be demonstrated between patients who remained in the same stage and patients who were upstaged by PET. Our results of 267 HL patients, with a longer follow up, shows that when staging takes full account of initial PET data, the separation of outcomes between early and advance stage HL becomes statistically significant regarding EFS, and clinically important with significant higher hazard ratios regarding OS and EFS. These differences are probably related to a better stratification of risk of these patients with FDG-PET, since no differences in therapy, supportive care and follow up were performed in this series of patients.

Also a great importance has been pointed that metabolic treatment response is more important than initial staging especially in HL[11,18-21]. Although current focus is on adapting therapy based on interim PET response, it is perhaps even more important to ensure the most appropriate initial staging, if taken into account the tendency is tailoring therapy with ABVD for early disease and BEACOPP for advance stage[22]. Therefore getting initial staging accuracy is even more important because it might influence primary therapy.

This study has some important limitations. Results are based on two series of cases, one staged conventionally and another subsequent series also staged with FDG-PET. However the spread of Ann Arbor stage and overall treatment outcome data is equivalent between the two series, demonstrating that both are equivalent in terms of patients and treatment. When the EFS of Era 2 patients classified according to metabolic staging was compared to the EFS of the same patients classified according to anatomical staging, it was also possible to observe a higher accuracy of the metabolic staging. Also, a randomized trial would be desirable, however in face of the amount of data showing the importance of MS, denying the FDG-PET evaluation in a group could be an ethical issue. Another limitation of the current study is the analysis of a patient population from a single health center. Several authors have extensively studied the performance of PET and PET/CT compared with CT over the past decades; as such, the compilation of multiple studies with

Table 3 The three- and five-year overall survival and event free survival of conventional staging and metabolic staging in initial staging of hodgkin lymphoma patients

Survival	150 Patients CS	117 Patients MS	267 Total patients
Three-year EFS			
Stage I	91.7%	100.0%	93.7%
Stage II	78.7%	84.4%	80.9%
Early stage	80.7%	85.6%	82.6%
Stage III	79.7%	76.7%	78.4%
Stage IV	63.7%	65.2%	64.5%
Advanced stage	71.0%	70.0%	70.5%
Five-year EFS			
Stage I	91.7%	100.0%	93.7%
Stage II	77.0%	84.4%	79.8%
Early stage	79.3%	85.6%	81.5%
Stage III	76.5%	69.0%	73.1%
Stage IV	58.6%	44.8%	53.7%
Advanced stage	66.7%	53.6%	61.9%
Three-year OS			
Stage I	91.7%	100.0%	93.7%
Stage II	93.2%	97.2%	94.8%
Early stage	93.0%	97.5%	94.6%
Stage III	94.2%	96.3%	95.2%
Stage IV	77.2%	74.2%	75.7%
Advanced stage	84.9%	82.8%	83.9%
Five-year OS			
Stage I	91.7%	100.0%	93.7%
Stage II	91.2%	97.2%	93.3%
Early stage	91.3%	97.5%	93.4%
Stage III	94.2%	90.9%	92.9%
Stage IV	71.1%	74.2%	72.5%
Advanced stage	81.5%	80.7%	81.1%

OS: Overall survival; EFS: Event free survival; CS: Conventional stage; MS: Metabolic staging.

larger series should be recommend.

COMMENTS

Background

Standard treatment for Hodgkin's Lymphoma (HL) was based on the ABVD regimen irrespective of disease stage at diagnosis. The aim of the current study was to establish whether positron emission tomography (PET) staging translates into more accurate prediction of outcome.

Research frontiers

This information is not only clinically important, but also relevant to future planning of clinical PET indications.

Innovations and breakthroughs

The results of the authors study indicate that Initial metabolic staging (MS) has impact in the determination of the event free survival (EFS) and overall survival (OS) in HL patients, also initial staging with 2-[18F]-fluoro-2-desoxy-D-glucose positron emission tomography (FDG-PET) is the strongest predictor of OS and EFS of the evaluated variables analyzed.

Applications

Initial staging with FDG-PET is the strongest predictor of OS and EFS of the evaluated variables analyzed. In the currently era of tailoring therapy to an individual level, initial staging might play an even more important role.

Peer review

The author reported the prognostic value and risk classification improvement of using MS with FDG-PET in initial staging of HL patients to predict 5 years OS and EFS, compared to conventional staging with computed tomography (CT). The conclusion is that initial staging of FDG-PET in HL is an accurate and independent predictor of OS and EFS. The difference in EFS and OS observed with two different staging systems may be explained by the fact that PET scan is more accurate in staging. Therefore, some of the early stages as determined by CT scan are upstaged to more advanced stages.

REFERENCES

1 **Carbone PP**, Kaplan HS, Musshoff K, Smithers DW, Tubiana M. Report of the Committee on Hodgkin's Disease Staging Classification. *Cancer Res* 1971; **31**: 1860-1861 [PMID: 5121694]

2 **Lister TA**, Crowther D, Sutcliffe SB, Glatstein E, Canellos GP, Young RC, Rosenberg SA, Coltman CA, Tubiana M. Report of a committee convened to discuss the evaluation and staging of patients with Hodgkin's disease: Cotswolds meeting. *J Clin Oncol* 1989; **7**: 1630-1636 [PMID: 2809679]

3 **Urba WJ**, Longo DL. Hodgkin's disease. *N Engl J Med* 1992; **326**: 678-687 [PMID: 1736106 DOI: 10.1056/NEJM199203053261006]

4 **Weihrauch MR**, Re D, Bischoff S, Dietlein M, Scheidhauer K, Krug B, Textoris F, Ansén S, Franklin J, Bohlen H, Wolf J, Schicha H, Diehl V, Tesch H. Whole-body positron emission tomography using 18F-fluorodeoxyglucose for initial staging of patients with Hodgkin's disease. *Ann Hematol* 2002; **81**: 20-25 [PMID: 11807631 DOI: 10.1007/s00277-001-0390-y]

5 **Jerusalem G**, Beguin Y, Fassotte MF, Najjar F, Paulus P, Rigo P, Fillet G. Whole-body positron emission tomography using 18F-fluorodeoxyglucose compared to standard procedures for staging patients with Hodgkin's disease. *Haematologica* 2001; **86**: 266-273 [PMID: 11255273]

6 **Hutchings M**, Loft A, Hansen M, Pedersen LM, Berthelsen AK, Keiding S, D'Amore F, Boesen AM, Roemer L, Specht L. Position emission tomography with or without computed tomography in the primary staging of Hodgkin's lymphoma. *Haematologica* 2006; **91**: 482-489 [PMID: 16585015]

7 **Pracchia LF**, Chaves AA, Cerci JJ, Soares Junior J, Meneghetti JC, Buccheri V. Metabolic test with fluorine-18-fluorodeoxyglucose in staging and detection of residual tumor or recurrence in Hodgkin lymphoma. *Clinics* (Sao Paulo) 2007; **62**: 121-126 [PMID: 17505695 DOI: 10.1590/S1807-59322007000200005]

8 **Cerci JJ**, Trindade E, Buccheri V, Fanti S, Coutinho AM, Zanoni L, Linardi CC, Celli M, Delbeke D, Pracchia LF, Pitela FA, Soares J, Zinzani PL, Meneghetti JC. Consistency of FDG-PET accuracy and cost-effectiveness in initial staging of patients with Hodgkin lymphoma across jurisdictions. *Clin Lymphoma Myeloma Leuk* 2011; **11**: 314-320 [PMID: 21816369 DOI: 10.1016/j.clml.2011.06.006]

9 **Hutchings M**, Loft A, Hansen M, Pedersen LM, Buhl T, Jurlander J, Buus S, Keiding S, D'Amore F, Boesen AM, Berthelsen AK, Specht L. FDG-PET after two cycles of chemotherapy predicts treatment failure and progression-free survival in Hodgkin lymphoma. *Blood* 2006; **107**: 52-59 [PMID: 16150944 DOI: 10.1182/blood-2005-06-2252]

10 **Gallamini A**, Hutchings M, Rigacci L, Specht L, Merli F, Hansen M, Patti C, Loft A, Di Raimondo F, D'Amore F, Biggi A, Vitolo U, Stelitano C, Sancetta R, Trentin L, Luminari S, Iannitto E, Viviani S, Pierri I, Levis A. Early interim 2-[18F]fluoro-2-deoxy-D-glucose positron emission tomography is prognostically superior to international prognostic score in advanced-stage Hodgkin's lymphoma: a report from a joint Italian-Danish study. *J Clin Oncol* 2007; **25**: 3746-3752 [PMID: 17646666 DOI: 10.1200/JCO.2007.11.6525]

11 **Cerci JJ**, Pracchia LF, Linardi CC, Pitella FA, Delbeke D, Izaki M, Trindade E, Soares J, Buccheri V, Meneghetti JC. 18F-FDG PET after 2 cycles of ABVD predicts event-free survival in early and advanced Hodgkin lymphoma. *J Nucl Med* 2010; **51**: 1337-1343 [PMID: 20720036 DOI: 10.2967/jnumed.109.073197]

12 **Uhm J**, Kuruvilla J. Treatment of newly diagnosed advanced stage Hodgkin lymphoma. *Blood Rev* 2012; **26**: 167-174 [PMID: 22542250 DOI: 10.1016/j.blre.2012.04.001]

13 **Cerci JJ**, Pracchia LF, Soares Junior J, Linardi Cda C, Meneghetti JC, Buccheri V. Positron emission tomography with 2-[18F]-fluoro-2-deoxy-D-glucose for initial staging of hodgkin lymphoma: a single center experience in Brazil. *Clinics*

(Sao Paulo) 2009; **64**: 491-498 [PMID: 19578651 DOI: 10.1590/S1807-59322009000600002]

14 **Bangerter M**, Moog F, Buchmann I, Kotzerke J, Griesshammer M, Hafner M, Elsner K, Frickhofen N, Reske SN, Bergmann L. Whole-body 2-[18F]-fluoro-2-deoxy-D-glucose positron emission tomography (FDG-PET) for accurate staging of Hodgkin's disease. *Ann Oncol* 1998; **9**: 1117-1122 [PMID: 9834825 DOI: 10.1023/A:1008486928190]

15 **Jerusalem G**, Hustinx R, Beguin Y, Fillet G. Positron emission tomography imaging for lymphoma. *Curr Opin Oncol* 2005; **17**: 441-445 [PMID: 16093792 DOI: 10.1097/01.cco.0000174041.29557.5c]

16 **Weihrauch MR**, Dietlein M, Schicha H, Diehl V, Tesch H. Prognostic significance of 18F-fluorodeoxyglucose positron emission tomography in lymphoma. *Leuk Lymphoma* 2003; **44**: 15-22 [PMID: 12691138 DOI: 10.1080/10428190210000402 51]

17 **Munker R**, Glass J, Griffeth LK, Sattar T, Zamani R, Heldmann M, Shi R, Lilien DL. Contribution of PET imaging to the initial staging and prognosis of patients with Hodgkin's disease. *Ann Oncol* 2004; **15**: 1699-1704 [PMID: 15520074 DOI: 10.1093/annonc/mdh426]

18 **Gallamini A**, Kostakoglu L. Interim FDG-PET in Hodgkin lymphoma: a compass for a safe navigation in clinical trials? *Blood* 2012; **120**: 4913-4920 [PMID: 22932799 DOI: 10.1182/blood-2012-03-403790]

19 **Mikhaeel NG**, Hutchings M, Fields PA, O'Doherty MJ, Timothy AR. FDG-PET after two to three cycles of chemotherapy predicts progression-free and overall survival in high-grade non-Hodgkin lymphoma. *Ann Oncol* 2005; **16**: 1514-1523 [PMID: 15980161 DOI: 10.1093/annonc/mdi272]

20 **Hutchings M**, Mikhaeel NG, Fields PA, Nunan T, Timothy AR. Prognostic value of interim FDG-PET after two or three cycles of chemotherapy in Hodgkin lymphoma. *Ann Oncol* 2005; **16**: 1160-1168 [PMID: 15939713 DOI: 10.1093/annonc/mdi200]

21 **Kostakoglu L**, Gallamini A. Interim 18F-FDG PET in Hodgkin lymphoma: would PET-adapted clinical trials lead to a paradigm shift? *J Nucl Med* 2013; **54**: 1082-1093 [PMID: 23818548 DOI: 10.2967/jnumed.113.120451]

22 **Blum KA**. Upcoming diagnostic and therapeutic developments in classical Hodgkin's lymphoma. *Hematology Am Soc Hematol Educ Program* 2010; **2010**: 93-100 [PMID: 21239777 DOI: 10.1182/asheducation-2010.1.93]

P- Reviewers: Chen F, Pan CX **S- Editor**: Ma YJ
L- Editor: A **E- Editor**: Liu SQ

World Journal of Radiology

Online Submissions: http://www.wjgnet.com/esps/
bpgoffice@wjgnet.com
doi:10.4329/wjr.v5.i12.491

World J Radiol 2013 December 28; 5(12): 491-497
ISSN 1949-8470 (online)

BRIEF ARTICLE

Hepatic abnormal perfusion visible by magnetic resonance imaging in acute pancreatitis

Wei Tang, Xiao-Ming Zhang, Zhao-Hua Zhai, Nan-Lin Zeng

Wei Tang, Xiao-Ming Zhang, Zhao-Hua Zhai, Nan-Lin Zeng, Sichuan Key Laboratory of Medical Image, Radiology Department, Affiliated Hospital of North Sichuan Medical College, Nanchong 637000, Sichuan Province, China

Author contributions: Tang W performed the majority of the procedures and wrote the manuscript; Zhang XM was involved in the conception and design of the study; Zhang XM and Zhai ZH edited the manuscript; and Zeng NL contributed to the data analysis and interpretation.

Correspondence to: Dr. Wei Tang, Sichuan Key Laboratory of Medical Image, Radiology Department, Affiliated Hospital of North Sichuan Medical College, Wenhua Road No. 63, Shunqing District, Nanchong 637000, Sichuan Province, China. tw-n-g-up@163.com
Telephone: +86-817-2262218 Fax: +86-817-2222856
Received: September 5, 2013 Revised: October 26, 2013
Accepted: November 18, 2013
Published online: December 28, 2013

Abstract

AIM: To study the prevalence and patterns of hepatic abnormal perfusion (HAP) visible by magnetic resonance imaging (MRI) in acute pancreatitis (AP).

METHODS: Enhanced abdominal MRI was performed on 51 patients with AP. These patients were divided into two groups according to the MRI results: those with signs of gallstones, cholecystitis, common bile duct (CBD) stones or dilatation of the CBD on MRI and those without. The prevalence, shape and distribution of HAP in the two groups were analyzed and compared. The severity of AP was graded using the MR severity index (MRSI). The correlation between the MRSI and HAP was then analyzed.

RESULTS: Of the 51 patients with AP, 32 (63%) showed at least one sign of gallbladder and CBD abnormalities on the MR images, while 19 (37%) showed no sign of gallbladder or CBD abnormalities. Nineteen patients (37%) had HAP visible in the enhanced images, including strip-, wedge- or patch-shaped HAP distributed in the hepatic tissue adjacent to the gallbladder and left and right liver lobes. There were no significant differences in the prevalence of HAP (χ^2 = 0.305, P = 0.581 > 0.05) or HAP distribution in the liver (χ^2 = 2.181, P = 0.536 > 0.05) between patients with and without gallbladder and CBD abnormalities. There were no significant differences in the MRSI score between patients with and without HAP (t = 0.559, P = 0.552 > 0.05). HAP was not correlated with the MRSI score.

CONCLUSION: HAP is common in patients with AP and appears strip-, patch- or wedge-shaped on MRI. HAP on MRI cannot be used to indicate the severity of AP.

Key words: Pancreatitis; Hepatic abnormal perfusion; Magnetic resonance imaging; Gallbladder

Core tip: Hepatic abnormal perfusion (HAP) due to acute pancreatitis on enhanced magnetic resonance imaging (MRI) presents as a strip-shaped abnormality of the hepatic tissue adjacent to the gallbladder or a patch- or wedge-shaped abnormality with lobar distribution in the liver, which is most likely caused by both the inflamed gallbladder and acute pancreatitis. Indications of HAP resulting from acute pancreatitis should not be misinterpreted as primary liver abnormalities. The presence of HAP on MRI cannot be used to indicate the severity of acute pancreatitis.

Tang W, Zhang XM, Zhai ZH, Zeng NL. Hepatic abnormal perfusion visible by magnetic resonance imaging in acute pancreatitis. *World J Radiol* 2013; 5(12): 491-497 Available from: URL: http://www.wjgnet.com/1949-8470/full/v5/i12/491.htm DOI: http://dx.doi.org/10.4329/wjr.v5.i12.491

INTRODUCTION

The pancreas is supplied by a rich plexus of arteries, derived from multiple branches of the coeliac trunk and superior mesenteric artery. Peripancreatic vessels are rich and complicated. Abnormal changes in major vessels and the microvasculature can be found in acute pancreatitis (AP), and the pathology of pancreatic and peripancreatic microcirculation has a significant impact on the early development and progression of the disease[1,2]. AP affects both the systematic and pancreatic vasculature[3-5]. The abnormal changes are not confined to the pancreas and may affect the gastrointestinal tract, liver, lung, kidney and skeletal muscle[6-11].

In AP, ex-pancreatic organ abnormalities are indicative of higher disease severity that can exacerbate pancreatic and systemic injury[1,10]. The identification of ex-pancreatic organ abnormalities is essential for predicting the severity of AP. Ex-pancreatic organ abnormalities have been found in the gallbladder and abdominal wall using magnetic resonance imaging (MRI); these abnormalities were correlated with the severity of AP[12,13].

The liver is adjacent to the pancreas; abnormalities may be observed in the liver early in the course of AP because of abnormal peripancreatic microcirculation[8]. Liver abnormality has also been identified using computed tomography (CT) in patients with AP, while hepatic perfusion disorder was found in a different anatomic site of the liver[14]. Other studies have used various terms for hepatic perfusion disorder including transient hepatic signal intensity differences, transient hepatic attenuation differences, or transient hepatic parenchyma enhancement[15-17]. This study refers to these phenomena as hepatic abnormal perfusion (HAP). Causes of HAP include hepatic vein abnormality, hepatic tumor, liver cirrhosis, inflammatory changes of the liver or organs adjacent to the liver, and others[15,16].

Imaging tools including CT and MRI play an important role in predicting the severity of AP by revealing abnormalities of the pancreas, peri-pancreas and ex-pancreatic organs[12,13,18-20]. Arita *et al*[14] reported that HAP in AP is most likely caused by increased arterial blood flow, the result of an inflamed lobe of the liver or inflamed gallbladder; HAP disappeared when AP had subsided in 5 of 28 patients (according to CT imaging). Is HAP related to the severity of AP and inflamed gallbladder?

To the best of our knowledge, this is the first report of HAP in AP on MRI. We present the spectrum of various HAP of AP visible by MRI, including the morphology, cause, prevalence, distribution, and pathogenesis of HAP as well as any association between HAP and the severity of AP.

MATERIALS AND METHODS

Patient population

This retrospective study was approved by our institutional review board. Patient informed consent was waived. Patients with AP admitted to our institution between February 2010 and February 2013 were considered for inclusion in this study. The diagnosis of AP was confirmed by the presence of acute typical abdominal pain and elevated serum levels of amylase or lipase, with levels three times normal indicating AP. The recruitment criteria for patients in this study were as follows: (1) AP at first onset; (2) enhanced abdominal MR examination; (3) upper abdominal MR examinations within 3 d of admission; (4) no related hepatic disease; (5) no hepatic vessel abnormality; and (6) the presence of a gallbladder.

Of the 51 patients enrolled in the study, there were 18 women and 33 men, with an average age of 49 ± 15 years (range 17 to 82 years).

MRI techniques

MRI was performed on a 1.5-T MR scanner with 38 mT/m gradients and 120 mT/m per second slope (Signa Excite; GE Medical Systems, Milwaukee, Wis), using a phased-array torso-pelvis coil. The sequences included axial fast spoiled gradient echo (FSPGR) T1-weighted imaging with fat suppression, gradient-echo (GRE) T1-weighted in-phase and out-of-phase MRI, respiratory-triggered (R-T) axial fast recovery fast spin-echo (FRFSE) T2-weighted MRI with fat suppression, coronal and axial single shot fast spin-echo (SSFSE) T2-weighted MRI, SSFSE radial series slabs MR cholangiopancreatography (MRCP), and three-dimension (3D) FSPGR dynamic enhanced MRI.

FSPGR T1-weighted imaging with fat suppression was obtained in 1 or 2 breath holds, with the following parameters: repetition time (TR, ms)/echo time (TE, ms) = 150-170/1.6; flip angle = 80°; matrix = 512 × 160-192; field of view (FOV) = 26-32 cm; section thickness = 5 mm; number of excitation (NEX) = 1; and sampling bandwidth = 20.8 kHz.

GRE in-phase and out-of-phase MRI were acquired during breath hold, with the following parameters: TR (ms)/TE (ms) = 150/4.4, 2.2; flip angle = 90°; matrix = 256 × 192-224; FOV = 26-32 cm; section thickness = 5 mm; NEX = 1; and sampling bandwidth = 31 or 62 kHz.

R-T FRFSE T2-weighted sequences were obtained with the following parameters: TR (ms)/TE (ms) = 10000-12000/90-100, TR determined by the frequency of respiration; section thickness = 5 mm; intersection gap = 0.5 mm; matrix = 256 × 192; NEX = 3; and FOV = 34 cm × 34 cm. The acquisition took approximately 3-4 min to complete.

Coronal and axial SSFSE T2-weighted images were obtained during breath hold, with the following parameters: TE = 90-100 ms; 2 s between slice acquisitions; section thickness = 5 mm; intersection gap = 0.5 mm; matrix = 384 × 224; one-half signal acquired; and FOV = 33 cm × 33 cm.

Radial oblique slab SSFSE images were obtained for MRCP with the following parameters: TE = 1300 ms; 6 s between image acquisitions; section thickness = 40 mm; matrix = 384 × 224; one-half signal acquired; and FOV = 30 cm × 30 cm.

Dynamic enhanced imaging was performed with an

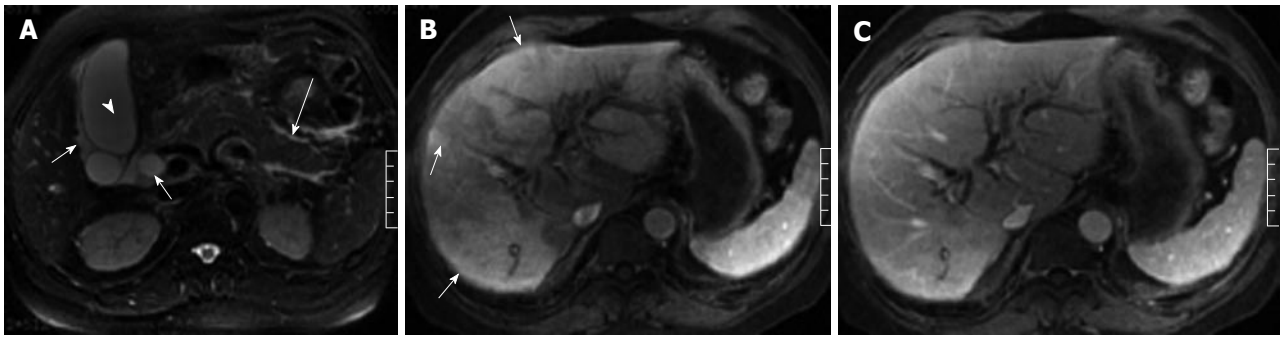

Figure 1 A 65-year-old man with acute pancreatitis combined with cholecystitis as well as common bile duct and intrahepatic bile duct dilatation. Fast recovery fast spin-echo T2-weighted image (A) shows gallbladder distention (arrowhead), perigallbladder fluid (short arrow), common bile duct dilatation (short arrow), and peripancreatic strand hyperintensity signal (long arrow). Patch- or wedge-shaped hepatic abnormal perfusion is found in the left and right lobes of the liver on the artery phase images (B, arrow) and returns to normal on the venous phase images (C).

axial fat saturated 3D FSPGR sequence. Gadolinium chelate was administered (0.2 mmol/L per kilogram of body weight) intravenously at approximately 3.5 mL/s by projector (Spectris MR Injection System, Medrad Inc., United States) injection, followed by a 20-mL saline solution flush. An additional delayed phase was acquired using 2D FSPGR fat suppression axial T1-weighted imaging.

MRI analysis

The original MRI data were loaded onto a computer workstation (GE, AW4.1, Sun Microsystems, Palo Alto, CA, United States) for review. Two observers (with 5 and 8 years' experience in interpreting abdominal MR images, respectively) independently reviewed MR images, and any discrepancies between the two reviewers were settled by consensus. The reviewed findings included: HAP was defined as an area of hepatic parenchyma enhancement that was different on the artery phase images, with a return to same signal intensity on venous phase images and delayed phase images compared with the surrounding normal hepatic tissues[15-17]. The presence or absence of HAP as well as the morphology and distribution of HAP in the liver were analyzed. Gallstones, cholecystitis, common bile duct (CBD) stones and dilatation of CBD: gallbladder and CBD stones were observed on T2 weight or MRCP images, which showed a hypointense area or a filling defect in the bright bile background[13]. Cholecystitis was diagnosed using MRI by identifying gallbladder wall thickening (more than 3 mm), gallbladder wall edema, gallbladder distention (diameter more than 40 mm), and pericholecystic fluid. The presence of one or more of the four criteria was indicative of cholecystitis[21,22]. Dilatation of the CBD was defined as the short diameter of the CBD over 7 mm on T2-weighted and MRCP images[23]. The severity of AP on the MRI was scored with the MR severity index (MRSI), which was derived from the CT severity index[18-20,24].

Statistical analyses

In China, the etiology of AP is closely related to the presence of gallbladder and common bile stones[13]. We therefore classified AP patients into two groups: those with gallbladder and CBD abnormalities (indicated by one or more signs of gallstones, cholecystitis, CBD stones and dilatation of CBD) and those without. The percentages of patients with HAP in all patients were calculated. The percentage of patients with HAP and the percentage of HAP distribution in the liver were calculated in each of the two groups. χ^2 tests were used to analyze the difference between the two groups for the prevalence of HAP and HAP distribution in the liver.

The MRSI is given as the range and the mean ± SD, and independent-sample *t* tests were used to test the difference between the patients with and without HAP.

Data analysis was performed using the Statistical Package for Social Sciences for Windows (Version 13.0, Chicago, IL, United States). $P \leqslant 0.05$ was considered significant.

RESULTS

Gallstones, cholecystitis, CBD stones and dilatation of CBD

Of the 51 patients with AP, 32 (63%) had at least one sign of gallbladder and CBD abnormalities on the MR images, and 19 (37%) showed no signs of gallbladder or CBD abnormalities. In the 32 patients with gallbladder and CBD abnormalities, gallbladder distention was found in 3 patients (Figure 1), pericholecystic fluid in 15 patients (Figures 1 and 2), gallbladder wall thickening in 19 patients, gallbladder wall edema in 4 patients, gallstones in 21 patients (Figure 3), CBD stones in 2 patients, and CBD dilation in 8 patients (Figures 1 and 3).

HAP

In the 51 patients with AP, 19 (37%) showed indications of HAP on enhanced images. Of the 19 patients with HAP, 15 (80%) had HAP on the arterial phase images and returned to normal on the venous phase images (Figures 1-4), while 4 (20%) had HAP on both the arterial and venous phase images with a return to normal on the delayed phase images (Figure 5).

In the 19 patients with HAP, there were 11 patients (58%) with gallbladder and CBD abnormalities and 8 patients (42%) without. The prevalence of HAP in patients with AP in combination with gallbladder or CBD abnor-

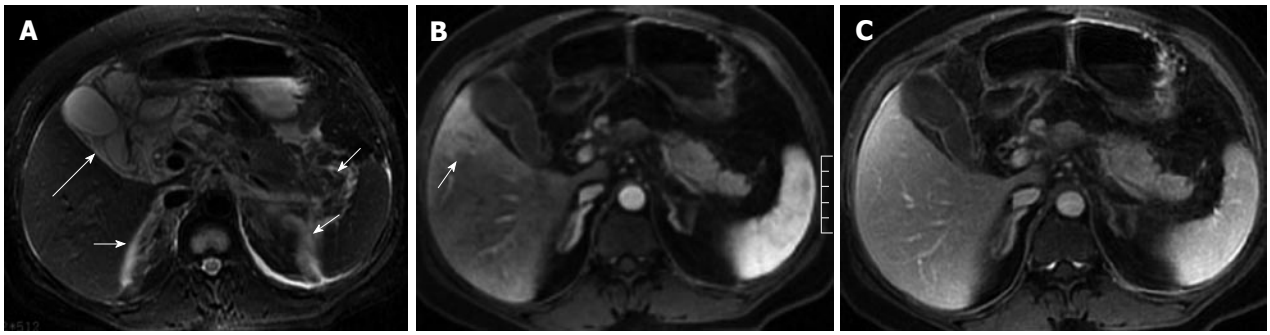

Figure 2 A 43-year-old woman with acute pancreatitis combined with cholecystitis. Respiratory-triggered axial fast recovery fast spin-echo T2-weighted image (A) shows the peripancreatic strand hyperintense signal and perinephric fluid collection (short arrow) as well as perigallbladder fluid (long arrow). Strip-shaped hepatic abnormal perfusion is found in the hepatic tissue adjacent to the gallbladder on the arterial phase images (B, arrow) and returns to normal on the venous phase images (C).

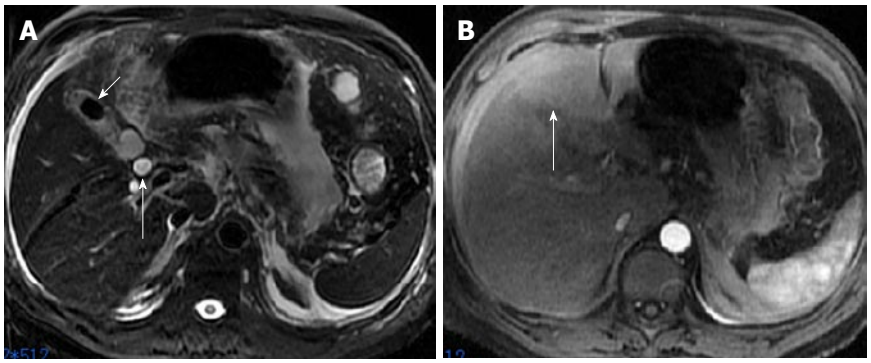

Figure 3 A 49-year-old man with acute pancreatitis combined with cholecystitis, gallbladder stone and common bile duct dilatation. Respiratory-triggered axial fast recovery fast spin-echo T2-weighted image (A) shows cholecystitis and gallbladder stones (short arrow) as well as common bile duct dilatation (long arrow). Patch- or wedge-shaped hepatic abnormal perfusion is found in the left lobe of the liver on arterial phase images (B, arrow).

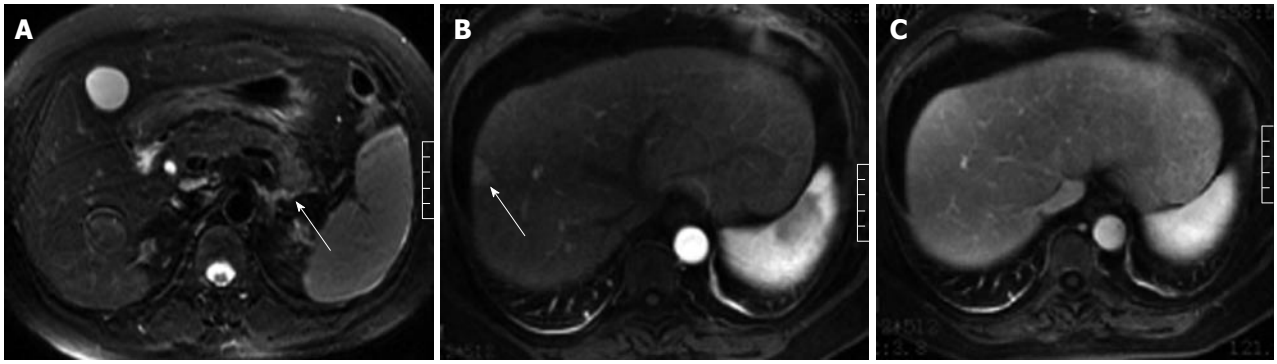

Figure 4 A 50-year-old woman with acute pancreatitis without gallbladder and common bile duct abnormalities. Fast recovery fast spin-echo T2-weighted image (A) shows peri-pancreatic strand hyperintensity signal (arrow). Wedge-shaped hepatic abnormal perfusion (arrow) is found in the right lobe of liver on the artery phase (B) and returns to normal on the venous phase images (C).

malities was greater than that in patients with AP without gallbladder or CBD abnormalities, but the difference between the two groups was not significant ($\chi^2 = 0.305$, $P = 0.581 > 0.05$) (Table 1).

Of the 11 patients with AP in combination with gallbladder and CBD abnormalities, 7 (64%) showed strip-shaped HAP in the hepatic tissues adjacent to the gallbladder (Figure 2), 2 (18%) showed wedge- or patch-shaped HAP in both the left and right hepatic lobes (Figure 1), 1 (9%) showed wedge- or patch-shaped HAP only in the right hepatic lobe, and 1 (9%) showed wedge- or patch-shaped HAP only in the left hepatic lobe (Figure 3).

In the 8 AP patients without gallbladder and CBD abnormalities, 3 (38%) showed strip-shaped HAP in hepatic tissues adjacent to the gallbladder, 1 (12%) showed wedge- or patch-shaped HAP in both the left and right hepatic lobes, 2 (25%) showed wedge- or patch-shaped HAP only in the right hepatic lobe (Figure 4), and 2 (25%) showed wedge- or patch-shaped HAP only in the left hepatic lobe (Figure 5).

There were no significant differences in the HAP distribution in the liver ($\chi^2 = 2.181$, $P = 0.536 > 0.05$) between the patients with and without gallbladder and CBD abnormalities (Table 2).

MRSI

In all 51 patients with AP, the mean MRSI was 2.7 ± 1.3, with scores ranging from 1 to 4. In the 19 patients with HAP, the mean MRSI was 3.2 ± 1.0, with scores ranging from 1 to 4. In the 32 patients without HAP, the mean

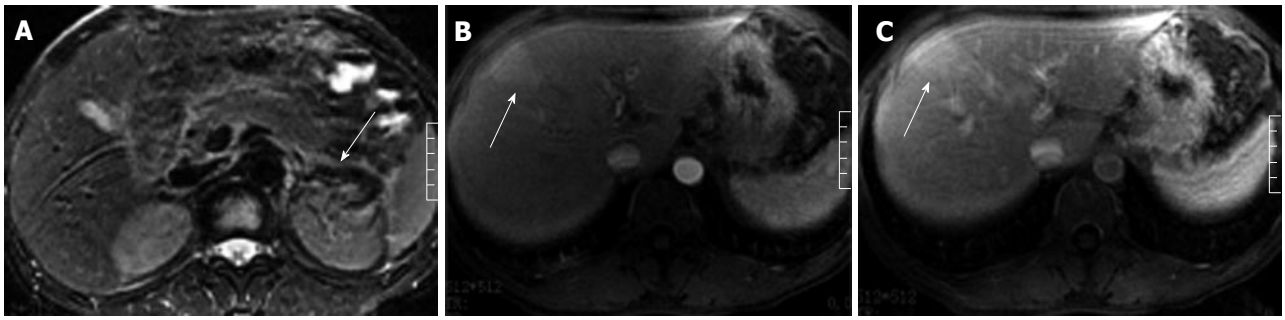

Figure 5 A 45-year-old man with acute pancreatitis without gallbladder or common bile duct abnormalities. Fast recovery fast spin-echo T2-weighted image (A) shows the left anterior pararenal space fluid collection (arrow). Wedge-shaped hepatic abnormal perfusion (arrow) is found in the left inner lobe of the liver on the arterial phase (B) and venous phase images (C).

Table 1 The visibility of hepatic abnormal perfusion in patients with acute pancreatitis

Acute pancreatitis (n = 51)	Visible hepatic abnormal perfusion	No visible hepatic abnormal perfusion
Acute pancreatitis combined with gallbladder and common bile duct abnormalities (group 1) (n = 32)	11	21
Acute pancreatitis without gallbladder and common bile duct abnormalities (group 2) (n = 19)	8	11

$\chi^2 = 0.305$, $P = 0.581 > 0.05$.

Table 2 Hepatic abnormal perfusion distribution in patients with hepatic abnormal perfusion

Patients with hepatic abnormal perfusion (n = 19)	Hepatic abnormal perfusion distribution in the liver			
	Adjacent to the gallbladder	Both left and right	Right	Left
Acute pancreatitis combined with gallbladder and common bile duct abnormalities (group 1) (n = 11)	7	2	1	1
Acute pancreatitis without gallbladder and common bile duct abnormalities (group 2) (n = 8)	3	1	2	2

$\chi^2 = 2.181$, $P = 0.536 > 0.05$.

MRSI was 3.0 ± 1.0, with scores ranging from 2 to 4. There were no significant differences in the MRSI scores between patients with and without HAP ($t = 0.559$, $P = 0.552 > 0.05$).

DISCUSSION

Pancreatic disease is related to gallbladder disorders because the gallbladder is located close to the pancreas[25,26]. Gallbladder abnormalities in carcinoma of the pancreatic head and AP have been reported[13,27]. In our study, 63% of patients with AP also showed signs of gallbladder and CBD abnormalities, which were discovered mainly by identifying cholecystitis on MRI images. The results demonstrate that gallbladder abnormalities are correlated with inflammation due to AP. Similarity, the inflammatory process of AP often spreads to the liver because the body of the pancreas is located close to the left lobe of the liver[14,28-30].

Inflammatory changes in the organs adjacent to liver can lead to HAP in the liver, as indicated by a previous study that reported HAP was found on CT images of patients with AP[14]. In our study, we used MRI images to categorize the patients with HAP into two groups: one group of patients with AP in combination with gallbladder and CBD abnormalities and another group of patients with AP and no gallbladder or CBD abnormality. Although the prevalence of HAP in patients with AP in combination with gallbladder and CBD abnormalities (58%) is higher than that in patients with AP but no gallbladder or CBD abnormalities (42%), there is no significant difference between the two groups. We speculate that the first cause of HAP in AP is the inflammatory process of AP spreading to the liver, while the second cause is the inflammatory process of cholecystitis spreading to the liver.

In the patients with AP and no gallbladder or CBD abnormalities, HAP was identified in hepatic tissue adjacent to the gallbladder (38%) and in the left and right lobes of the liver (62%). In patients with AP in combination with gallbladder and CBD abnormalities, HAP was identified in hepatic tissue adjacent to the gallbladder (64%) and in the left and right lobes of the liver (36%). There were no significant differences in the HAP distribution between the two groups. The distribution of HAP in AP is different from that of HAP caused only by

cholecystitis. HAP caused by cholecystitis is mainly distributed in hepatic tissue adjacent to the gallbladder, with no distribution on the left or right lobes of the liver[31,32]. Our results of the HAP distribution indicate that the biliary and pancreatic diseases influence each other because of their close anatomic site and related functions[25].

We found that HAP was strip, patch or wedge-shaped on enhanced MR images of patients with AP. Our results are similar to those obtained by Arita *et al*[14] by CT. The shape of HAP can elucidate the pathogenic mechanisms by which AP causes HAP. Strip-shaped HAP adjacent to the gallbladder is attributable to hepatic arterial hyperemia and increased venous drainage caused by the inflammatory process in the gallbladder[14,31]. Patch- and wedge-shaped HAP in the left and right lobes of the liver are caused by the inflammatory process of AP, which may spread to the liver through the hepatoduodenal ligament or gastrohepatic ligament toward the porta hepatis, finally spreading along the Glisson sheath; another pathway is through the lesser sac to the left lobe of the liver[28-30]. Understanding the pathway of AP spread can help predict the severity of AP.

MRSI is used for staging AP by grading both the degree of pancreatic and peripancreatic fluid and the extent of pancreatic necrosis. The sum of these parameters resulted in the development of an MRSI[18-20]. The MRSI has more advantages for predicting local complications and has a limited role in predicting systemic complications[19]. Ex-pancreatic organ abnormalities in patients with AP reflect systemic complications, as abdominal wall edema and gallbladder abnormalities were reported on MRI images. The presence of these abnormalities had a positive correlation with the severity of AP and may be a supplementary factor for grading the severity of AP[12,13]. In our study, HAP in AP had no correlation with the severity of AP identified using MRI. We speculate that HAP in AP is caused by both cholecystitis and AP, which is the reason for the correlation between HAP and the severity of AP.

In addition, in our study, 4 patients (20%) had HAP on the both arterial phase and venous phase images that returned to normal on the delayed phase images (Figure 1). This finding differs from another study on HAP. Another study reported that HAP was found on arterial phase images and returned to normal on venous phase images[15-17]. These special findings warrant further study.

In conclusion, the presence of HAP on enhanced MRI is common in patients with AP, which presents as strip-shaped in the hepatic tissue adjacent to the gallbladder and with a patch- or wedge-shaped lobar distribution in the liver. HAP is most likely caused by increased arterial blood flow attributable to both inflamed gallbladder and AP, and should not be misinterpreted as other primary liver abnormalities. The presence of HAP on MRI images cannot be used to determine the severity of AP.

COMMENTS

Background

In acute pancreatitis (AP), ex-pancreatic organ abnormality is a feature of disease severity that has the potential to exacerbate pancreatic and systemic injury. The identification of ex-pancreatic organ abnormality is essential in predicting the severity of AP. Hepatic abnormal perfusion (HAP) in AP is most likely caused by increased arterial blood flow due to the inflamed lobe of the liver or the inflamed gallbladder. Is HAP related to the severity of AP and the inflamed gallbladder?

Research frontiers

The abnormal changes in AP are not confined to the pancreas and may affect the gastrointestinal tract, liver, lung, kidney and skeletal muscle. In the area of AP, current research has focused on predicting the relationship between the severity of AP and ex-pancreatic organ abnormality using imaging tools.

Innovations and breakthroughs

In a previous study, HAP due to AP was found using computed tomography. However, there are no previous reports on the use of magnetic resonance imaging (MRI) to evaluate HAP in AP. the authors study presents information on HAP in patients with AP by using MRI, and discusses the morphology, cause, prevalence, distribution, and pathogenesis of HAP and any association with the severity of AP.

Applications

The study results suggest that HAP on enhanced MRI presents as strip-shaped in the hepatic tissue adjacent to the gallbladder, and as patch-shaped or wedge-shaped with lobar distribution in the liver. HAP on MRI cannot be used to determine the severity of AP.

Terminology

HAP is defined as an area with a hepatic parenchymal enhancement difference on arterial phase images that returns to the same signal intensity on venous phase images and delayed phase images compared with the surrounding normal hepatic tissues.

Peer review

This is a good descriptive study in which the authors analyze HAP due to AP visible by MRI. The results are interesting and suggest that HAP is common in AP and cannot be used to determine the severity of AP.

REFERENCES

1 **Cuthbertson CM**, Christophi C. Disturbances of the microcirculation in acute pancreatitis. *Br J Surg* 2006; **93**: 518-530 [PMID: 16607683 DOI: 10.1002/bjs.5316]

2 **Zhou ZG**, Chen YD, Sun W, Chen Z. Pancreatic microcirculatory impairment in experimental acute pancreatitis in rats. *World J Gastroenterol* 2002; **8**: 933-936 [PMID: 12378645]

3 **Beattie GC**, Hardman JG, Redhead D, Siriwardena AK. Evidence for a central role for selective mesenteric angiography in the management of the major vascular complications of pancreatitis. *Am J Surg* 2003; **185**: 96-102 [PMID: 12559436 DOI: 10.1016/S0002-9610(02)01199-6]

4 **Bergert H**, Hinterseher I, Kersting S, Leonhardt J, Bloomenthal A, Saeger HD. Management and outcome of hemorrhage due to arterial pseudoaneurysms in pancreatitis. *Surgery* 2005; **137**: 323-328 [PMID: 15746787 DOI: 10.1016/j.surg.2004.10.009]

5 **Inoue K**, Hirota M, Beppu T, Ishiko T, Kimura Y, Maeda K, Ogawa M. Angiographic features in acute pancreatitis: the severity of abdominal vessel ischemic change reflects the severity of acute pancreatitis. *JOP* 2003; **4**: 207-213 [PMID: 14614201]

6 **Schiller WR**, Anderson MC. Microcirculation of the normal and inflamed canine pancreas. *Ann Surg* 1975; **181**: 466-470 [PMID: 1130866]

7 **Chen HM**, Sunamura M, Shibuya K, Yamauchi JI, Sakai Y, Fukuyama S, Mikami Y, Takeda K, Matsuno S. Early microcirculatory derangement in mild and severe pancreatitis models in mice. *Surg Today* 2001; **31**: 634-642 [PMID: 11495159 DOI: 10.1007/s005950170098]

8 **Kelly DM**, McEntee GP, McGeeney KF, Fitzpatrick JM. Microvasculature of the pancreas, liver, and kidney in cerulein-induced pancreatitis. *Arch Surg* 1993; **128**: 293-295 [PMID: 8442685 DOI: 10.1001/archsurg.1993.01420150049009]

9 **Dobosz M**, Mionskowska L, Hac S, Dobrowolski S, Dymecki D, Wajda Z. Heparin improves organ microcirculatory dis-

turbances in caerulein-induced acute pancreatitis in rats. *World J Gastroenterol* 2004; **10**: 2553-2556 [PMID: 15300904]
10 **Foitzik T**, Eibl G, Hotz B, Hotz H, Kahrau S, Kasten C, Schneider P, Buhr HJ. Persistent multiple organ microcirculatory disorders in severe acute pancreatitis: experimental findings and clinical implications. *Dig Dis Sci* 2002; **47**: 130-138 [PMID: 11837713]
11 **Nishiwaki H**, Ko I, Hiura A, Ha SS, Satake K, Sowa M. Renal microcirculation in experimental acute pancreatitis of dogs. *Ren Fail* 1993; **15**: 27-31 [PMID: 8441833 DOI: 10.3109/08860229309065568]
12 **Yang R**, Jing ZL, Zhang XM, Tang W, Xiao B, Huang XH, Yang L, Feng ZS. MR imaging of acute pancreatitis: correlation of abdominal wall edema with severity scores. *Eur J Radiol* 2012; **81**: 3041-3047 [PMID: 22571930 DOI: 10.1016/j.ejrad.2012.04.005]
13 **Ji YF**, Zhang XM, Li XH, Jing ZL, Huang XH, Yang L, Zhai ZH. Gallbladder patterns in acute pancreatitis: an MRI study. *Acad Radiol* 2012; **19**: 571-578 [PMID: 22366559 DOI: 10.1016/j.acra.2012.01.004]
14 **Arita T**, Matsunaga N, Takano K, Hara A, Fujita T, Honjo K. Hepatic perfusion abnormalities in acute pancreatitis: CT appearance and clinical importance. *Abdom Imaging* 1999; **24**: 157-162 [PMID: 10024402 DOI: 10.1007/s002619900466]
15 **Colagrande S**, Centi N, Galdiero R, Ragozzino A. Transient hepatic intensity differences: part 1, Those associated with focal lesions. *AJR Am J Roentgenol* 2007; **188**: 154-159 [PMID: 17179358 DOI: 10.2214/AJR.05.1368]
16 **Colagrande S**, Centi N, Galdiero R, Ragozzino A. Transient hepatic intensity differences: part 2, Those not associated with focal lesions. *AJR Am J Roentgenol* 2007; **188**: 160-166 [PMID: 17179359 DOI: 10.2214/AJR.05.1367]
17 **Lupescu IG**, Grasu M, Capsa R, Pitrop A, Georgescu SA. Hepatic perfusion disorders: Computer-tomographic and magnetic resonance imaging. *J Gastrointestin Liver Dis* 2006; **15**: 273-279 [PMID: 17013453]
18 **Arvanitakis M**, Koustiani G, Gantzarou A, Grollios G, Tsitouridis I, Haritandi-Kouridou A, Dimitriadis A, Arvanitakis C. Staging of severity and prognosis of acute pancreatitis by computed tomography and magnetic resonance imaging-a comparative study. *Dig Liver Dis* 2007; **39**: 473-482 [PMID: 17363349 DOI: 10.1016/j.dld.2007.01.015]
19 **Tang W**, Zhang XM, Xiao B, Zeng NL, Pan HS, Feng ZS, Xu XX. Magnetic resonance imaging versus Acute Physiology And Chronic Healthy Evaluation II score in predicting the severity of acute pancreatitis. *Eur J Radiol* 2011; **80**: 637-642 [PMID: 20843620 DOI: 10.1016/j.ejrad.2010.08.020]
20 **Arvanitakis M**, Delhaye M, De Maertelaere V, Bali M, Winant C, Coppens E, Jeanmart J, Zalcman M, Van Gansbeke D, Devière J, Matos C. Computed tomography and magnetic resonance imaging in the assessment of acute pancreatitis. *Gastroenterology* 2004; **126**: 715-723 [PMID: 14988825 DOI: 10.1053/j.gastro.2003.12.006]
21 **Smith EA**, Dillman JR, Elsayes KM, Menias CO, Bude RO. Cross-sectional imaging of acute and chronic gallbladder inflammatory disease. *AJR Am J Roentgenol* 2009; **192**: 188-196 [PMID: 19098200 DOI: 10.2214/AJR.07.3803]
22 **Altun E**, Semelka RC, Elias J, Braga L, Voultsinos V, Patel J, Balci NC, Woosley JT. Acute cholecystitis: MR findings and differentiation from chronic cholecystitis. *Radiology* 2007; **244**: 174-183 [PMID: 17581902 DOI: 10.1148/radiol.2441060920]
23 **Songür Y**, Temuçin G, Sahin B. Endoscopic ultrasonography in the evaluation of dilated common bile duct. *J Clin Gastroenterol* 2001; **33**: 302-305 [PMID: 11588544 DOI: 10.1097/00004836-200110000-00009]
24 **Lecesne R**, Taourel P, Bret PM, Atri M, Reinhold C. Acute pancreatitis: interobserver agreement and correlation of CT and MR cholangiopancreatography with outcome. *Radiology* 1999; **211**: 727-735 [PMID: 10352598]
25 **Kimura W**. Surgical anatomy of the pancreas for limited resection. *J Hepatobiliary Pancreat Surg* 2000; **7**: 473-479 [PMID: 11180873 DOI: 10.1007/s005340070017]
26 **Jaffray C**, Yang J, Norman J. Elastase mimics pancreatitis-induced hepatic injury via inflammatory mediators. *J Surg Res* 2000; **90**: 95-101 [PMID: 10792947 DOI: 10.1006/jsre.2000.5832]
27 **Zhang XM**, Mitchell DG, Byun JH, Verma SK, Bergin D, Witkiewicz A. Gallbladder abnormalities in carcinoma of pancreatic head: findings on MR imaging. *Abdom Imaging* 2009; **34**: 507-513 [PMID: 18546035 DOI: 10.1007/s00261-008-9422-6]
28 **Meyers MA**, Oliphant M, Berne AS, Feldberg MA. The peritoneal ligaments and mesenteries: pathways of intraabdominal spread of disease. *Radiology* 1987; **163**: 593-604 [PMID: 3575702]
29 **Fujiwara T**, Takehara Y, Ichijo K, Tooyama N, Kodaira N, Yamamoto H, Watahiki H. Anterior extension of acute pancreatitis: CT findings. *J Comput Assist Tomogr* 1995; **19**: 963-966 [PMID: 8537534 DOI: 10.1097/00004728-199511000-00023]
30 **Siegelman SS**, Copeland BE, Saba GP, Cameron JL, Sanders RC, Zerhouni EA. CT of fluid collections associated with pancreatitis. *AJR Am J Roentgenol* 1980; **134**: 1121-1132 [PMID: 6770619 DOI: 10.2214/ajr.134.6.1121]
31 **Yamashita K**, Jin MJ, Hirose Y, Morikawa M, Sumioka H, Itoh K, Konish J. CT finding of transient focal increased attenuation of the liver adjacent to the gallbladder in acute cholecystitis. *AJR Am J Roentgenol* 1995; **164**: 343-346 [PMID: 7839966 DOI: 10.2214/ajr.164.2.7839966]
32 **Matsui O**, Takashima T, Kadoya M, Konishi H, Kawamura I, Hirose J, Kameyama T, Chohtou S. Staining in the liver surrounding gallbladder fossa on hepatic arteriography caused by increased cystic venous drainage. *Gastrointest Radiol* 1987; **12**: 307-312 [PMID: 2442058 DOI: 10.1007/BF01885168]

P- Reviewers: Pan CX, Sun ZH, **S- Editor**: Ma YJ
L- Editor: Wang TQ **E- Editor**: Liu SQ

World Journal of Radiology

Online Submissions: http://www.wjgnet.com/esps/
bpgoffice@wjgnet.com
doi:10.4329/wjr.v5.i12.498

World J Radiol 2013 December 28; 5(12): 498-502
ISSN 1949-8470 (online)

CASE REPORT

Dynamic ^{18}F-fluorodeoxyglucose positron emission tomography/CT in hibernoma: Enhanced tracer uptake mimicking liposarcoma

Christos Sachpekidis, Safwan Roumia, Matthias Schwarzbach, Antonia Dimitrakopoulou-Strauss

Christos Sachpekidis, Safwan Roumia, Antonia Dimitrakopoulou-Strauss, Medical Positron Emission Tomography Group-Biological Imaging, Clinical Cooperation Unit Nuclear Medicine, German Cancer Research Center, 69115 Heidelberg, Germany
Matthias Schwarzbach, Surgical Clinic, Klinikum Frankfurt Höchst, 65929 Frankfurt, Germany
Author contributions: Sachpekidis C performed positron emission tomography/CT scanning and wrote paper; Roumia S was attending physician and wrote paper; Schwarzbach M performed surgical operations; Dimitrakopoulou-Strauss A performed positron emission tomography/CT evaluations, organized and overviewed the report.
Correspondence to: Christos Sachpekidis, MD, Medical Positron Emission Tomography Group -Biological Imaging, Clinical Cooperation Unit Nuclear Medicine, German Cancer Research Center, Im Neuenheimer Feld 280, 69115 Heidelberg, Germany. christos_saxpe@yahoo.g
Telephone: +49-62-21422477 Fax: +49-62-21422476
Received: September 3, 2013 Revised: October 14, 2013
Accepted: October 18, 2013
Published online: December 28, 2013

Abstract

We report on two cases of patients with fat-equivalent masses in computed tomography (CT), referred to our department for dynamic positron emission tomography/CT (dPET/CT) with ^{18}F-fluorodeoxyglucose (^{18}F-FDG) in order to investigate their dignity. Both qualitative and quantitative information, as derived from dPET/CTs, couldn't exclude a high-grade liposarcoma: Visual evaluation, revealed a large hypermetabolic focus of intense ^{18}F-FDG uptake in each patient (average SUVs 8.3 and 11.3). Regression-based parametric imaging demonstrated an enhanced distribution volume, which correlates to perfusion, and a high phosphorylation rate that correlates to cell viability. Kinetic analysis, based on a two-tissue compartment model demonstrated an enhanced FDG transport k_1 and an enhanced phosphorylation rate k_3. A non-compartmental approach based on fractal dimension revealed also enhanced values. However, final diagnosis was based on biopsy, which revealed hibernoma, a benign brown fat tumor. Brown adipose contains increased numbers of mitochondria and a high-rate of glucose metabolism. Therefore, they have increased FDG uptake. The evaluation of lipomatous lesions on CT, with high FDG uptake, should include the possibility of hibernoma as a differential diagnosis.

Key words: Hibernoma; Dynamic positron emission tomography/CT; ^{18}F-fluorodeoxyglucose; Kinetic Modeling; Parametric imaging

Core tip: We report on two cases of patients with fat-equivalent masses in computed tomography (CT), referred to our department for dynamic positron emission tomography/CT (dPET/CT) with ^{18}F-fluorodeoxyglucose (^{18}F-FDG) in order to investigate their dignity. Both qualitative and quantitative information, as derived from dPET/CTs, couldn't exclude a high-grade liposarcoma. The evaluation of lipomatous lesions on CT, with high FDG uptake, should include the possibility of hibernoma as a differential diagnosis.

Sachpekidis C, Roumia S, Schwarzbach M, Dimitrakopoulou-Strauss A. Dynamic ^{18}F-fluorodeoxyglucose positron emission tomography/CT in hibernoma: Enhanced tracer uptake mimicking liposarcoma. *World J Radiol* 2013; 5(12): 498-502 Available from: URL: http://www.wjgnet.com/1949-8470/full/v5/i12/498.htm DOI: http://dx.doi.org/10.4329/wjr.v5.i12.498

INTRODUCTION

Hibernomas are benign soft tissue tumors arising from

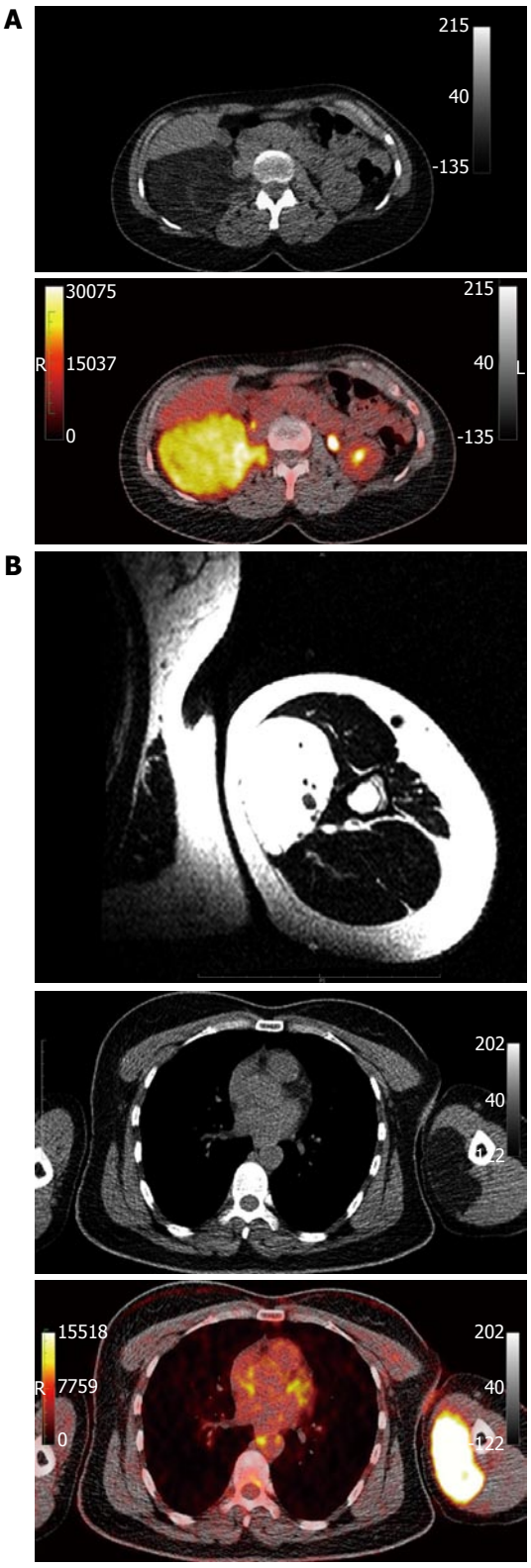

Figure 1 Computed tomography and magnetic resonance imaging. A: Computed tomography (upper row) and fused positron emission tomography/CT (PET/CT) (lower row) images of the retroperitoneal tumor; B: Magnetic resonance imaging (upper row), CT (middle row) and fused positron emission tomography/CT (PET/CT) (lower low) images of the tumor located in the left upper arm. Magnetic resonance imaging demonstrates a well-circumscribed mass without infiltration of the surrounding tissues. CT reveals a fat-equivalent mass, while PET/CT demonstrates intense fluorodeoxyglucose accumulation in the tumor area. CT: Computed tomography.

brown adipose tissue. Their pathogenesis is unknown and they give no symptoms. They are distinctly rare accounting for 1.6% of benign lipomatous tumors and approximately 1.1% of all adipocytic tumors[1]. Their peak incidence is in the third and fourth decades of life. Hibernomas are usually found in sites where brown fat persists beyond fetal life *e.g.*, shoulder, neck, retroperitoneum, back, thorax. As neither malignant transformation nor recurrence is expected, complete surgical resection is the treatment of choice[1,2]. The evaluation of hibernomas is a diagnostic challenge not only because of the rarity of the disease, but also because they are asymptomatic and present with atypical, non-specific imaging findings. Herein, we report on two cases of patients with fat-equivalent masses in computed tomography (CT) referred to our department for dynamic positron emission tomography/CT (dPET/CT) with ^{18}F-fluorodeoxyglucose (^{18}F-FDG). The main indication for their referral was the investigation of their metabolism and, more specifically, the differential diagnosis between lipomas and liposarcomas.

CASE REPORT

Two female patients (35 and 46 years old) were referred to our department from the surgical clinic for ^{18}F-FDG dPET/CT. These, otherwise healthy, patients demonstrated well-circumscribed fat-equivalent masses in CT in the anatomical areas of the retroperitoneum (7.8 cm × 10.2 cm × 17 cm) and the left upper arm (7 cm × 3 cm × 10 cm) respectively (Figure 1). The patients had also already gone through magnetic resonance imaging (MRI) that demonstrated a slight enhancement of contrast material without infiltration of the surrounding tissues; therefore, liposarcomas could not be excluded. The main indication for the referral of the patients for PET/CT was the metabolic/functional characterization of these masses, so that further information regarding their dignity would be derived. Moreover, whole body evaluation for potential metastases before treatment was another indication for the PET/CT scan.

The patients underwent dPET/CT after bolus application of ^{18}F-FDG. Evaluation of dPET/CTs was based on visual qualitative assessment of the fused PET/CT images, SUV calculation, parametric imaging, and absolute quantitative evaluation after application of a two-tissue compartment model and a non-compartment analysis. PET/CT images of the patients demonstrated two large hypermetabolic foci in the right retroperitoneum and the left medial part of the left upper arm (Figure 1). The average SUVs of these masses were 8.3 and 7.7, while their maximum SUVs were 11.3 and 13.5 respectively.

Regression-based parametric imaging was performed, leading to the calculation of intercept- and slope-parametric images. Intercept images revealed an enhanced distribution volume in both lesions, finding related to enhanced perfusion and blood volume; slope images demonstrated also an enhanced signal, implying a high

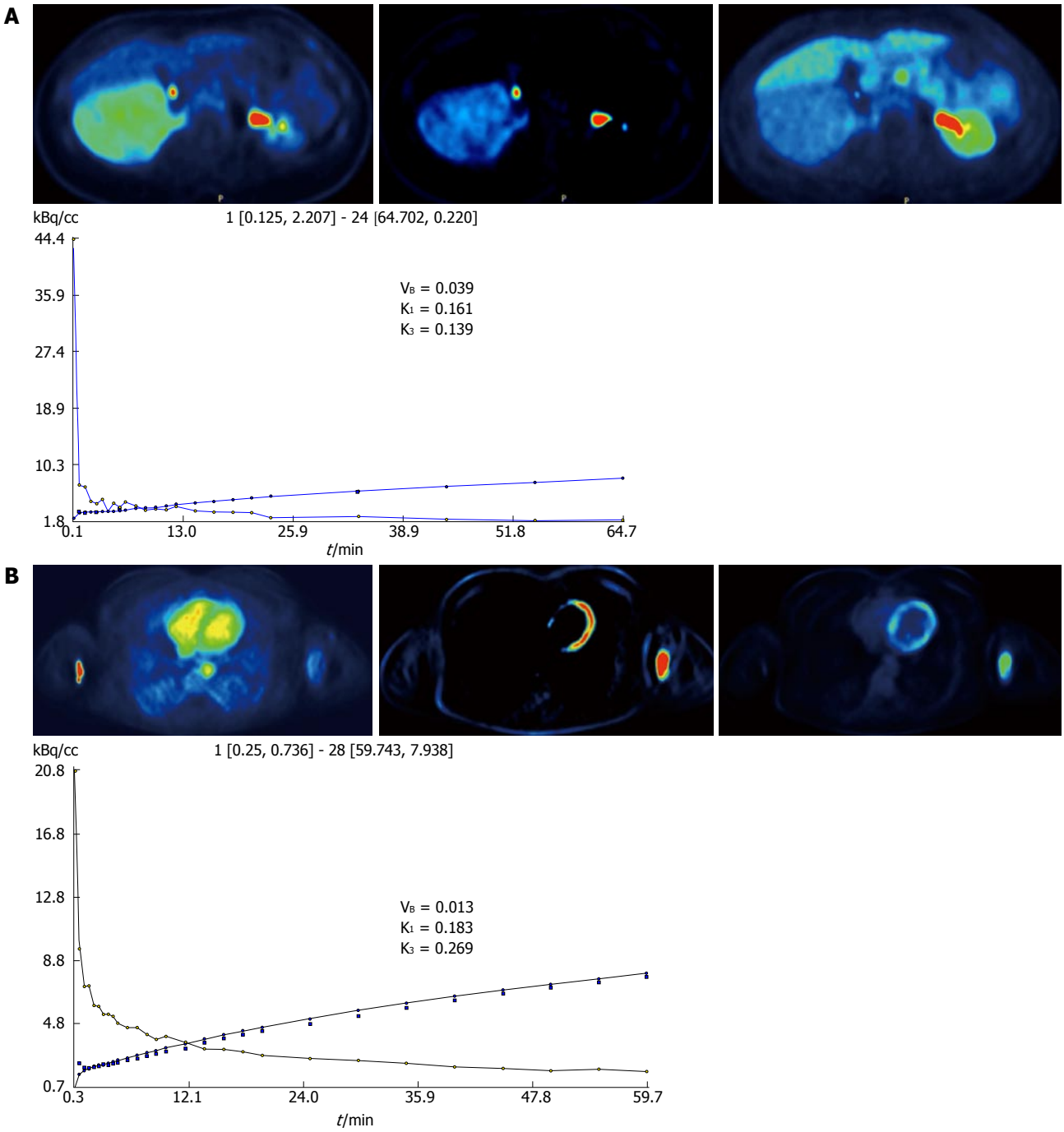

Figure 2 ^{18}F-fluorodeoxyglucose positron emission tomography study. A: ^{18}F-fluorodeoxyglucose (^{18}F-FDG) positron emission tomography (PET) study of the retroperitoneal tumor; B: ^{18}F-FDG PET study of the left upper arm tumor. Left row, FDG images (55-60 min after tracer injection) demonstrating an enhanced uptake in the left upper arm. Middle row, parametric images of the slope demonstrating an intense signal in the tumor area. Right row parametric images of the intercept demonstrating also an enhancement within the tumor area. The coordinate figure, corresponding time-activity curve of the ^{18}F-FDG kinetics after application of a two-tissue compartment model.

phosphorylation rate, which is related to cell viability (Figure 2)[3].

The application of a two-tissue compartment model led to the extraction of ^{18}F-FDG kinetic parameters that had high values. In particular, the parameter k_1, an indicator of intracellular FDG transport, had the values of 0.161 and 0.183 in the two tumors, while the indice k_3, which is a parameter of phosphorylation rate, was 0.139 and 0.269 respectively (Figure 2). A non-compartmental approach was also performed resulting in the acquisition of fractal dimension (FD), a parameter of tissue heterogeneity[4]. This analysis also revealed high FD values for the two patients (1.265 and 1.358 respectively).

Both qualitative and quantitative evaluation of dPET/CT studies revealed two tumors of highly active metabolism and perfusion. The features of these tumors led to the exclusion of lipomas as a potential diagnosis, rendering higher the possibility of high grade liposar-

comas. Although, their characteristics were not typical of this entity, since liposarcomas don't present with so intense characteristics in dPET/CT according to our experience, it was not possible to exclude a liposarcoma based on the PET data exclusively[5].

Final diagnosis was based on CT-guided biopsy, which revealed a hibernoma. The patients were treated with complete surgical resection of their tumors.

DISCUSSION

Hibernomas are benign, asymptomatic brown fat tumors with no malignant potential. They usually occur in the third to fourth decade of life, earlier than other soft tissue tumors. Macroscopically, they are well defined, encapsulated, hypervascular and soft, while their color ranges from tan to red brown, depending on the amount of intracellular lipids[6]. From a microscopical perspective, the tumor is characterized by the "hibernoma cells". These are large multivacuolated fat cells with eccentric nuclei, no/rare atypia and a small single round central nucleolus. There have been recognized four histologic variants of hibernomas: typical, myxoid, lipoma-like, and spindle cell hibernoma, all of them with a benign course[1]. Lipomas, the most common soft tissue tumors, typically occur in the fifth to sixth decade. Macroscopically, they are well-circumscribed masses, usually encapsulated, with a distinct lobular pattern. They have a pale yellow to tan color, with a lobular to smooth and variably greasy to myxoid cut surface. Microscopically, the mass consists of uniform in size and shape mature fat cells (adipocytes), while fat necrosis and other inflammatory changes may be seen when lipomas are traumatised[7]. Liposarcomas, on the other hand are the second most common soft tissue sarcomas following malignant fibrous histiocytomas[8]. They are typically deep seated and tend to affect adults between the ages of 40 and 60. The histologic spectrum of liposarcomas is very wide which is also reflected in the tumor's imaging. Liposarcomas are classified into four main groups: well differentiated (low grade; most common subtype), dedifferentiated (low grade), myxoid (intermediate grade) and pleomorphic liposarcomas (high grade)[9].

Since hibernomas are typically slow growing and asymptomatic, their early diagnosis is difficult. Differential diagnosis is not simple and includes lipoma, liposarcoma, rhabdomyosarcoma, resolving hematoma, and giant cell tumor; in the pediatric population, one should consider rhabdomyosarcoma and lymphoma. Therefore, imaging modalities are crucial in tumor detection and characterization. Among anatomical imaging modalities, CT and MRI play the most important role. CT depicts hibernoma as a well-defined mass with signal intensity intermediate between subcutaneous fat and muscle, which enhances variably after contrast injection[6]. MRI also shows the well-circumscribed mass, which, on T1- and T2-weighted images demonstrates high signal intensity but slightly less than that of the subcutaneous fat[10]. Although these radiologic findings help in differentiation and exclusion of some other tumor types, they are not hibernoma-specific. Lipomas appear on CT identical to subcutaneous fat demonstrating a homogeneous low attenuation, and no enhancement after administration of intravenous contrast. Similarly, on MRI signal intensity of a lipoma is identical to that of the subcutaneous adipose tissue on all pulse sequence. Regarding liposarcoma, its appearance on CT and MRI reflects the degree of tumor differentiation; the more differentiated the tumor, the more it resembles adipose fat tissue. Well-differentiated liposarcomas present as predominantly fat masses (at least 75% adipose tissue) with septa of variable thickness and shape. The other histologic subtypes of liposarcoma appear radiologically as tumors that typically contain less fat with significant amounts of soft-tissue, thus resulting in inhomogeneous CT and signal intensity (MRI)[11,12].

Despite their benign nature, many studies have shown that hibernomas demonstrate increased ^{18}F-FDG uptake in PET[13-15]. Moreover, the intense ^{18}F-FDG uptake observed in hibernomas has been proposed as a very meaningful technique to differentiate these tumors from liposarcomas[16]. In clinical oncological practice, increased FDG uptake raises the concern of a suspected mass to be malignant. However, ^{18}F-FDG is not a specific tumor tracer; any cause of increased glucose consumption can lead to enhanced FDG uptake. Brown fat uptake is a known, well-documented, normal variant of FDG uptake[17]. Brown adipose tissue contains increased numbers of mitochondria and a high rate of glucose metabolism. Therefore, brown fat cells have increased FDG uptake because of their high level of glucose metabolism rather than from tumor growth activity. This explains the intense FDG uptake of hibernomas, despite their lack of malignant potential. Except ^{18}F-FDG, other PET radiotracers have also been studied in soft tissue sarcomas; our group has evaluated the behavior of carbon-11-labeled aminoisobutyric acid and oxygen-15-labeled water (^{15}O-labeled water) in eleven histopathologically confirmed soft tissue sarcoma patients. Both radiotracers showed an increased activity in viable tumor with a significant differentiation from normal tissue, however the results were not tumor-specific[18].

In our cases, two well-circumscribed, fat-equivalent on CT masses were detected in two female patients of 35 and 46 years old. Both masses demonstrated very high FDG uptake on dPET/CT, with SUVs significantly higher than even SUVs detected in sarcomas[5]. Moreover, their parametric (intercept, slope) images were positive, indicating both enhanced perfusion and phosphorylation. The application of two-tissue compartment analysis and non-compartmental modeling also demonstrated high values (k_1, k_3, FD), rendering malignancy (high grade liposarcoma in our cases) a more possible diagnosis than a benign tumor (lipoma)[5,19]. However, despite all these malignancy-indicating qualitative and quantitative PET/CT findings, histopathology proved that both masses were benign and were characterized as hibernomas. Therapists moved on with complete tumor excision.

Hibernomas may be a diagnostic challenge based on the imaging findings, since they mimic often malignant

lesions. The evaluation of lipomatous lesions on CT, with high FDG uptake, should include the possibility of hibernoma as a differential diagnosis.

COMMENTS

Case characteristics

Hibernoma is a distinctly rare tumor, without specific symptoms or imaging features, representing therefore a diagnostic challenge.

Clinical diagnosis

We describe two cases of lipomatous tumors in two otherwise asymptomatic patients, eventually found out to suffer from hibernomas.

Differential diagnosis

Differential diagnosis is not simple and includes lipoma, liposarcoma, rhabdomyosarcoma, resolving hematoma, and giant cell tumor.

Laboratory diagnosis

No specific tumor marker or other biochemical index is specifically raised in the tumor.

Imaging diagnosis

Magnetic resonance imaging demonstrated well-circumscribed masses without infiltration of the surrounding tissues, computed tomography (CT) revealed fat-equivalent masses, while positron emission tomography/CT (PET/CT) demonstrated intense fluorodeoxyglucose (FDG) accumulation in the tumor areas.

Pathological diagnosis

CT-guided biopsy revealed hibernomas.

Treatment

Total surgical resection.

Term explanation

Dynamic PET/CT (dPET/CT) is an imaging modality that (in contrary to "classical" whole body PET/CT protocols) is based on dynamic scanning of the patient after bolus iv injection of a radiotracer. In addition to the standard diagnostic information acquired from static whole-body PET/CT studies, dPET/CT allows absolute quantitative data acquisition, based on compartment and non-compartment modeling, and furthermore renders possible the calculation of parametric images.

Experiences and lessons

In masses that appear as fat-equivalent on CT and also demonstrate enhanced FDG uptake on PET, the diagnosis of hibernoma should be considered.

Peer review

The authors first published dynamic PET/CT study in the rare tumor hibernoma. The semi-quantitative data (after SUV calculations), the absolute quantitative data (after application of two-tissue compartment modeling and non-compartment modeling) and parametric images that our group presents, are the first published for hibernomas.

REFERENCES

1 **Mavrogenis AF**, Coll-Mesa L. Soft tissue: Hibernom. Atlas Genet Cytogenet Oncol Haematol, 2012. Availabel from: URL: http://atlasgeneticsoncology.org/Tumors/HibernomaID5166.html

2 **Rigor VU**, Goldstone SE, Jones J, Bernstein R, Gold MS, Weiner S. Hibernoma. A case report and discussion of a rare tumor. *Cancer* 1986; **57**: 2207-2211 [PMID: 3697918 DOI: 10.1002/1097-0142(19860601)57:11<2207::AID-CNCR2820571122>3.0.CO;2-#]

3 **Dimitrakopoulou-Strauss A**, Pan L, Strauss LG. Quantitative approaches of dynamic FDG-PET and PET/CT studies (dPET/CT) for the evaluation of oncological patients. *Cancer Imaging* 2012; **12**: 283-289 [PMID: 23033440 DOI: 10.1102/1470-7330.2012.0033]

4 **Dimitrakopoulou-Strauss A**, Strauss LG, Burger C, Mikolajczyk K, Lehnert T, Bernd L, Ewerbeck V. On the fractal nature of positron emission tomography (PET) studies. *W J Nucl Med* 2003; **2**: 306-313

5 **Dimitrakopoulou-Strauss A**, Strauss LG, Schwarzbach M, Burger C, Heichel T, Willeke F, Mechtersheimer G, Lehnert T. Dynamic PET 18F-FDG studies in patients with primary and recurrent soft-tissue sarcomas: impact on diagnosis and correlation with grading. *J Nucl Med* 2001; **42**: 713-720 [PMID: 11337565]

6 **da Motta AC**, Tunkel DE, Westra WH, Yousem DM. Imaging findings of a hibernoma of the neck. *AJNR Am J Neuroradiol* 2006; **27**: 1658-1659 [PMID: 16971608]

7 **Weiss SW**, Goldblum JR. Enzinger and Weiss's Soft Tissue Tumors. 4th ed. St. Louis: Mosby, 2001: 571-641

8 **Kransdorf MJ**. Malignant soft-tissue tumors in a large referral population: distribution of diagnoses by age, sex, and location. *AJR Am J Roentgenol* 1995; **164**: 129-134 [PMID: 7998525 DOI: 10.2214/ajr.164.1.7998525]

9 **Fletcher DM**, Unni KK, Mertens F. Adipocytic tumors. In: WHO Classification of Soft Tissue Tumors. Pathology and Genetics: Tumors of Soft Tissue and Bone. Lyon, France: IARC Press, 2002: 19

10 **Meyers SP**. MRI of Bone and Soft Tissue Tumors and Tumorlike Lesions, Differential Diagnosis and Atlas. New York: Thieme Medical Pub, 2008: 543-554

11 **Kransdorf MJ**, Murphey MD. Imaging of Soft Tissue Tumors. 2nd ed. Lippincott Williams & Wilkins, Philadelphia, 2006: 80-150

12 **Kransdorf MJ**, Bancroft LW, Peterson JJ, Murphey MD, Foster WC, Temple HT. Imaging of fatty tumors: distinction of lipoma and well-differentiated liposarcoma. *Radiology* 2002; **224**: 99-104 [PMID: 12091667 DOI: 10.1148/radiol.2241011113]

13 **Chatterton BE**, Mensforth D, Coventry BJ, Cohen P. Hibernoma: intense uptake seen on Tc-99m tetrofosmin and FDG positron emission tomographic scanning. *Clin Nucl Med* 2002; **27**: 369-370 [PMID: 11953578 DOI: 10.1097/00003072-200205000-00016]

14 **Klein MA**, Scalcione LR, Youn T, Shah RA, Katz DS, Sung WW, Yung EY. Intensely hypermetabolic lipomatous hypertrophy of the interatrial septum on 18-FDG PET with MRI and CT correlation. *Clin Nucl Med* 2010; **35**: 972-973 [PMID: 21206236 DOI: 10.1097/RLU.0b013e3181f9dfeb]

15 **Nishida J**, Ehara S, Shiraishi H, Tada H, Satoh T, Okada K, Shimamura T. Clinical findings of hibernoma of the buttock and thigh: rare involvements and extremely high uptake of FDG-PET. *Med Sci Monit* 2009; **15**: CS117-CS122 [PMID: 19564831]

16 **Tsuchiya T**, Osanai T, Ishikawa A, Kato N, Watanabe Y, Ogino T. Hibernomas show intense accumulation of FDG positron emission tomography. *J Comput Assist Tomogr* 2006; **30**: 333-336 [PMID: 16628059]

17 **Lin E**, Alavi A. PET and PET/CT: a clinical guide. Thieme medical publisher, Inc. 2005: 32-55

18 **Schwarzbach M**, Willeke F, Dimitrakopoulou-Strauss A, Strauss LG, Mechtersheimer G, Hinz U, Lehnert T, Herfarth C. [Biologic characterization of soft tissue sarcomes by positron emission tomography (initial results)]. *Langenbecks Arch Chir Suppl Kongressbd* 1998; **115**: 635-639 [PMID: 14518332]

19 **Strauss LG**, Klippel S, Pan L, Schönleben K, Haberkorn U, Dimitrakopoulou-Strauss A. Assessment of quantitative FDG PET data in primary colorectal tumours: which parameters are important with respect to tumour detection? *Eur J Nucl Med Mol Imaging* 2007; **34**: 868-877 [PMID: 17219134 DOI: 10.1007/s00259-006-0319-8]

P- Reviewers: Chen F, El-Ghar MA, Triantopoulou C
S- Editor: Ma YJ **L- Editor**: A **E- Editor**: Liu XM

World Journal of Radiology

Online Submissions: http://www.wjgnet.com/esps/
bpgoffice@wjgnet.com
www.wjgnet.com

World J Radiol 2013 December 28; 5(12): I-V
ISSN 1949-8470 (online)

GENERAL INFORMATION

World Journal of Radiology (*World J Radiol*, *WJR*, online ISSN 1949-8470, DOI: 10.4329) is a peer-reviewed open access (OA) academic journal that aims to guide clinical practice and improve diagnostic and therapeutic skills of clinicians.

Aim and scope

WJR covers topics concerning diagnostic radiology, radiation oncology, radiologic physics, neuroradiology, nuclear radiology, pediatric radiology, vascular/interventional radiology, medical imaging achieved by various modalities and related methods analysis. The current columns of *WJR* include editorial, frontier, diagnostic advances, therapeutics advances, field of vision, mini-reviews, review, topic highlight, medical ethics, original articles, case report, clinical case conference (clinicopathological conference), and autobiography.

We encourage authors to submit their manuscripts to *WJR*. We will give priority to manuscripts that are supported by major national and international foundations and those that are of great basic and clinical significance.

WJR is edited and published by Baishideng Publishing Group (BPG). BPG has a strong professional editorial team composed of science editors, language editors and electronic editors. BPG currently publishes 41 OA clinical medical journals, and is one of the leading medical publishers, with the first-class editing and publishing capacity and production.

Columns

The columns in the issues of *WJR* will include: (1) Editorial: The editorial board members are invited to make comments on an important topic in their field in terms of its current research status and future directions to lead the development of this discipline; (2) Frontier: The editorial board members are invited to select a highly cited cutting-edge original paper of his/her own to summarize major findings, the problems that have been resolved and remain to be resolved, and future research directions to help readers understand his/her important academic point of view and future research directions in the field; (3) Diagnostic Advances: The editorial board members are invited to write high-quality diagnostic advances in their field to improve the diagnostic skills of readers. The topic covers general clinical diagnosis, differential diagnosis, pathological diagnosis, laboratory diagnosis, imaging diagnosis, endoscopic diagnosis, biotechnological diagnosis, functional diagnosis, and physical diagnosis; (4) Therapeutics Advances: The editorial board members are invited to write high-quality therapeutic advances in their field to help improve the therapeutic skills of readers. The topic covers medication therapy, psychotherapy, physical therapy, replacement therapy, interventional therapy, minimally invasive therapy, endoscopic therapy, transplantation therapy, and surgical therapy; (5) Field of Vision: The editorial board members are invited to write commentaries on classic articles, hot topic articles, or latest articles to keep readers at the forefront of research and increase their levels of clinical research. Classic articles refer to papers that are included in Web of Knowledge and have received a large number of citations (ranking in the top 1%) after being published for more than years, reflecting the quality and impact of papers. Hot topic articles refer to papers that are included in Web of Knowledge and have received a large number of citations after being published for no more than 2 years, reflecting cutting-edge trends in scientific research. Latest articles refer to the latest published high-quality papers that are included in PubMed, reflecting the latest research trends. These commentary articles should focus on the status quo of research, the most important research topics, the problems that have now been resolved and remain to be resolved, and future research directions. Basic information about the article to be commented (including authors, article title, journal name, year, volume, and inclusive page numbers); (6) Minireviews: The editorial board members are invited to write short reviews on recent advances and trends in research of molecular biology, genomics, and related cutting-edge technologies to provide readers with the latest knowledge and help improve their diagnostic and therapeutic skills; (7) Review: To make a systematic review to focus on the status quo of research, the most important research topics, the problems that have now been resolved and remain to be resolved, and future research directions; (8) Topic Highlight: The editorial board members are invited to write a series of articles (7-10 articles) to comment and discuss a hot topic to help improve the diagnostic and therapeutic skills of readers; (9) Medical Ethics: The editorial board members are invited to write articles about medical ethics to increase readers' knowledge of medical ethics. The topic covers international ethics guidelines, animal studies, clinical trials, organ transplantation, *etc.*; (10) Clinical Case Conference or Clinicopathological Conference: The editorial board members are invited to contribute high-quality clinical case conference; (11) Original Articles: To report innovative and original findings in radiology; (12) Brief Articles: To briefly report the novel and innovative findings in radiology; (13) Meta-Analysis: Covers the systematic review, mixedtreatment comparison, meta-regression, and overview of reviews, in order to summarize a given quantitative effect, *e.g.*, the clinical effectiveness and safety of clinical treatments by combining data from two or more randomized controlled trials, thereby providing more precise and externally valid estimates than those which would stem from each individual dataset if analyzed separately from the others; (15) Letters to the Editor: To discuss and make reply to the contributions published in *WJR*, or to introduce and comment on a controversial issue of general interest; (16) Book Reviews: To introduce and comment on quality monographs of radiology; and (17) Autobiography: The editorial board members are invited to write their autobiography to provide readers with stories of success or failure in their scientific research career. The topic covers their basic personal information and information about when they started doing research work, where and how they did research work, what they have achieved, and their lessons from success or failure.

Name of journal

World Journal of Radiology

ISSN

ISSN 1949-8470 (online)

Launch date

December 31, 2009

Frequency

Monthly

Editor-in-Chief

Filippo Cademartiri, MD, PhD, FESC, FSCCT, Professor, Cardio-Vascular Imaging Unit - Giovanni XXIII Hospital, Via Giovanni XXIII, 7 - 31050 - Monastier di Treviso (TV), Italy. filippocademartiri@gmail.com

Editorial Office
Jian-Xia Cheng, Director
Jin-Lei Wang, Vice Director
World Journal of Radiology
Room 903, Building D, Ocean International Center,
No. 62 Dongsihuan Zhonglu, Chaoyang District,
Beijing 100025, China
Telephone: +86-10-85381891
Fax: +86-10-85381893
E-mail: bpgoffice@wjgnet.com
http://www.wjgnet.com

Publisher
Baishideng Publishing Group Co., Limited
Flat C, 23/F., Lucky Plaza, 315-321 Lockhart Road,
Wanchai, Hong Kong, China
Telephone: +852-31779906
Fax: +852-65557188
E-mail: bpgoffice@wjgnet.com
http://www.wjgnet.com

Production center
Beijing Baishideng BioMed Scientific Co., Limited
Room 903, Building D, Ocean International Center,
No. 62 Dongsihuan Zhonglu, Chaoyang District,
Beijing 100025, China
Telephone: +86-10-85381892
Fax: +86-10-85381893

Representative office
USA Office
8226 Regency Drive,
Pleasanton, CA 94588-3144, United States
Telephone: +1-925-2238242
Fax: +1-925-2238243

Instructions to authors
Full instructions are available online at http://www.wjgnet.com/1948-5204/g_info_20100312180518.htm.

Indexed and Abstracted in
PubMed Central, PubMed, Digital Object Identifier, and Directory of Open Access Journals.

SPECIAL STATEMENT

All articles published in this journal represent the viewpoints of the authors except where indicated otherwise.

Biostatistical editing
Statisital review is performed after peer review. We invite an expert in Biomedical Statistics to evaluate the statistical method used in the paper, including *t*-test (group or paired comparisons), chi-squared test, Ridit, probit, logit, regression (linear, curvilinear, or stepwise), correlation, analysis of variance, analysis of covariance, *etc*. The reviewing points include: (1) Statistical methods should be described when they are used to verify the results; (2) Whether the statistical techniques are suitable or correct; (3) Only homogeneous data can be averaged. Standard deviations are preferred to standard errors. Give the number of observations and subjects (*n*). Losses in observations, such as drop-outs from the study should be reported; (4) Values such as ED50, LD50, IC50 should have their 95% confidence limits calculated and compared by weighted probit analysis (Bliss and Finney); and (5) The word 'significantly' should be replaced by its synonyms (if it indicates extent) or the *P* value (if it indicates statistical significance).

Conflict-of-interest statement
In the interests of transparency and to help reviewers assess any potential bias, *WJR* requires authors of all papers to declare any competing commercial, personal, political, intellectual, or religious interests in relation to the submitted work. Referees are also asked to indicate any potential conflict they might have reviewing a particular paper. Before submitting, authors are suggested to read "Uniform Requirements for Manuscripts Submitted to Biomedical Journals: Ethical Considerations in the Conduct and Reporting of Research: Conflicts of Interest" from International Committee of Medical Journal Editors (ICMJE), which is available at: http://www.icmje.org/ethical_4conflicts.html.

Sample wording: [Name of individual] has received fees for serving as a speaker, a consultant and an advisory board member for [names of organizations], and has received research funding from [names of organization]. [Name of individual] is an employee of [name of organization]. [Name of individual] owns stocks and shares in [name of organization]. [Name of individual] owns patent [patent identification and brief description].

Statement of informed consent
Manuscripts should contain a statement to the effect that all human studies have been reviewed by the appropriate ethics committee or it should be stated clearly in the text that all persons gave their informed consent prior to their inclusion in the study. Details that might disclose the identity of the subjects under study should be omitted. Authors should also draw attention to the Code of Ethics of the World Medical Association (Declaration of Helsinki, 1964, as revised in 2004).

Statement of human and animal rights
When reporting the results from experiments, authors should follow the highest standards and the trial should conform to Good Clinical Practice (for example, US Food and Drug Administration Good Clinical Practice in FDA-Regulated Clinical Trials; UK Medicines Research Council Guidelines for Good Clinical Practice in Clinical Trials) and/or the World Medical Association Declaration of Helsinki. Generally, we suggest authors follow the lead investigator's national standard. If doubt exists whether the research was conducted in accordance with the above standards, the authors must explain the rationale for their approach and demonstrate that the institutional review body explicitly approved the doubtful aspects of the study.

Before submitting, authors should make their study approved by the relevant research ethics committee or institutional review board. If human participants were involved, manuscripts must be accompanied by a statement that the experiments were undertaken with the understanding and appropriate informed consent of each. Any personal item or information will not be published without explicit consents from the involved patients. If experimental animals were used, the materials and methods (experimental procedures) section must clearly indicate that appropriate measures were taken to minimize pain or discomfort, and details of animal care should be provided.

SUBMISSION OF MANUSCRIPTS

Manuscripts should be typed in 1.5 line spacing and 12 pt. Book Antiqua with ample margins. Number all pages consecutively, and start each of the following sections on a new page: Title Page, Abstract, Introduction, Materials and Methods, Results, Discussion, Acknowledgements, References, Tables, Figures, and Figure Legends. Neither the editors nor the publisher are responsible for the opinions expressed by contributors. Manuscripts formally accepted for publication become the permanent property of Baishideng Publishing Group Co., Limited, and may not be reproduced by any means, in whole or in part, without the written permission of both the authors and the publisher. We reserve the right to copy-edit and put onto our website accepted manuscripts. Authors should follow the relevant guidelines for the care and use of laboratory animals of their institution or national animal welfare committee. For the sake of transparency in regard to the performance and reporting of clinical trials, we endorse the policy of the ICMJE to refuse to publish papers on clinical trial results if the trial was not recorded in a publicly-accessible registry at its outset. The only register now available, to our knowledge, is http://www.clinicaltrials.gov sponsored by the United States National Library of Medicine and we encour-

age all potential contributors to register with it. However, in the case that other registers become available you will be duly notified. A letter of recommendation from each author's organization should be provided with the contributed article to ensure the privacy and secrecy of research is protected.

Authors should retain one copy of the text, tables, photographs and illustrations because rejected manuscripts will not be returned to the author(s) and the editors will not be responsible for loss or damage to photographs and illustrations sustained during mailing.

Online submissions

Manuscripts should be submitted through the Online Submission System at: http://www.wjgnet.com/esps/. Authors are highly recommended to consult the ONLINE INSTRUCTIONS TO AUTHORS (http://www.wjgnet.com/1948-5204/g_info_20100312180518.htm) before attempting to submit online. For assistance, authors encountering problems with the Online Submission System may send an email describing the problem to bpgoffice@wjgnet.com, or by telephone: +86-10-85381891. If you submit your manuscript online, do not make a postal contribution. Repeated online submission for the same manuscript is strictly prohibited.

MANUSCRIPT PREPARATION

All contributions should be written in English. All articles must be submitted using word-processing software. All submissions must be typed in 1.5 line spacing and 12 pt. Book Antiqua with ample margins. Style should conform to our house format. Required information for each of the manuscript sections is as follows:

Title page

Title: Title should be less than 12 words.

Running title: A short running title of less than 6 words should be provided.

Authorship: Authorship credit should be in accordance with the standard proposed by International Committee of Medical Journal Editors, based on (1) substantial contributions to conception and design, acquisition of data, or analysis and interpretation of data; (2) drafting the article or revising it critically for important intellectual content; and (3) final approval of the version to be published. Authors should meet conditions 1, 2, and 3.

Institution: Author names should be given first, then the complete name of institution, city, province and postcode. For example, Xu-Chen Zhang, Li-Xin Mei, Department of Pathology, Chengde Medical College, Chengde 067000, Hebei Province, China. One author may be represented from two institutions, for example, George Sgourakis, Department of General, Visceral, and Transplantation Surgery, Essen 45122, Germany; George Sgourakis, 2nd Surgical Department, Korgialenio-Benakio Red Cross Hospital, Athens 15451, Greece

Author contributions: The format of this section should be: Author contributions: Wang CL and Liang L contributed equally to this work; Wang CL, Liang L, Fu JF, Zou CC, Hong F and Wu XM designed the research; Wang CL, Zou CC, Hong F and Wu XM performed the research; Xue JZ and Lu JR contributed new reagents/analytic tools; Wang CL, Liang L and Fu JF analyzed the data; and Wang CL, Liang L and Fu JF wrote the paper.

Supportive foundations: The complete name and number of supportive foundations should be provided, e.g. Supported by National Natural Science Foundation of China, No. 30224801

Correspondence to: Only one corresponding address should be provided. Author names should be given first, then author title, affiliation, the complete name of institution, city, postcode, province, country, and email. All the letters in the email should be in lower case. A space interval should be inserted between country name and email address. For example, Montgomery Bissell, MD, Professor of Medicine, Chief, Liver Center, Gastroenterology Division, University of California, Box 0538, San Francisco, CA 94143, United States. montgomery.bissell@ucsf.edu

Telephone and fax: Telephone and fax should consist of +, country number, district number and telephone or fax number, e.g. Telephone: +86-10-85381891 Fax: +86-10-85381893

Peer reviewers: All articles received are subject to peer review. Normally, three experts are invited for each article. Decision on acceptance is made only when at least two experts recommend publication of an article. All peer-reviewers are acknowledged on Express Submission and Peer-review System website.

Abstract

There are unstructured abstracts (no less than 200 words) and structured abstracts. The specific requirements for structured abstracts are as follows:

An informative, structured abstract should accompany each manuscript. Abstracts of original contributions should be structured into the following sections: AIM (no more than 20 words; Only the purpose of the study should be included. Please write the Aim in the form of "To investigate/study/…"), METHODS (no less than 140 words for Original Articles; and no less than 80 words for Brief Articles), RESULTS (no less than 150 words for Original Articles and no less than 120 words for Brief Articles; You should present *P* values where appropriate and must provide relevant data to illustrate how they were obtained, e.g. 6.92 ± 3.86 *vs* 3.61 ± 1.67, $P < 0.001$), and CONCLUSION (no more than 26 words).

Key words

Please list 5-10 key words, selected mainly from *Index Medicus*, which reflect the content of the study.

Core tip

Please write a summary of less than 100 words to outline the most innovative and important arguments and core contents in your paper to attract readers.

Text

For articles of these sections, original articles and brief articles, the main text should be structured into the following sections: INTRODUCTION, MATERIALS AND METHODS, RESULTS and DISCUSSION, and should include appropriate Figures and Tables. Data should be presented in the main text or in Figures and Tables, but not in both. The main text format of these sections, editorial, topic highlight, case report, letters to the editors, can be found at: http://www.wjgnet.com/1948-5204/g_info_list.htm.

Illustrations

Figures should be numbered as 1, 2, 3, *etc*., and mentioned clearly in the main text. Provide a brief title for each figure on a separate page. Detailed legends should not be provided under the figures. This part should be added into the text where the figures are applicable. Keeping all elements compiled is necessary in line-art image. Scale bars should be used rather than magnification factors, with the length of the bar defined in the legend rather than on the bar itself. File names should identify the figure and panel. Avoid layering type directly over shaded or textured areas. Please use uniform legends for the same subjects. For example: Figure 1 Pathological changes in atrophic gastritis after treatment. A: ...; B: ...; C: ...; D: ...; E: ...; F: ...; G: …*etc*. It is our principle to publish high resolution-figures for the E-versions.

Tables

Three-line tables should be numbered 1, 2, 3, *etc*., and mentioned clearly in the main text. Provide a brief title for each table. Detailed legends should not be included under tables, but rather added into the text where applicable. The information should complement, but not duplicate the text. Use one horizontal line under the title, a second under column heads, and a third below the Table, above any footnotes. Vertical and italic lines should be omitted.

Notes in tables and illustrations

Data that are not statistically significant should not be noted. [a]$P < 0.05$, [b]$P < 0.01$ should be noted ($P > 0.05$ should not be noted). If there are other series of P values, [c]$P < 0.05$ and [d]$P < 0.01$ are used. A third series of P values can be expressed as [e]$P < 0.05$ and [f]$P < 0.01$. Other notes in tables or under illustrations should be expressed as [1]F, [2]F, [3]F; or sometimes as other symbols with a superscript (Arabic numerals) in the upper left corner. In a multi-curve illustration, each curve should be labeled with ●, ○, ■, □, ▲, △, *etc*., in a certain sequence.

Acknowledgments

Brief acknowledgments of persons who have made genuine contributions to the manuscript and who endorse the data and conclusions should be included. Authors are responsible for obtaining written permission to use any copyrighted text and/or illustrations.

REFERENCES

Coding system

The author should number the references in Arabic numerals according to the citation order in the text. Put reference numbers in square brackets in superscript at the end of citation content or after the cited author's name. For citation content which is part of the narration, the coding number and square brackets should be typeset normally. For example, "Crohn's disease (CD) is associated with increased intestinal permeability[1,2]". If references are cited directly in the text, they should be put together within the text, for example, "From references[19,22-24], we know that..."

When the authors write the references, please ensure that the order in text is the same as in the references section, and also ensure the spelling accuracy of the first author's name. Do not list the same citation twice.

PMID and DOI

Pleased provide PubMed citation numbers to the reference list, e.g. PMID and DOI, which can be found at http://www.ncbi.nlm.nih.gov/sites/entrez?db=pubmed and http://www.crossref.org/SimpleTextQuery/, respectively. The numbers will be used in E-version of this journal.

Style for journal references

Authors: the name of the first author should be typed in bold-faced letters. The family name of all authors should be typed with the initial letter capitalized, followed by their abbreviated first and middle initials. (For example, Lian-Sheng Ma is abbreviated as Ma LS, Bo-Rong Pan as Pan BR). The title of the cited article and italicized journal title (journal title should be in its abbreviated form as shown in PubMed), publication date, volume number (in black), start page, and end page [PMID: 11819634 DOI: 10.3748/wjg.13.5396].

Style for book references

Authors: the name of the first author should be typed in bold-faced letters. The surname of all authors should be typed with the initial letter capitalized, followed by their abbreviated middle and first initials. (For example, Lian-Sheng Ma is abbreviated as Ma LS, Bo-Rong Pan as Pan BR) Book title. Publication number. Publication place: Publication press, Year: start page and end page.

Format

Journals

English journal article (list all authors and include the PMID where applicable)

1 **Jung EM**, Clevert DA, Schreyer AG, Schmitt S, Rennert J, Kubale R, Feuerbach S, Jung F. Evaluation of quantitative contrast harmonic imaging to assess malignancy of liver tumors: A prospective controlled two-center study. *World J Gastroenterol* 2007; **13**: 6356-6364 [PMID: 18081224 DOI: 10.3748/wjg.13.6356]

Chinese journal article (list all authors and include the PMID where applicable)

2 **Lin GZ**, Wang XZ, Wang P, Lin J, Yang FD. Immunologic effect of Jianpi Yishen decoction in treatment of Pixu-diarrhoea. *Shijie Huaren Xiaohua Zazhi* 1999; **7**: 285-287

In press

3 **Tian D**, Araki H, Stahl E, Bergelson J, Kreitman M. Signature of balancing selection in Arabidopsis. *Proc Natl Acad Sci USA* 2006; In press

Organization as author

4 **Diabetes Prevention Program Research Group**. Hypertension, insulin, and proinsulin in participants with impaired glucose tolerance. *Hypertension* 2002; **40**: 679-686 [PMID: 12411462 DOI:10.1161/01.HYP.0000035706.28494.09]

Both personal authors and an organization as author

5 **Vallancien G**, Emberton M, Harving N, van Moorselaar RJ; Alf-One Study Group. Sexual dysfunction in 1, 274 European men suffering from lower urinary tract symptoms. *J Urol* 2003; **169**: 2257-2261 [PMID: 12771764 DOI:10.1097/01.ju.0000067940.76090.73]

No author given

6 21st century heart solution may have a sting in the tail. *BMJ* 2002; **325**: 184 [PMID: 12142303 DOI:10.1136/bmj.325.7357.184]

Volume with supplement

7 **Geraud G**, Spierings EL, Keywood C. Tolerability and safety of frovatriptan with short- and long-term use for treatment of migraine and in comparison with sumatriptan. *Headache* 2002; **42** Suppl 2: S93-99 [PMID: 12028325 DOI:10.1046/j.1526-4610.42.s2.7.x]

Issue with no volume

8 **Banit DM**, Kaufer H, Hartford JM. Intraoperative frozen section analysis in revision total joint arthroplasty. *Clin Orthop Relat Res* 2002; (**401**): 230-238 [PMID: 12151900 DOI:10.1097/00003086-200208000-00026]

No volume or issue

9 Outreach: Bringing HIV-positive individuals into care. *HRSA Careaction* 2002; 1-6 [PMID: 12154804]

Books

Personal author(s)

10 **Sherlock S**, Dooley J. Diseases of the liver and billiary system. 9th ed. Oxford: Blackwell Sci Pub, 1993: 258-296

Chapter in a book (list all authors)

11 **Lam SK**. Academic investigator's perspectives of medical treatment for peptic ulcer. In: Swabb EA, Azabo S. Ulcer disease: investigation and basis for therapy. New York: Marcel Dekker, 1991: 431-450

Author(s) and editor(s)

12 **Breedlove GK**, Schorfheide AM. Adolescent pregnancy. 2nd ed. Wieczorek RR, editor. White Plains (NY): March of Dimes Education Services, 2001: 20-34

Conference proceedings

13 **Harnden P**, Joffe JK, Jones WG, editors. Germ cell tumours V. Proceedings of the 5th Germ cell tumours Conference; 2001 Sep 13-15; Leeds, UK. New York: Springer, 2002: 30-56

Conference paper

14 **Christensen S**, Oppacher F. An analysis of Koza's computational effort statistic for genetic programming. In: Foster JA, Lutton E, Miller J, Ryan C, Tettamanzi AG, editors. Genetic programming. EuroGP 2002: Proceedings of the 5th European Conference on Genetic Programming; 2002 Apr 3-5; Kinsdale, Ireland. Berlin: Springer, 2002: 182-191

Electronic journal (list all authors)

15 Morse SS. Factors in the emergence of infectious diseases. Emerg Infect Dis serial online, 1995-01-03, cited 1996-06-05; 1(1): 24 screens. Available from: URL: http://www.cdc.gov/ncidod/eid/index.htm

Patent (list all authors)

16 **Pagedas AC**, inventor; Ancel Surgical R&D Inc., assignee. Flexible endoscopic grasping and cutting device and positioning tool assembly. United States patent US 20020103498. 2002 Aug 1

Statistical data

Write as mean ± SD or mean ± SE.

Statistical expression

Express *t* test as *t* (in italics), *F* test as *F* (in italics), chi square test as χ^2 (in Greek), related coefficient as *r* (in italics), degree of freedom as υ (in Greek), sample number as *n* (in italics), and probability as *P* (in italics).

Units

Use SI units. For example: body mass, m (B) = 78 kg; blood pressure, p (B) = 16.2/12.3 kPa; incubation time, t (incubation) = 96 h, blood glucose concentration, c (glucose) 6.4 ± 2.1 mmol/L; blood CEA mass concentration, p (CEA) = 8.6 24.5 μg/L; CO_2 volume fraction, 50 mL/L CO_2, not 5% CO_2; likewise for 40 g/L formaldehyde, not 10% formalin; and mass fraction, 8 ng/g, *etc*. Arabic numerals such as 23, 243, 641 should be read 23243641.

The format for how to accurately write common units and quantums can be found at: http://www.wjgnet.com/1948-5204/g_info_20100312183048.htm.

Abbreviations

Standard abbreviations should be defined in the abstract and on first mention in the text. In general, terms should not be abbreviated unless they are used repeatedly and the abbreviation is helpful to the reader. Permissible abbreviations are listed in Units, Symbols and Abbreviations: A Guide for Biological and Medical Editors and Authors (Ed. Baron DN, 1988) published by The Royal Society of Medicine, London. Certain commonly used abbreviations, such as DNA, RNA, HIV, LD50, PCR, HBV, ECG, WBC, RBC, CT, ESR, CSF, IgG, ELISA, PBS, ATP, EDTA, mAb, can be used directly without further explanation.

Italics

Quantities: *t* time or temperature, *c* concentration, *A* area, *l* length, *m* mass, *V* volume.
Genotypes: *gyrA*, *arg* 1, *c myc*, *c fos*, *etc*.
Restriction enzymes: *Eco*RI, *Hin*dI, *Bam*HI, *Kbo* I, *Kpn* I, *etc*.
Biology: *H. pylori*, *E coli*, *etc*.

Examples for paper writing

All types of articles' writing style and requirement will be found in the link: http://www.wjgnet.com/esps/NavigationInfo.aspx?id=15

SUBMISSION OF THE REVISED MANUSCRIPTS AFTER ACCEPTED

Authors must revise their manuscript carefully according to the revision policies of Baishideng Publishing Group Co., Limited. The revised version, along with the signed copyright transfer agreement, responses to the reviewers, and English language Grade B certificate (for non-native speakers of English), should be submitted to the online system via the link contained in the e-mail sent by the editor. If you have any questions about the revision, please send e-mail to esps@wjgnet.com.

Language evaluation

The language of a manuscript will be graded before it is sent for revision. (1) Grade A: priority publishing; (2) Grade B: minor language polishing; (3) Grade C: a great deal of language polishing needed; and (4) Grade D: rejected. Revised articles should reach Grade A or B.

Copyright assignment form

Please download a Copyright assignment form from http://www.wjgnet.com/1948-5204/g_info_20100312182928.htm.

Responses to reviewers

Please revise your article according to the comments/suggestions provided by the reviewers. The format for responses to the reviewers' comments can be found at: http://www.wjgnet.com/1948-5204/g_info_20100312182841.htm.

Proof of financial support

For papers supported by a foundation, authors should provide a copy of the approval document and serial number of the foundation.

STATEMENT ABOUT ANONYMOUS PUBLICATION OF THE PEER REVIEWERS' COMMENTS

In order to increase the quality of peer review, push authors to carefully revise their manuscripts based on the peer reviewers' comments, and promote academic interactions among peer reviewers, authors and readers, we decide to anonymously publish the reviewers' comments and author's responses at the same time the manuscript is published online.

PUBLICATION FEE

WJR is an international, peer-reviewed, OA online journal. Articles published by this journal are distributed under the terms of the Creative Commons Attribution Non-commercial License, which permits use, distribution, and reproduction in any medium and format, provided the original work is properly cited. The use is non-commercial and is otherwise in compliance with the license. Authors of accepted articles must pay a publication fee. Publication fee: 600 USD per article. All invited articles are published free of charge.

百世登

Baishideng®

Published by **Baishideng Publishing Group Co., Limited**
Flat C, 23/F., Lucky Plaza,
315-321 Lockhart Road, Wan Chai,
Hong Kong, China
Fax: +852-65557188
Telephone: +852-31779906
E-mail: bpgoffice@wjgnet.com
http://www.wjgnet.com